

Impact of connection details of architectural components on seismic induced repair cost in a shear wall building

by

Seyyed Roozbeh DAREGHOLI

MANUSCRIPT-BASED THESIS PRESENTED TO ÉCOLE DE
TECHNOLOGIE SUPÉRIEURE IN PARTIAL FULFILLEMENT OF A
MASTER'S DEGREE WITH THESIS IN CONSTRUCTION ENGINEERING
M. A. Sc.

MONTREAL, JANUARY 18, 2024

ÉCOLE DE TECHNOLOGIE SUPÉRIEURE
UNIVERSITÉ DU QUÉBEC



Seyyed Roozbeh Daregholi, 2023



This Creative Commons licence allows readers to download this work and share it with others as long as the author is credited. The content of this work can't be modified in any way or used commercially.

BOARD OF EXAMINERS

THIS THESIS HAS BEEN EVALUATED

BY THE FOLLOWING BOARD OF EXAMINERS

Mrs. Rola Assi, Thesis Supervisor
Department of Construction Engineering at École de technologie supérieure

Mr. Ahmad Abo-El-Ezz, Thesis Co-supervisor
Department of Construction Engineering at École de technologie supérieure

Mr. Wahid Maref, President of the Board of Examiners
Department of Construction Engineering at École de technologie supérieure

Mr. Reda Snaiki, Member of the jury
Department of Construction Engineering at École de technologie supérieure

THIS THESIS WAS PRESENTED AND DEFENDED

IN THE PRESENCE OF A BOARD OF EXAMINERS AND PUBLIC

ON DECEMBER 14, 2023

AT ÉCOLE DE TECHNOLOGIE SUPÉRIEURE

ACKNOWLEDGMENTS

I am profoundly grateful to my dedicated supervisor, Professor Rola Assi, and co-supervisor, Professor Ahmad Abo-El-Ezz for their invaluable guidance, unwavering support, and expert mentorship throughout the journey of crafting this thesis. Their insightful feedback, patient encouragement, and genuine belief in my capabilities have been instrumental in shaping my research and refining my ideas. This thesis is a testament to their dedication, and I am honored to have had the privilege of working under their tutelage.

In the tapestry of my academic pursuits, a profound debt of gratitude is owed to my cherished wife, Gilda Shayanmehr and our precious newborn daughter, Ariana Daregholi. Your unwavering love and steadfast encouragement have provided me with the strength to navigate the intricate pathways of research and reach this significant milestone. Your presence has been a constant source of inspiration, reminding me of the greater purpose behind my endeavors.

Impact des détails de connexion des composants architecturaux sur les pertes économiques directes induites par les séismes dans un bâtiment à murs de refend

Seyyed Roozbeh DAREGHOLI

RÉSUMÉ

Les pertes associées à la défaillance des composants non structuraux (CNS) lors des séismes représentent la contribution la plus significative aux pertes économiques totales des bâtiments. Par conséquent, les études récentes se sont concentrées sur la proposition de modifications aux détails de connexion, aux dimensions et aux matériaux des composants afin d'améliorer leur performance sismique. Dans une première étape, cette étude évalue l'effet de l'utilisation de différentes méthodes pour estimer les paramètres de demande en ingénierie (PDI) sur les pertes des bâtiments. Ensuite, elle examine quantitativement les pertes économiques directes et les avantages potentiels résultant de l'amélioration des détails de connexion de trois composants architecturaux couramment utilisés, à savoir les cloisons de séparation, les plafonds suspendus et les rideaux soumis à différentes intensités sismiques. De plus, elle examine la répartition des coûts de réparation associés à l'emplacement des CNS le long de la hauteur du bâtiment. Pour atteindre ces objectifs, un immeuble de bureaux en béton armé de 12 étages avec des murs de refend, situé à Montréal sur un sol de classe D (sol rigide), a été choisi comme étude de cas. L'étude utilise la méthodologie d'estimation des pertes spécifiques aux bâtiments proposée dans le document FEMA-P58 pour estimer les pertes économiques directes en termes de coût de réparation. Les résultats ont révélé la variation des PDI estimés (exprimés sous forme de taux de déplacement inter-étages et d'accélération horizontale maximale des planchers) lors de l'utilisation de différentes méthodes de prédiction et mettent en évidence la corrélation entre les PDI calculés et coûts de réparation correspondants. De plus, les résultats ont montré que l'amélioration des détails de connexion peut réduire les coûts de réparation des cloisons de séparation, des plafonds suspendus et des rideaux de plus de 30 % à l'intensité sismique de conception correspondant à une probabilité de dépassement de 2 % en 50 ans. De plus, il est observé qu'il existe une corrélation entre l'intensité du séisme, les valeurs prédites des PDI dans chaque étage et la répartition des coûts de réparation le long de la hauteur du bâtiment. Dans

VIII

le bâtiment considéré, les pertes estimées dues à la défaillance des composants sélectionnés sont principalement concentrées dans le tiers supérieur de la hauteur du bâtiment, représentant plus de 50 % des coûts de réparation.

Mots-clés : composante architecturale, estimation des pertes, coût de réparation, FEMA P-58, fonctions de fragilité, états d'endommagement, fonctions de conséquences

Impact of connection details of architectural components on seismic induced repair cost in a shear wall building

Seyyed Roozbeh DAREGHOLI

ABSTRACT

Losses associated with the failure of Non-Structural Components (NSCs) during earthquakes are the most significant contributor to overall building economic loss. Consequently, recent studies have focused on proposing modifications to connection details, element sizes, and materials of NSCs to enhance their seismic performance. In the first step, this study evaluates the effect of using different prediction methods for estimating Engineering Demand Parameters (EDPs) on repair cost of architectural components. Then it quantitatively investigates the repair costs and potential benefits that result from improving the connection details for three commonly used architectural components, namely partition walls, suspended ceilings, and curtain walls subjected to different earthquake intensities. Additionally, it examines the distribution of repair costs associated with the location of the architectural components along the building height. To achieve these goals, a 12-story reinforced concrete shear wall office building located in Montreal on site Class D (stiff soil), was selected as a case study. The study employs the FEMA-P58 building-specific loss estimation methodology to estimate the direct economic loss in terms of repair cost. The results revealed the variation of estimated EDPs (expressed as inter-story drift ratio and peak horizontal floor acceleration) while using different prediction methods and highlight the correlation between calculated EDPs and their corresponding repair costs. Moreover, the results demonstrated that enhancing connection detailing can reduce repair costs of partition walls, suspended ceilings, and curtain walls, by more than 30% at the design level earthquake intensity corresponding to 2% probability of exceedance in 50 years. Furthermore, it is observed that there is a correlation between the earthquake intensity, predicted values of EDPs in each story, and the distribution of repair cost along building height. In the case study building, the estimated loss due to the failure of the

X

selected components is mainly concentrated in the upper third of the building's height accounting for more than 50% of repair cost.

Keywords: architectural component, loss estimation, repair cost, FEMA P-58, fragility curves, damage states, consequences functions

TABLE OF CONTENTS

	Page
INTRODUCTION	1
0.1 Background and problem statement.....	1
0.2 Objectives	4
0.3 Methodology.....	4
0.4 Limitations of study	5
0.5 Thesis organization.....	6
CHAPTER 1 LITERATURE REVIEW	7
1.1 Introduction.....	7
1.2 Performance-based loss estimation framework	10
1.2.1 Hazard analysis.....	12
1.2.2 Methods of predict EDPs.....	14
1.2.2.1 Simplified analysis based on FEMA P-58.....	14
1.2.2.2 Equations proposed in NBC 2015	15
1.2.2.3 Equations proposed in ASCE7-22.....	15
1.2.3 Damage analysis and fragility curve definitions for NSCs	16
1.2.3.1 Fragility curve definition.....	16
1.2.3.2 Fragility curves of architectural components	17
1.3 Loss estimation and consequences functions.....	23
1.3.1 Loss estimation.....	23
1.3.2 Previous studies on loss estimation	24
1.4 Summary.....	26
CHAPTER 2 ASSESSMENT OF INFLUENCE OF EDP PREDICTION METHOD ON INDUCED REPAIR COST	27
2.1 Description of the case study building.....	27
2.1.1 Building information	27
2.1.2 Description of input ground motions.....	28
2.1.3 Selected architectural components	30
2.1.4 Estimated replacement costs:	31
2.2 Finite element modelling of the building.....	33
2.3 EDPs comparison.....	36
2.3.1 IDR comparison.....	36
2.3.1.1 Comparison of IDR obtained from different methods	36
2.3.1.2 Validation of IDR results with previous studies.....	39
2.3.2 PFA comparison:	40
2.3.2.1 Comparison of PFA obtained from different methods	40
2.3.2.2 Validation of PFA results with previous studies.....	43
2.4 Sensitivity of estimated loss to the EDPs calculation method.....	47
2.4.1 Assumed fragility curves and replacement costs.....	48
2.4.2 Comparison of calculated repair costs.....	48

2.4.3	Contribution of selected architectural components and effect of their location along building height in the repair cost.....	49
2.4.4	Synthesizing the results of loss estimation.....	54
CHAPTER 3 INFLUENCE OF CONNECTION DETAILS ON THE SEISMIC RESPONSE OF ARCHITECTURAL NON-STRUCTURAL COMPONENTS AND INDUCED LOSSES IN REINFORCED CONCRETE SHEAR WALL BUILDINGS.....57		
3.1	Abstract.....	57
3.2	Introduction.....	57
3.3	Description of the studied building and NSCs.....	60
3.3.1	Building information	60
3.3.2	Selected architectural components and their estimated replacement cost.....	61
3.3.3	Seismic intensities	63
3.4	Structural analysis.....	64
3.5	Selection of component fragility curves and repair cost consequences functions.....	66
3.5.1	Partition Walls	66
3.5.2	Suspended Ceilings	67
3.5.3	Curtain Walls.....	68
3.6	Results of loss estimation before and after improving the connection details.....	74
3.7	Conclusion	78
CONCLUSIONS.....		79
RECOMMENDATIONS.....		83
APPENDIX I	CALCULATION OF EDPs USING SIMPLIFIED ANALYSIS BASED ON ASCE 7 METHOD.....	85
APPENDIX II	CALCULATION OF EDPs USING SIMPLIFIED ANALYSIS BASED ON METHOD OF NBC 2015.....	93
APPENDIX III	CALCULATION OF EDPs USING SIMPLIFIED ANALYSIS BASED ON EQUIVALENT LATERAL FORCE METHOD OF FEMA P-58	103
APPENDIX IV	PERFORMANCE CALCULATION USING PACT.....	115
APPENDIX V	AN EXAMPLE FOR CALCULATION OF REPAIR COST.....	121
APPENDIX VI	CURVE FITTING USING REGRESSION MODEL TO VERIFY ESTIMATED PFA	123
LIST OF BIBLIOGRAPHICAL REFERENCES.....		127

LIST OF TABLES

		Page
Table 2.1	Spectral values associated with 5% damped response spectra	29
Table 2.2	Estimated quantity for selected architectural components based on FEAM P-58 Normative quantity estimation tool.....	31
Table 2.3	Assumed total replacement costs of building and selected components	32
Table 2.4	Comparison of the periods obtained from FEM model with the values in the CDH (2016)	34
Table 2.5	Comparison of base shears obtained from FEM model and the values provided in CDH (2016) in both principal directions.....	36
Table 2.6	Comparison and validation of maximum IDR predicted by the four selected methods	40
Table 2.7	Comparison of code defined height factors and the equation provided by Fathali and Lizundia (2011).....	43
Table 2.8	Comparison and verification of FEMA P-58, ASCE7-22, and NBC2015 methods with previous studies.....	47
Table 2.9	Selected fragilities for architectural components Taken from FEMA P-58 Fragility Specification (FEMA, 2018)	48
Table 3.1	Estimated quantity and maximum possible repair cost for each NSCs based on FEAM P-58 Normative quantity estimation tool	62
Table 3.2	Definition of Damage States for PWs, SCs, and CWs based on FEMA P-58 Fragility Specification (FEMA, 2018)	70
Table 3.3	Selected fragilities for PWs, SCs, and CWs Taken from FEMA P-58 Fragility Specification (FEMA, 2018)	71

LIST OF FIGURES

		Page
Figure 1.1	Building components Taken from CSA S-832 (2014).....	8
Figure 1.2	Recommended seismic performance objectives of Vision 2000 Taken from Structural Engineers Association of California (1995).....	11
Figure 1.3	PEER approach for PBEE Taken from Porter (2003)	12
Figure 1.4	Example of the fragility curves for different damage states of a partition wall	17
Figure 1.5	Typical gypsum partition walls: a) configuration; b) friction connection, fixed bottom and a slip track at top; c) friction connection with a double slip track (top and bottom); d) full connection (fix at top and bottom).....	19
Figure 1.6	Typical acoustic lay-in panel suspended ceilings: a) general configuration ; b)transversal section; c) fix connection to adjacent wall; (d) free connection adjacent wall Taken from FEMA E-74 (2012)	21
Figure 1.7	Typical curtain wall: a) glass and frame configuration; b) Mullion section and connection detailing; c) Transom head and connection detailing; d) Transom sill and connection detailing Taken from FEMA E-74 (2012)	23
Figure 1.8	Calculation of a repair cost for a PG Taken from Zeng et al. (2016)	24
Figure 2.1	Plan and elevation of the 12-storey office building Taken from Concrete design handbook (2016)	28
Figure 2.2	Montreal 5% damped response spectrum used in this section based on the NBC 2015 seismic hazard values	29
Figure 2.3	Maximum possible repair cost: a) Partition Walls; b) Suspended Ceilings; c) Curtain Walls.....	33
Figure 2.4	Obtained mode shapes and corresponding lateral periods of vibrations from SAP 2000 model	35

Figure 2.5	Estimated IDR using three different methods due to increasing earthquakes intensities	38
Figure 2.6	Verification of calculated IDR with previous study	39
Figure 2.7	Estimated PFA/PGA ratio using three different methods due to increasing earthquake intensities	42
Figure 2.8	General non-linear relation between PFA/PGA and z/h Taken from Fathali & Lizundia (2011).....	44
Figure 2.9	Validation of PFA calculated by different methods with previous studies considering 2% in 50 years earthquake	46
Figure 2.10	Sensitivity of the repair cost of architectural components to the EDPs estimation method.....	49
Figure 2.11	Contribution of each NSC in estimated loss ratio due to different calculated EDP method.....	50
Figure 2.12	Variation of loss ratio of each architectural components along building height considering different methods for EDPs calculation.....	52
Figure 2.13	Variation of repair ratio of each architectural components along building height considering different methods for EDPs calculation.....	53
Figure 2.14	a) Total repair cost; b) Loss ratio of three selected NSCs; (c), (d), (e) Repair cost associated with each selected NSCs	55
Figure 3.1	Framework of FEMA P-58 loss estimation methodology used in this study	60
Figure 3.2	Plan and elevation views of the 12-story office building Taken from Concrete design handbook (2016)	61
Figure 3.3	Maximum possible repair cost: a) Partition Walls; b) Suspended Ceilings; c) Curtain Walls.....	63
Figure 3.4	Utilized response spectra - Montreal (site class-D) based on the NBC 2020 hazard values	64
Figure 3.5	calculation of IDR and PFA based on the simplified linear method presented in FEMA P-58-1 (FEMA, 2018)	65
Figure 3.6	Fragility curves for standard and improved conditions of selected PWs (a) and (b); SCs (c) and (d); CWs (e) and (f); Taken from FEMA P-58 Fragility Specification Manager (2011)	72

Figure 3.7	Consequences functions for standard and improved conditions of selected PWs SCs, and CWs Taken from FEMA P-58 Fragility Specification Manager (2011)73
Figure 3.8	Total Repair cost: a) PWs; b) SCs; c) CWs; Loss ratio: c) PWs; d) SCs; e) CWs; Repair ratio: f) PWs; g) SCs; h) CWs; based on spectral acceleration at the fundamental period of the building76
Figure 3.9	Effect of Location of architectural componentss on their contribution to repair cost77

LIST OF ABBREVIATIONS AND ACRONYMS

ASCE	American Society of Civil Engineers
BF	Bare Frame
Can\$	Canadian Dollar
CBD	Central Business District
CHD	Concrete Design Handbook
CNB	Code National du bâtiment- Canada
CNS	Composants Non-Structraux
CQC	Complete Quadratic Combination
CSA	Canadian Standard Association
CW	Curtain Wall
DBE	Design Base Earthquake
DDOF	Dynamic Degree of Freedom
DM	Demand Measures
DS	Damage State
DV	Decision Variables
EAL	Estimated Annual Loss
EDPs	Engineering Demand Parameters
FEM	Finite Element Model
FEMA	Federal Emergency Management Agency
FRS	Floor Response Spectra
gsf	Gross Square feet
IDA	Incremental Dynamic Analysis

XX

IDR	Inter-story Drift Ratio
IM	Intensity Measures
Lf	Linear feet
MAFE	Mean Annual Frequency of Exceedance
MCS	Multi-story Concentrated-mass Shear
MCE	Maximum Credible Earthquake
MCEER	Multidisciplinary Center of Earthquake Engineering Research
MEP	Mechanical, Electrical, and Plumbing
MPMR	Modal Participation Mass Ratio
NBC	National Building Code of Canada
NSCs	Non-Structural Components
OFC	Operational and Functional Components
PACT	Performance Assessment Calculation Tool
PBEE	Performance-Based Earthquake Engineering
PDI	Paramètre de Demande en Ingénierie
PEER	Pacific Earthquake Engineering Research
PFA	Peak Floor Acceleration
PG	Performance Group
PGA	Peak Ground Acceleration
PW	Partition Wall
RC	Reinforced Concrete
RSA	Response Spectrum Analysis

SEAOC	Structural Engineers Association of California
SEESL	Structural Engineering and Earthquake Simulation Library
SFRS	Seismic Force Resisting System
SLE	Service Level Earthquake
SRSS	Square Root of the Sum of the Squares
UBC	Uniform Building Code
THA	Time History Analysis
UIF	Uniformly In-filled Frame
UIF-s	Uniformly In-filled frame with shear columns

LIST OF SYMBOLS AND UNITS OF MEASUREMENTS

Lowercase Latin alphabet

f_c	Concrete characteristic strength
h	Average roof height of structure from the base
h_i	Height above the effective base of the building for level i
h_x	Height above the effective base of the building for level x
h_n	Total height of the structure
w_i	Lumped weight at each floor level i .
z	Height of the point of the attachment of the component above the base of the structure

Uppercase Latin alphabet

A_g	Shear area
A_r	Dynamic amplification factor of non-structural component
A_x	Acceleration height factor
C_1	Adjustment factor for inelastic response
C_2	Adjustment factor for cyclic degradation
C_{AR}	Component resonance ductility factor
C_d	Deflection amplification factor
C_p	Non-structural component factor to take into consideration the likelihood of component failure
C_{vx}	Vertical distribution factor
EA_g	Gross axial rigidity
EI_g	Gross flexural rigidity
F_a	Acceleration-based site coefficient
F_p	Seismic design force of non-structural component
F_t	Concentrated load at the top level to consider the effects of higher mode
F_x	Vertical distribution of lateral forces at level x
F_y	Yield strength
H	Total height of the building
H_{ai}	Floor acceleration modification factor

$H_{\Delta i}$	Inter-story drift ratio modification factor
H_f	Force amplification factor
I	Importance factor
IE	Importance factor
I_g	Moment of inertia
I_p	Component importance factor
M_v	Higher mode factor
R	Response modification factor
R_d	Ductility-related force modification factors
R_o	Overstrength-related force modification factors
R_p	Response modification factor of non-structural component
R_{po}	Component strength factor
R_{μ}	Structure ductility reduction factor
S	Strength ratio
$S_a(0.2)$	Spectral response acceleration at period of 0.2 seconds
$S_a(T_1)$	5% damped spectral acceleration at the fundamental period of the building
S_{DS}	5% damped site-specific spectral acceleration at short period
S_p	Horizontal force factor for non-structural component
T_a	Design period
U_x	Modal participation mass ratio X-direction
U_y	Modal participation mass ratio Y-direction
$V_{s30}(X_V)$	Average shear wave velocity in the upper 30m of a ground profile
V	Base shear
V_p	Design lateral force for non-structural components
V_{y1}	First mode response estimated yield strength
W	Total building seismic weight
W_1	The first modal effective weight in the considered direction
W_p	Component operating weight
W_x	Effective seismic weight at level x

Greek alphabet

β	Standard deviation of ln of intensity measure
β_{gm}	Ground motion dispersion
β_m	Modeling dispersion
$\beta_{a\Delta}$	Computed displacement dispersion
β_{aa}	Computed acceleration dispersion
β_{SD}	Inter-story drift dispersion
β_{FA}	Floor acceleration dispersion
Δ_i	Unmodified inter-story drift ratio
Δ_i^*	Modified inter-story drift ratio
Ω_0	Building overstrength factor
Θ	Median of the fragility curve

INTRODUCTION

0.1 Background and problem statement

A building is composed of two main components, structural components (SCs) and non-structural components (NSCs). In a typical building, NSCs usually contribute for the majority of the total investment. NSCs make up approximately 82 percent, 87 percent, and 92 percent of total monetary investment in office, hotel, and hospital buildings in the United States respectively (Miranda and Taghavi, 2003).

NSCs in buildings can be categorized as: (1) architectural components, such as exterior cladding, interior partition walls, suspended ceilings; (2) mechanical components, piping systems, electrical equipment, and telecommunication devices; and (3) building contents such as office equipment's, furniture, cabinets (CSA S-832, 2014; Assi et al., 2016). NSCs do not act as load-bearing systems in a building; however, they are subjected to dynamic loads during an earthquake and they must be designed to withstand the forces and displacements that arise from the building's seismic response (Filiatrault & Sullivan, 2014), defined as Engineering Demand Parameters (EDPs). Therefore, NSCs can be damaged mainly because of excessive displacement (i.e., drift-sensitive) or excessive acceleration (i.e. acceleration-sensitive)(Pardalopoulos & Pantazopoulou, 2015).

In Performance Based Earthquake Engineering (PBEE), one of the crucial factors is the computation of EDPs (Engineering Demand Parameters). These parameters, such as inter-storey drift and peak floor horizontal acceleration, are derived from structural analysis and serve as inputs for damage analysis. They are then used in loss analysis to provide quantitative outputs such as repair cost and repair time. While estimating loss, it is important to consider that different methods used to estimate EDPs can have an impact on the estimated economic loss.

Although numerous studies have compared calculated EDPs using various methods available in the literature, their effect on building loss has been rarely addressed. Time history analysis is a precise yet laborious and time-consuming method to determine the values of EDPs.

Alternatively, simplified methods based on building codes can be employed to compute the EDPs and assess their impact on the building's economic loss. Furthermore, by analyzing the variation of EDPs along the height of the building and understanding its impact on building loss, valuable insights can be gained, which can help in planning for post-earthquake repair sequences.

Damage to NSCs can pose life safety hazards, for both occupants and passers-by, cause difficulty in evacuating the building safely during an incident or preventing rescuers to access to the building interior in case of an earthquake event, and limit the post-earthquake building functionality (D'Amore et al., 2023; Villaverde R, 2004). It is expressed in reconnaissance reports from past earthquakes (Filiatrault et al., 2001; Miranda et al., 2012) that damage to NSCs occurs at much lower earthquake intensities than those required to cause structural damage, and their failure could have a substantial impact on the performance and operation of buildings (Perrone et al., 2019), such as the 1994 Northridge earthquake (McGauvin and Patrucco, 1994) and the 2010 Maule earthquake in Chile (Miranda et al., 2012).

Based on the observations after an earthquake event, for countries where the structural failure is the main concern, usually the NSCs deficiencies are overshadowed, like the earthquake on 12 January 2010 in Haiti (Fierro et al., 2011). Yet, damage to NSCs has greatly outweighed structural damage in most impacted buildings in several large earthquakes that struck North America in the twentieth century (Filiatrault & Sullivan, 2014).

For example, observations from earthquakes such as the 1989 Loma Prieta and 1994 Northridge earthquakes in California, showed that modern code requirements in high seismicity zones are relatively reliable in preventing life-threatening structural damage. Both events resulted in less than 100 fatalities despite their huge magnitudes and epicentral placements close to the concentrated population locations. The economic loss linked with these earthquakes, which totaled \$7 billion for Loma Prieta and almost \$30 billion for Northridge, were significantly high (Hamburger, 1996).

In modern code-compliant buildings, NSCs could make a significant contribution in the building loss (Goulet et al., 2007). For example, a study on seismic performance assessment of a code-conforming building in New Zealand, showed that 26% of predicted building loss was due to drift-sensitive NSCs like partitions and facades, and 49% of predicted loss was

caused by acceleration-sensitive NSCs like ceilings, equipment, egress systems, and contents (Bradley et al., 2009). A regional loss prediction in the campus of Tsinghua University in China, including buildings with different occupancies and structural systems indicated significant portion of losses are from architectural NSCs like exterior walls, partitions, wall finishes, and ceiling systems with predicted loss ratio of 35% (defined as repair cost to replacement cost ratio) for maximum credible earthquake shaking (Zeng et al., 2016). Another study by Ni et al. (2018) on two tall buildings in Manila and Bangkok located on a high and moderate seismic zones showed that in the first building the damage ratio (defined as number of damaged components divided by total number of component in a performance group) for architectural NSCs vary from 3.5% to 11% and for the second buildings loss ratio for architectural NSCs is between 2.7 to 4.7%.

Additionally, the observation has demonstrated that failures of NSCs often result from inadequate or insufficient anchoring and bracing (Miranda et al., 2012). In recent years, damage-mitigation solutions have been developed to regulate and minimize damage to either vertical (facades, partitions) or horizontal (ceilings) architectural components (Bianchi et al., 2021). These solutions involve studying the effects of connection detailing on the fragility of partition walls (Retamales et al., 2013; Sousa & Monteiro, 2018; Preti & Bolis, 2017; Hassani & Ryan, 2022), suspended ceilings (Ryu & Reinhorn, 2019; Brandolese et al., 2019; Dhakal et al., 2016), and curtain walls (Baird, Palermo, Pampanin, et al., 2011), by taking into account adequate bracing, internal and lateral gaps, and energy dissipation mechanism of connections (Bianchi et al., 2021).

Based on previous research efforts, significant progress has been made in estimation of EDPs, as well as the analysis of damage to NSCs. Nevertheless, previous studies have not specifically determined the exact extent of loss reduction resulting from the implementation of seismically improved connections, and there is limited research work done to evaluate quantitatively the potential impact of optimizing the improved seismic connection detailing of NSCs on reducing seismic loss in code-conforming buildings.

0.2 Objectives

The main objective of this study is to quantify the impact of the connection details of architectural components including partition walls, suspended ceilings, and curtain walls, on the expected repair cost in a code-conforming shear wall building subjected to various levels of ground motion intensities. The specific objectives of this study are as follows:

1. Compare the effect of the selected seismic demand prediction methods on the repair cost of building architectural components.
2. Evaluate the sensitivity of the building repair cost of architectural components to the effect of the type of the connection of selected architectural components in a code-conforming building subjected to eight different earthquake intensities, by comparing two standard and improved connections detailing conditions.
3. Evaluate the effect of the location of the architectural components along the height of the building on the distribution of repair costs and determine the portion of the repair cost for each of the lower, the middle, and the upper thirds along the building height.

0.3 Methodology

In this study, the following procedure has been considered to achieve the research objectives:

1. Performing a comprehensive literature review on estimation of the required EDPs and economic loss in the buildings.
2. Identifying a case study shear wall building designed according to the NBCC 2015, characterization of its structural components and estimate the quantity of architectural components including partition walls, curtain walls, and suspended ceilings using the Normative Quantity Estimation tool of FEMA P-58 (FEMA, 2018).
3. Conducting structural analysis on a 3D model of the building using the software SAP2000 (CSI-SAP2000, V 21,1,0) to obtain the modal dynamic parameters.
4. Choosing ground motion input for structural analysis by utilizing the 5% damped response spectra of Montreal, site class D, obtained from the National building Code

of Canada seismic hazard calculation tool (NRC, 2015) with three different earthquake intensities (40% in 50 years, 10% in 50 years, and 2% in 50 years) for comparative analyses of EDPs predicted from previous studies on the same case study building.

5. Calculating the EDPs (inter-story drift ratio and peak floor horizontal acceleration) using existing methods such as FEMA-P58 simplified analysis procedure (FEMA, 2018); equivalent static procedure of NBC (NBC, 2015) and ASCE 7-22 (ASCE, 2022) for the different earthquake intensities.
6. Performing a loss analysis using the software PACT (FEMA, 2018), by considering a set of architectural components with conventional standard connection and evaluate the sensitivity of the estimated repair cost of these components to the EDPs calculated with different methods.
7. Selecting the same architectural components with improved connection detailing condition, based on their seismic performance, by considering damage state fragility curves and corresponding repair cost consequences functions.
8. Calculating EDPs by FEMA P-58 simplified analysis procedure and considering the 5% damped response spectra of Montreal, site class D, obtained from the National building Code of Canada seismic hazard calculation tool (NBC, 2020) with eight different earthquake intensities (from 40% in 50 years to 2% in 50 years).
9. Performing a loss analysis using the software PACT (FEMA, 2018) to evaluate the impact of considering conventional and improved connections on architectural components predicted repair cost.

0.4 Limitations of the study

The study has the following limitations:

1. In the building numerical model, only the concrete shear wall core has been modeled, and the effect of accidental torsion was ignored given the symmetry of the building.
2. The assessments are conducted in one mid-rise building located in Montreal, and the low-rise or high-rise buildings and the effect of different seismic zones are not considered.

3. In this study, the focus is on architectural components, therefore the machinery, electrical and mechanical equipment, and building contents are not considered.
4. In this study, the office (commercial) occupancy has been considered for the building, the effect of changing occupancy on the repair cost is not considered.
5. The focus of the study is on assessing the repair costs of architectural components of the building. Additional factors, such as business interruption during the repair period and the potential loss of building functionality are not considered.

0.5 Thesis organization

This thesis comprises three chapters. Chapter 1 presents a comprehensive literature review on the contribution of NSCs to damage and economic losses, performance-based loss assessment framework, estimation of the EDPs, fragility curves and economic loss calculation, and the effect of architectural components connection improvement on the corresponding damage state fragility curves and repair cost consequences functions; Chapter 2 is dedicated to identifying the case study building, its components, and the applied earthquake intensities, as well as calculating and comparing EDPs using various methods (including simplified analysis method of FEMA P-58, standardized procedures in NBC2015 and ASCE 7-22) and resulting repair cost. Chapter 3 investigates the improved connection detailing for the selected architectural components and the quantitative assessment of the repair cost reduction due to the connection detailing improvement, by conducting a loss analysis of the case study building subjected to different earthquake intensities. Conclusions and recommendations are then presented in the final section of the thesis.

CHAPTER 1

LITERATURE REVIEW

This chapter begins with an introduction discussing the contribution of NSCs to damages and resulting direct or indirect economic losses following an earthquake event. It then presents the performance-based loss assessment framework. Subsequently, it covers each step of performance-based design procedure such as hazard analysis, structural analysis methods used to predict EDPs, the development of fragility curves and damage analysis, then, it explores the calculation of performance and the estimation method for losses. Finally, the chapter concludes with a summary of the main findings derived from the review of previous studies.

1.1 Introduction

Structural components refer to the elements specifically designed and constructed to safely bear and transfer all imposed gravity and lateral loads to the ground, ensuring that the structure remains intact without experiencing total or partial collapse. Non-structural components, also known as operational and functional components according to CSA S832, are other types of existing elements in the buildings (Figure 1.1). NSCs are divided to three main categories: (1) architectural, like partition walls, suspended ceilings, curtain walls, etc. (2) building services, including mechanical, plumbing, electrical, and telecommunications. (3) building contents such as office equipment, kitchen equipment, hazardous material, etc.

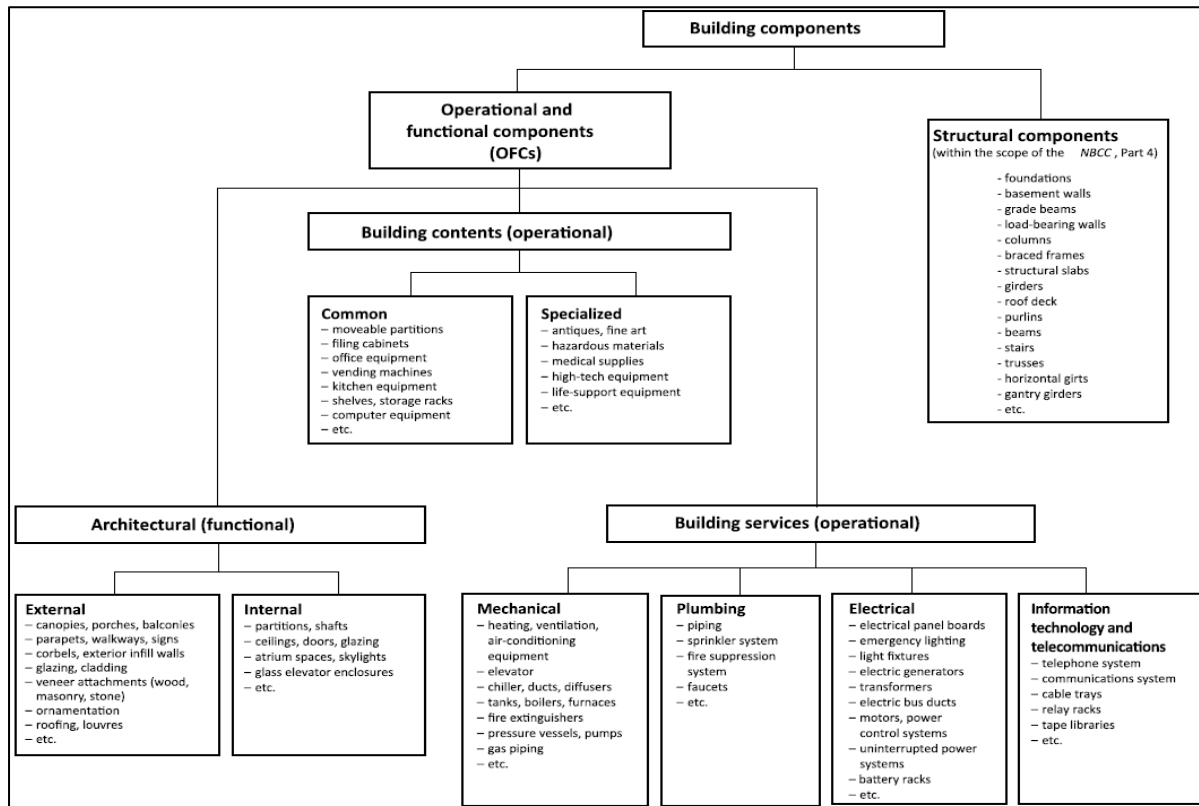


Figure 1.1 Building components
Taken from CSA S-832 (2014)

Earthquakes are one of the most important hazards which could threaten the safety of the structures and impose significant social and economic losses. During recent earthquakes which occurred in countries with reliable and modern building design codes, unlike the structural components, the performance of non-structural components was not satisfactory and caused a significant portion of losses after an event. After significant earthquakes such as the 1906 M_w 7.8 earthquake in San Francisco, USA and the 1923 M_w 7.9 earthquake in Kanto, Japan the effect of seismic load has started to be gradually considered quantitatively in the building designs however, paying attention to the NSCs failure (mostly the architectural components) started decades later, after the 1971 M_L 6.6 earthquake in San Fernando, USA, and the 1972 M_w 6.2 earthquake in Managua, Nicaragua. (CSA S832-14).

Seismic reconnaissance reports revealed the significant contribution of NSCs in building loss due to an earthquake. The February 2010 M_w 8.8 earthquake in Maule, Chile, caused a widespread damage to the building with different occupancies such as hospitals, office, commercial, and residential buildings, university campuses, and industrial facilities. Observed NSC damages includes damage to ceilings, fire sprinklers, partitions, cable trays, glazing, curtain walls, and facades, elevator, emergency power generation, etc. (Miranda et al., 2012). The most common types of NSCs failure due to the February 2001 M_w 6.8 earthquake in Nisqually, USA, was the failure of suspended ceilings. Moreover, the failure of unanchored building contents, cracking of interior and exterior wall finish materials, and shattering of glass windows were observed in many cases (Filiatrault et al., 2001). The February 2011 M_w 6.6 earthquake in Christchurch, New Zealand resulted in extensive damage to the multi-storey buildings located in the central business district (CBD) of Christchurch. Notably, the facades of these buildings played a significant role in contributing to the overall damage sustained by the structures. It has been observed that among the surveyed facade systems, 64% were assessed as operational, 14% were classified as immediate occupancy, 12% were designated as life safety, and 10% were categorized as high hazard (Baird et al., 2011). Due to the January 2010 M_w 7.0 earthquake in Haiti, there was widespread structural damage that overshadowed reports of non-structural damage. However, it is important to highlight that a significant portion of the structural damage resulted from the unintended interaction between NSCs, such as rigid masonry infills, and structural components, such as lightly reinforced concrete frames. Additionally, numerous schools and hospitals were forced to close due to non-structural damage. Most of the non-structural damage in Haiti was observed in heavy block partitions, which were severely impacted to the point where the buildings became unusable for inhabitants. Notably, several wards in the main Hospital in Port-au-Prince had to be closed due to partition damage. Schools also faced closures due to damage to partitions, ceilings, and the collapse of air conditioning equipment in Port-au-Prince (Fierro et al., 2011).

Causes of damage to NSCs can be classified into four main reasons: (1) Inertial effects which are caused by acceleration at various levels of structures and can lead to sliding or overturning. (2) Inter-story displacement of regular buildings or building distortion for the buildings with torsional irregularities, which is caused by eccentricity between center of stiffness and center

of mass which results non-uniform transitional inter-story displacements in each story. Generally, the NSCs affected by this type of damage are drift-sensitive non-structural components. (3) Pounding of closely located adjacent buildings may occur during earthquakes and can cause damage to the either acceleration or displacement- sensitive NSCs crossing the separation. (4) NSCs interaction, which might happen for adjacent NSCs that move independently in a limited share area (FEMA E74, 2012).

1.2 Performance-based loss estimation framework

Performance-based design is a procedure that aims to accomplish predefined performance objectives while designing a new building or seismically upgrading an existing one. It is one of the most promising strategies to minimize the extent of damages and losses following an earthquake or similar disaster. Enhancing the performance of NSCs is one of the issues with an utmost importance to mitigate the earthquake-induced damages (FEMA, 2018).

Performance-based design originated in the 1990s, and one of the earliest representations of this concept was developed by the Structural Engineering Association of California in a Vision 2000 report (1995). The motivation behind this approach stemmed from the recognition of a disconnection between the expectations of building owners and engineers. While most building codes typically aim for Life Safety as the engineering expectation, the owners' expectations often extend beyond this level. Thus, performance-based engineering introduced a matrix (Figure 1.2) that depicted the desired system performance at different levels of seismic excitation (Porter, 2003).

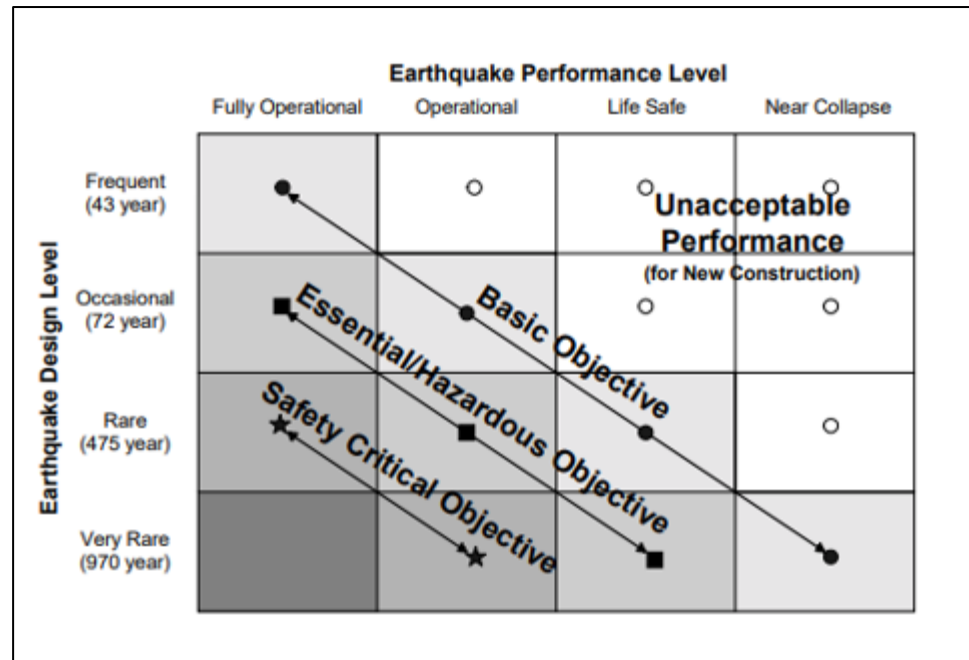


Figure 1.2 Recommended seismic performance objectives of Vision 2000
Taken from Structural Engineers Association of California (1995)

In 1997, the Pacific Earthquake Engineering Research Center (PEER) project aimed at furthering the quantitative understanding of Performance-Based Earthquake Engineering (PBEE). This marked a significant leap forward as engineers moved beyond relying solely on engineering parameters to make decisions. During discussions with building owners, EDPs like drift, displacement, acceleration, and base shear often failed to grab their attention or make sense to them effectively. PBEE introduced parameters related to loss analysis, such as repair cost, casualties, and downtime instead of the aforementioned EDPs (Porter, 2003).

Figure 1.3 depicts the framework of performance-based design which incorporates multiple factors such as ground motion characteristics, structural properties, and the vulnerability of NSCs. It offers a systematic approach to quantifying the potential damage and loss scenarios based on the performance of both structural and non-structural components.

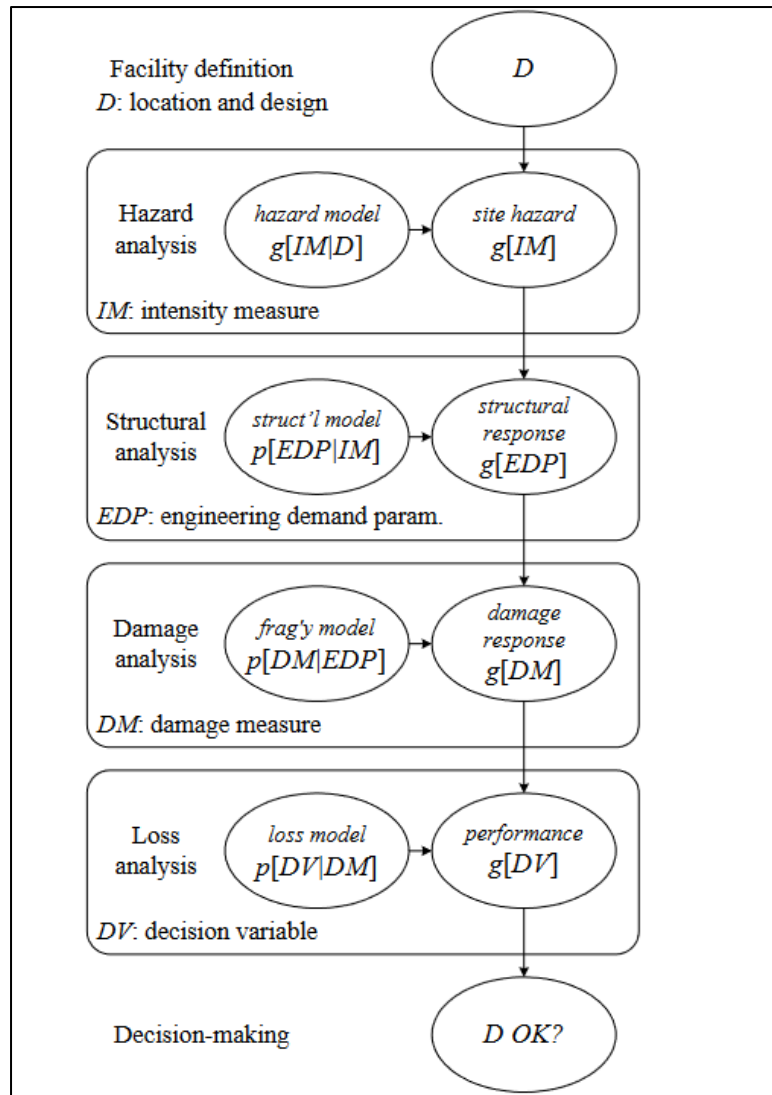


Figure 1.3 PEER approach for PBEE
Taken from Porter (2003)

1.2.1 Hazard analysis

Hazard analysis is the first step in the performance-based analysis which considers site hazard, geotechnical considerations, and ground motion intensities. Earthquake impact can appear by ground shaking, ground fault rupture, liquefaction, lateral spreading, land sliding. Each of these effects may take place within a range of severity, spanning from imperceptible consequences

to substantial damages. Building performance levels for both structural components and NSCs are always assessed at a specified seismic hazard level. Earthquake hazard expresses a quantitative estimation of the intensity of these effects considering the site-specific probability of experiencing the effects of a specific magnitude (FEMA P-58-1, 2018).

The seismic hazard input for structural analysis can be approached using two main methods. The most precise yet demanding approach is nonlinear response history analysis, which entails assessing shaking effects by simultaneously analyzing the response to orthogonal pairs of horizontal ground motion components. These ground motion pairs are appropriately scaled to align with the target response spectrum for the intended ground shaking intensity level. Alternatively, for a more simplified analysis, the shaking can be characterized by spectral response accelerations at the first mode's period along each axis of the structure.

The delineation of earthquake hazards differs based on the approach to performance assessment. In the intensity-based assessments, the ground shaking intensity can be portrayed using a user-defined acceleration response spectrum, such as a designated code design spectrum. On the other hand, in scenario-based assessments, the ground shaking intensity is depicted by acceleration response spectra generated for specific magnitude-distance pairs using attenuation relationships. In the context of time-based assessments, ground-shaking intensity is characterized by a sequence of seismic hazard curves and the corresponding acceleration response spectra derived from these curves, considering selected annual frequencies of exceedance (FEMA, 2018). The National Building Code of Canada seismic hazard tool allows to obtain seismic hazard values for specific sites within Canada, based on different versions of this code (2005, 2010, 2015, and 2020), by entering the site's location. Furthermore, the effect of site class is considered in the obtained values of spectral accelerations, and there is a tab called "site designation" that allows to enter a shear wave velocity or to select a site class.

(<https://earthquakescanada.nrcan.gc.ca/hazard-alea/interpolat/index-en.php>).

Regarding the outputs, the older versions of the tool (2005, 2010, and 2015) provide spectral values for the 2%, 5%, 10%, and 40% probabilities in 50 years. However, the 2020 version offers additional values, including 2.5%, 3.5%, 7%, 14%, 20%, and 30% probabilities in 50 years. These additional values can be useful for assessing the performance of NSCs in different

intensities. Because, even in code-conforming buildings, NSCs often experience damage at lower intensities than the design-based earthquake (2% in 50 years).

1.2.2 Methods of EDP prediction

This section covers the structural analysis methods used to predict EDPs. Commonly employed EDPs include peak floor acceleration, PFA, and inter-story drift ratio, IDR, peak floor velocity, PFV, and residual drift ratio, RDR. These parameters are selected based on the type of NSCs and their sensitivity to evaluate the corresponding damages and losses (FEMA, 2018).

Various methods exist for computing acceleration and displacement demands used in the design of NSCs or for calculating related losses. These methods include simplified formulations provided in different building codes. Moreover, the finite element method can be utilized to model buildings and conduct analyses using different approaches, such as static analysis, response spectrum analysis, and the most accurate one, time history analysis. In this study, the focus is on the evaluation of IDR using simplified analysis in FEMA P-58 (FEMA, 2018), equivalent lateral force procedure of ASCE 7-22 (ASCE, 2022), and equivalent static analysis based on NBC (NRC, 2015) and on the evaluation of PFA using simplified analysis in FEMA P-58 (FEMA, 2018), acceleration height amplification factor of ASCE 7-22 (ASCE, 2022) considering inelastic behavior of building, and elastic acceleration height amplification factor presented in NBC (NRC, 2015). A brief overview of each method is presented in the next sub-sections. The reader is referred to Appendix I, II, and III for full details related to the equations and step-by-step procedures for each method.

1.2.2.1 Simplified analysis based on FEMA P-58

According to FEMA P-58-1 (FEMA P-58, 2018) the simplified analysis based on equivalent lateral force method is valid only for regular, low-rise, and mid-rise buildings to predict IDR and PFA at each floor level. The principal assumptions made in this procedure are as follows:

- Each of the building's horizontal axes has different frame systems with uncoupled response and the effect of torsional response is negligible.

- The building shall be regular in plan and elevation and its height must be less than 15 stories. Moreover, the contribution of higher modes should not be significant.
- Story drift ratios are less than 4 times of the yield drift, and they are limited to 4% (P-delta effect is insignificant), and bilinear elastic-plastic component behavior can be reasonably assumed.

Details of calculations using this method are shown in the Appendix III.

1.2.2.2 Equations proposed in NBC 2015

In order to compute IDR, the distributed lateral forces should be calculated by equivalent static procedure outlined in NBC2015 (Appendix II). These forces can then be applied to a linear static model to obtain floor displacement and story drift ratio, Δ_i .

Finally, to consider inelastic effects, the displacement obtained from equivalent static force procedure, shall be modified by multiplying it by ductility- and overstrength-related force modification factor ($R_d.R_o$), and dividing by importance factor (I_E).

According to the section 5.3.3.1 of the CSA S832-14 (CSA, 2014), all the restraints and connections of operational and functional components (OFC or NSC) must be designed to withstand a minimum amount of lateral force, V_p , which is determined in accordance with NBC Article 4.1.8.18. (Appendix II).

The PFA depends on the spectral acceleration, acceleration-based site class coefficient and horizontal force factor for NSCs which depends on dynamic amplification and response modification factor of NSCs as well as their location along building height. NBC approach consider only the elastic PFA.

1.2.2.3 Equations proposed in ASCE7-22

To estimate the IDR, the distributed lateral forces should be calculated using the equivalent lateral force procedure outlined in ASCE7-22 (Appendix I). These forces can then be applied to a linear static model to obtain the floor displacement and story drift ratio, denoted as Δ_i . Finally, to account for inelastic effects, the displacement obtained from the equivalent lateral

force procedure is modified by multiplying it with the deflection amplification factor (C_d) and dividing it by the importance factor (I_e).

According to Article 13.3.1 of ASCE7-22, non-structural components, with some exceptions based on the seismic design category (SDC), are required to withstand the effects of horizontal seismic design forces, F_p , in the most vulnerable direction. The details of calculation for this force are provided in Appendix I.

This method considers inelastic PFA by taking into account the structure ductility reduction factor. The obtained PFA equals to the product of PGA and height modification factor which also depends on the first modal period of structure and the location of NSCs along building height.

1.2.3 Damage analysis and fragility curve definitions for NSCs

1.2.3.1 Fragility curve definition

The nature and magnitude of damage that a component may undergo is uncertain. Fragility curves are statistical distributions that depict the conditional probability of an undesired event or physical damage occurring at a specific engineering demand parameter (Figure 1.4).

The fragility curves provide valuable insights into the vulnerability of the NSCs and enable a quantitative assessment of the potential damage levels associated with different levels of seismic intensity. These curves can serve as a useful tool for risk assessment, decision-making, and optimizing mitigation strategies for non-structural components in seismic design and even retrofitting processes (FEMA, 2018).

More than 700 fragilities for various structural and non-structural components of buildings are presented in Volume 3 of FEMA P-58 (FEMA, 2018) This volume includes information on damage states, required repair actions, as well as fragility parameters such as median and dispersion for each distribution.

Fragility curves for components can be derived using a variety of approaches, including laboratory testing, gathering data from earthquake events that caused damage, analysis techniques, expert engineering judgment, or a combination of these methods (FEMA, 2018).

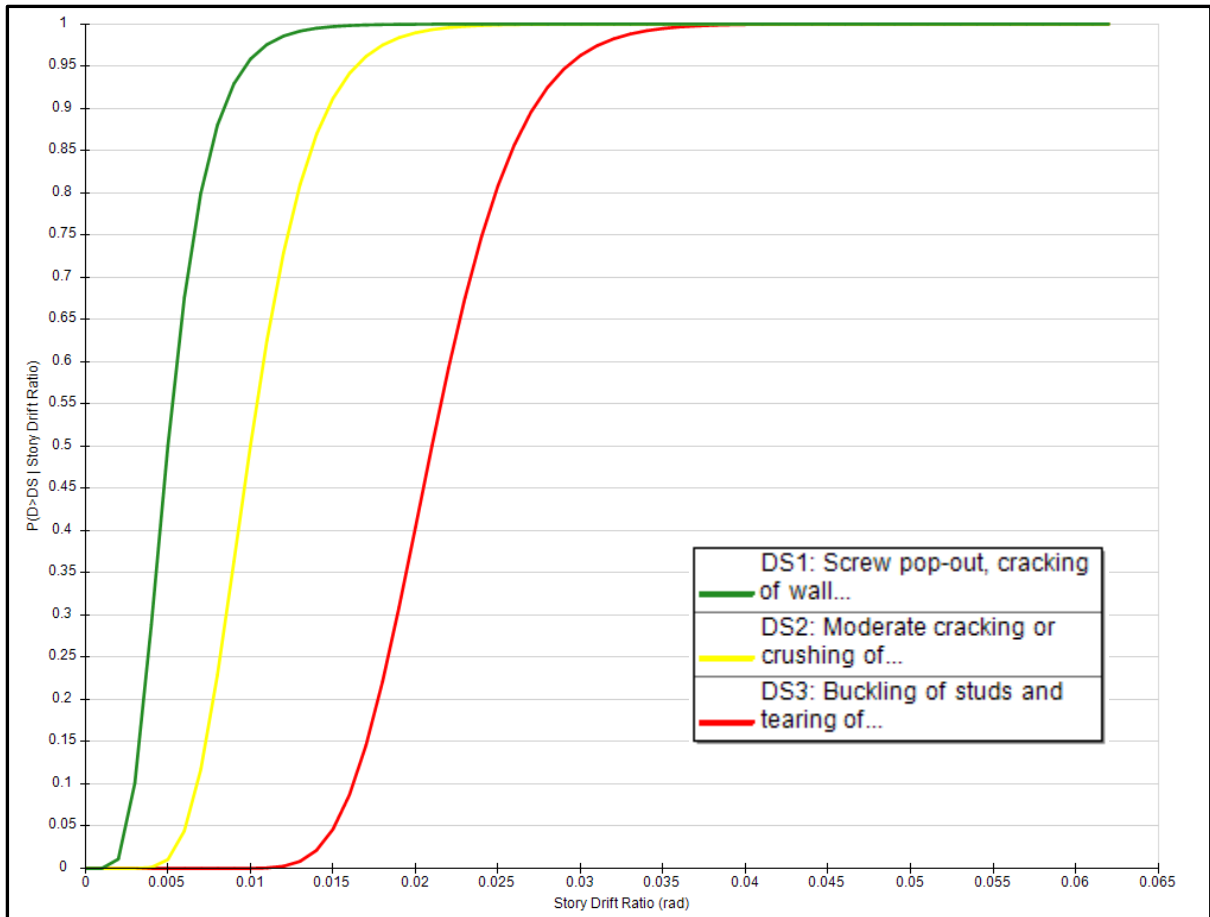


Figure 1.4 Example of the fragility curves for different damage states of a partition wall
Taken from FEMA P-58 (FEMA, 2018)

1.2.3.2 Fragility curves of architectural components

Experimental studies have been conducted in the last two decades with a focus on enhancing our understanding and knowledge of the seismic performance and damage mechanisms of NSCs including damage mitigation solutions to both vertical architectural components such as facades and partitions, and horizontal components such as ceilings (Bianchi et al., 2021).

Technical report MCEER-11-0005 (Davais R. et al., 2011) investigated the seismic performance of cold-framed gypsum partition walls by constructing 50 large scale specimens with 22 various configurations to study both in-plane and out-of-plane behaviour of partition

walls. Figure 1.5 presents typical configuration of partition walls and three typical connections' detailing used in this research to simulate fixed connection and two alternative friction connections in order to study in-plane behaviour of partition walls. For the purpose of fragility analysis, the observed damage during testing was categorized into three damage states, which are defined as follows. The first damage state (DS1) represents superficial damage that can be fixed by cosmetic repairs. DS2 typically occurs at higher drift ratios and involves damage that necessitates the replacement of portions of the partition wall assembly. DS3 is associated with severe damage to the wall assembly, requiring complete removal and replacement of the wall.

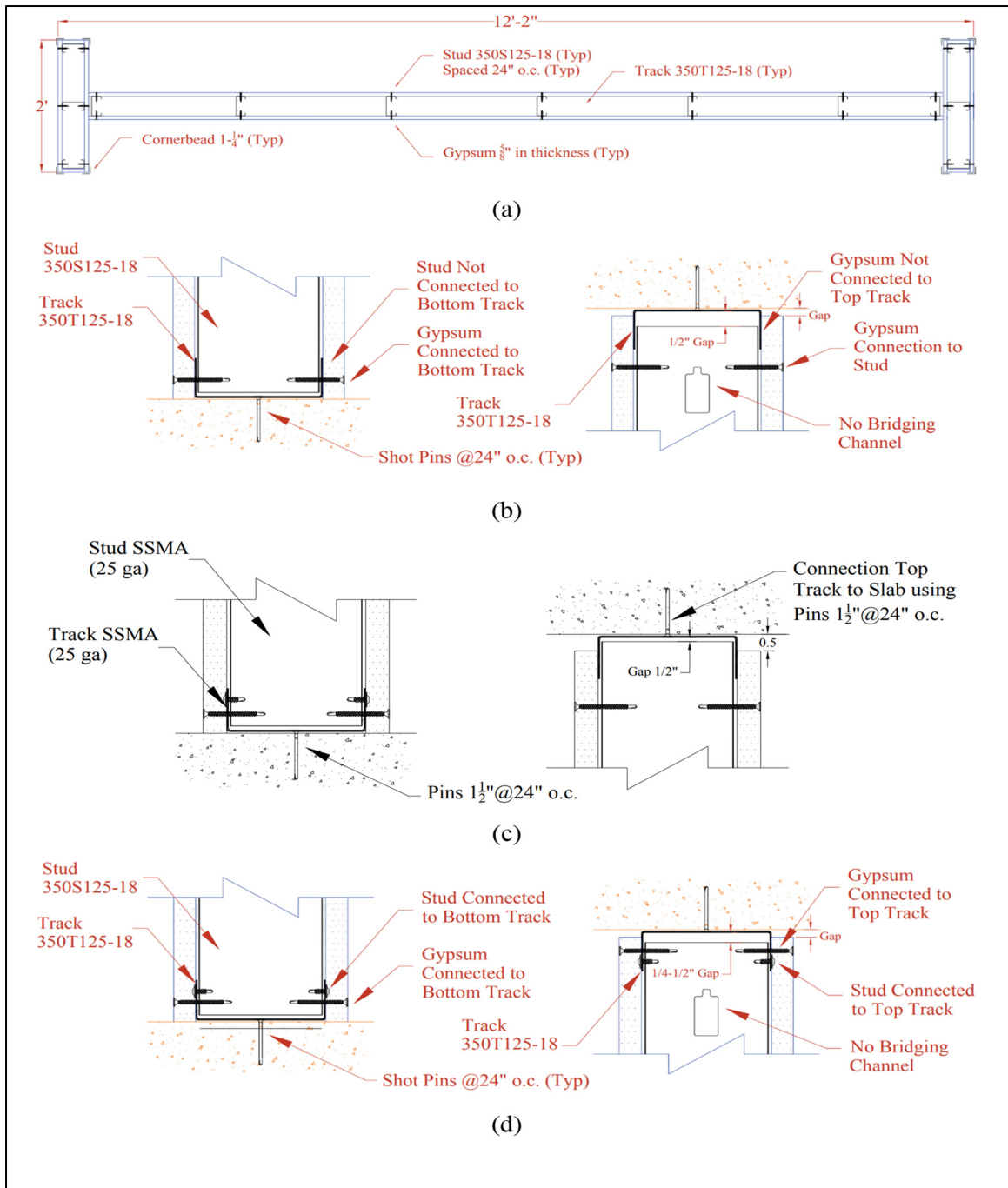


Figure 1.5 Typical gypsum partition walls: a) configuration; b) friction connection, fixed bottom and a slip track at top; c) friction connection with a double slip track (top and bottom); d) full connection (fix at top and bottom)
 Taken from MCEER-11-0005 technical report (2011)

An experimental study on large area suspended ceilings was conducted by Ki P. Ryu et al. (2017). The study aimed to investigate the dynamic behavior of suspended ceiling systems through a series of full-scale shake table tests. These tests were performed on 20 ft × 53 ft and 20 ft × 20 ft ceiling systems at the Structural Engineering and Earthquake Simulation Laboratory (SEESL) at the University at Buffalo (UB). In order to assess the impact of different system conditions and evaluate the effectiveness of various protective systems mandated by the seismic design standard ASTM E580 (ASTM E580, 2014)) on performance of ceiling system, a range of test configurations were chosen. Based on the observations, four main failure mechanism have been detected: (a) failure of perimeter pop rivets, (b) failure of connection in the grid, (c) fallen panels, and (d) complex global system collapse. A set of fragility curves has been generated as a function of PFA (Ryu & Reinhorn, 2017).

Figure 1.6 shows general configuration of an acoustic lay-in panel suspended ceiling, considering the mitigation details such as diagonal bracing and connection detailing to the adjacent walls to improve seismic performance of the system.

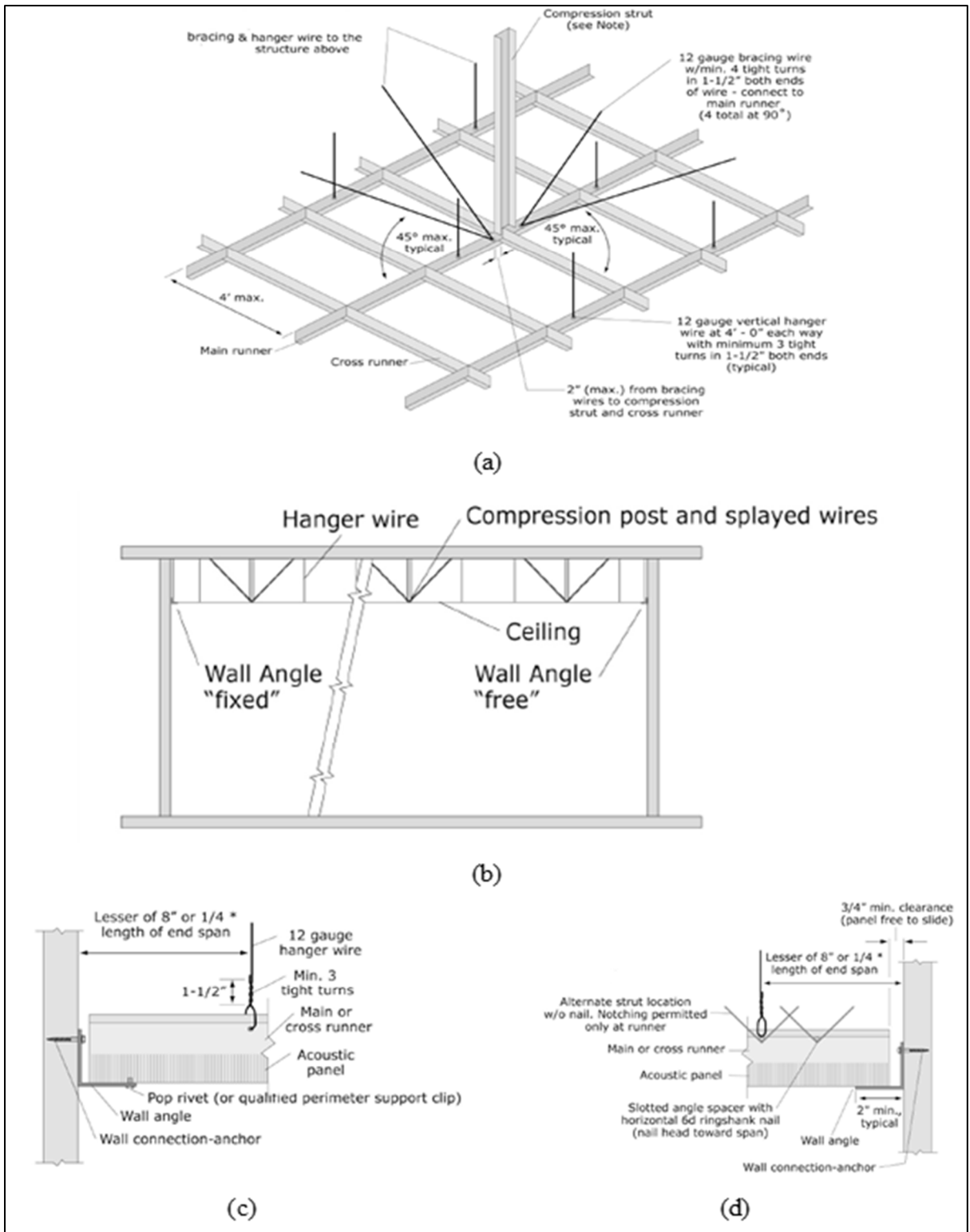


Figure 1.6 Typical acoustic lay-in panel suspended ceilings: a) general configuration; b) transversal section; c) fix connection to adjacent wall; (d) free connection adjacent wall
 Taken from FEMA E-74 (2012)

The effect of different parameters on the in-plane dynamic performance and failure mechanism of the curtain walls have been assessed by means of racking cyclic tests and shake table tests (Memari et al. 2004; Weggel et al. 2007; Memari 2011; Sivanerupan et al. 2014; Arifin et al. 2020; Lu et al. 2016, 2017; Bianchi et al. 2021). In all these studies, altering the connection details, leads to variations in the derived fragility curves (Bianchi et al., 2022). The damage states of glazing can be classified into four groups, (1) glass cracking, (2) glass fallout, (3) gasket seal degradation, and (4) damage to glazing frame (FEMA P-58-3, 2018). Figure 1.7 shows the detailing of a glazing curtain wall. The most common proposed mitigation measures to improve the performance of glazing can be enumerated as (1) using safety glasses like tempered glazing which break into small dull parts instead of large shards, or laminated glazing which reduce the hazards by remaining in place, even after breaking, (2) increasing the clearance between glass and frame which prevent imposing the frame deflection directly to the glass edges.

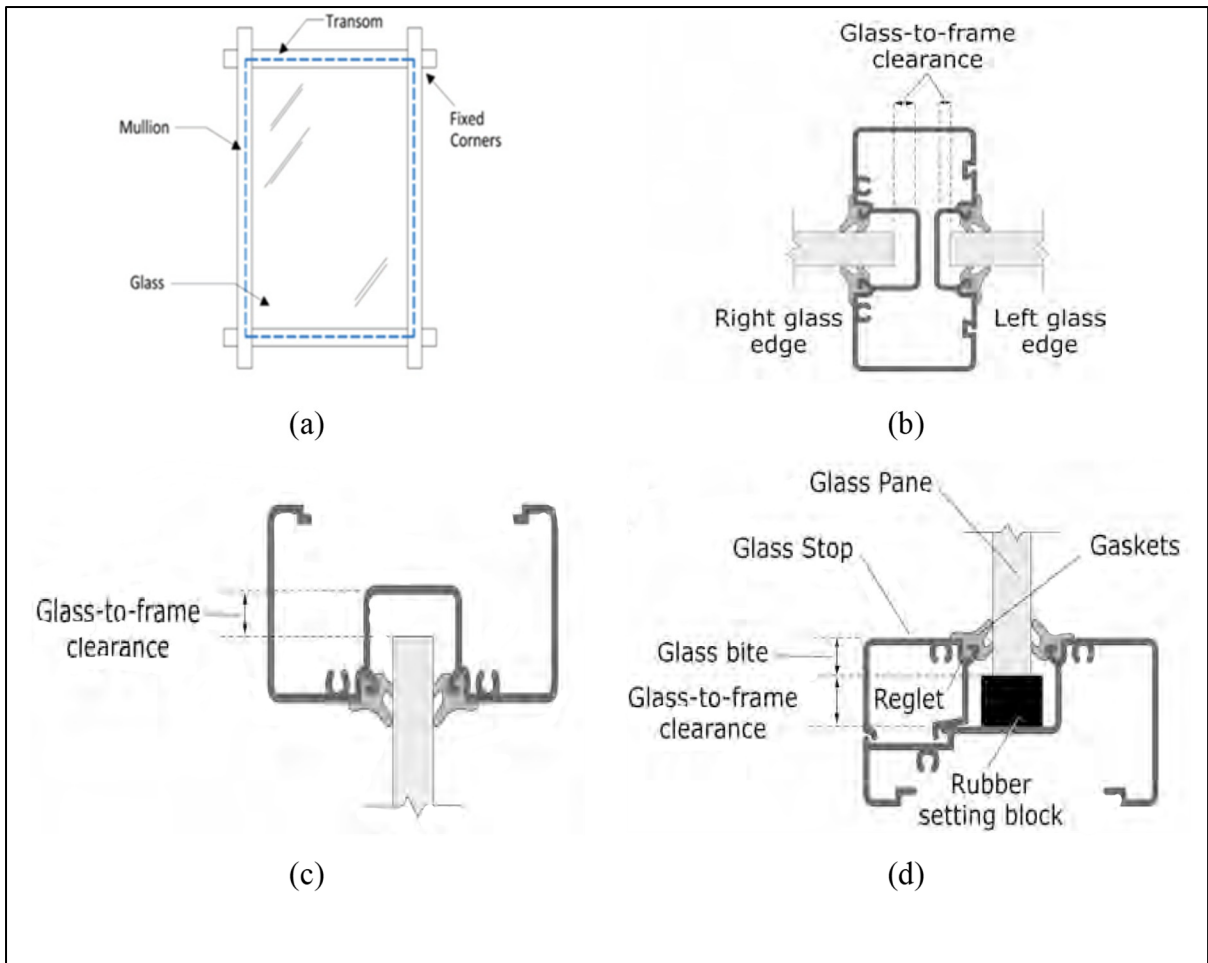


Figure 1.7 Typical curtain wall: a) glass and frame configuration; b) Mullion section and connection detailing; c) Transom head and connection detailing; d) Transom sill and connection detailing

Taken from FEMA E-74 (2012)

1.3 Loss estimation and consequences functions

1.3.1. Loss estimation

According to FEMA P-58, the following procedure can be followed to calculate the performance and estimate the repair cost of NSCs (Figure 1.8). In this methodology, the probability of a particular damage state occurring for each Performance Group (PG) is calculated using a fragility curve and based on the value of an EDP. Subsequently, the repair

cost of each PG can be calculated using the corresponding consequence function for the determined damage state. (Zeng et al., 2016)

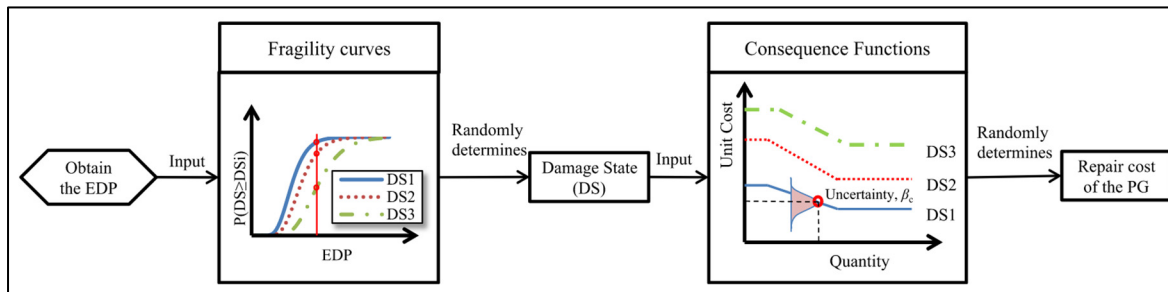


Figure 1.8 Calculation of a repair cost for a PG
Taken from Zeng et al. (2016)

Consequence functions are mathematical representations revealing how losses may be distributed in relation to the level of damage incurred. The repair cost consequence functions convert damage into estimations of potential repairs and replacements cost. To explain the above procedure a numerical example has been provided in Appendix V.

1.3.2. Previous studies on loss estimation

Several research have been done during recent years to calculate the building total loss. Majdi (2020) conducted a study to assess the expected losses, including economic and social aspects, for concrete buildings with moment-resisting frames at Al-Hillah City, Iraq. Engineering demand parameters were computed using dynamic time history analysis with twelve ground motion records with PGA values ranging from 0.14g to 0.7g. The study evaluated performance and losses using a probabilistic approach based on FEMA-P58 and PACT (FEMA, 2018). These losses were quantified in terms of repair time, repair costs, and casualties. The worst-case scenario was considered for each intensity level, and the corresponding performance level was determined for both horizontal directions. The findings indicate that wall partitions are more vulnerable and prone to losses, including potential collapse, across various intensity levels. The study also identified that upper floors and wall partitions require the most extensive repairs (Majdi, 2020).

Xiang Zeng et al. (2016) conducted a case study at Tsinghua University campus in Beijing to evaluate seismic vulnerability. The authors employed FEMA P-58 methodology to assess the

fragility of both structural and non-structural components. The researchers utilized field inspections and design drawings to gather building data as well as information on structural and non-structural components. Detailed loss assessments were carried out on two demonstration buildings at three different hazard levels: SLE (Service Level Earthquake), DBE (Design Basis Earthquake), and MCE (Maximum Credible Earthquake). The study concluded that at lower hazard levels, earthquake losses were primarily attributed to repair costs of NSCs. However, as the hazard level increased, the cost of replacing irreparable building's components also increased. The percentage of loss due to building collapse remained relatively low. Architectural components, such as exterior walls, partitions, wall finishes, and ceiling systems, accounted for a significant portion of losses, with a predicted loss ratio of 35% (defined as the repair cost to replacement cost ratio) for MCE intensity (Zeng et al., 2016).

Ni et al. (2018) conducted a comparative study on the performance of non-structural components in two different tall buildings subjected to (SLE), (DBE), and (MCE). The first building, a 37-story structure, is located in a moderate seismic zone in Bangkok, while the second building, a 50-story structure, is situated in a high seismic zone in Manila.

The study assessed direct economic and social losses, as well as downtime and business interruption losses, using both FEMA P-58 default normative database and actual quantities of components. The findings reveal that non-structural damage in both buildings occurs under MCE events. However, in the moderate seismic zone, damage is predominantly associated with drift-sensitive components on multiple floors, while in the high seismic zone, acceleration-sensitive and velocity-sensitive components play a more significant role in overall losses. For the first building, the damage ratio (defined as number of damaged components divided by total number of components in a performance group) of architectural components ranged from 2.7% to 4.7%. In the case of the second building, their damage ratio was found to be between 3.5% and 11%. Furthermore, in the 37-story building, architectural components contribute significantly to damage at all hazard levels. In contrast, in the 50-story building, the contents of the building have a notable impact on total losses, especially at higher hazard levels. The study also identifies that downtime results in business interruption, and the loss incurred due to business interruption is significantly higher than the direct economic loss. Therefore, reducing downtime is crucial to mitigating business interruption losses (Ni et al., 2018).

1.4 Summary

This chapter discussed the importance of NSCs and their contribution to building economic loss. It provided a detailed explanation of the performance-based assessment framework, reviewing each step of the procedure, including hazard analysis, structural analysis, damage analysis, and loss analysis.

By examining previous studies, it is evident that numerous investigations have been conducted on calculating engineering demand parameters (EDPs), developing fragility curves, and analyzing the damage of NSCs with different types of connections to the structure. Additionally, researchers have estimated losses resulting from earthquake events. However, it should be noted that limited research has specifically determined the exact extent of loss reduction achieved through the implementation of seismically improved connections. The issue is addressed in this thesis by conducting quantitative analysis on the impact of connection details on seismic induced repair cost of selected architectural components.

CHAPTER 2

ASSESSMENT OF INFLUENCE OF EDP PREDICTION METHOD ON INDUCED REPAIR COST OF ARCHITECTURAL COMPONENTS

In this chapter, a detailed description of the selected case study building, the 3D static modelling, and ground motion characteristic are provided. Then, to quantify the sensitivity of repair cost of architectural components to the EDP prediction method, a comparative assessment was conducted using different simplified EDP prediction methods, including FEMA-P58 (FEMA, 2018), ASCE 7-22 (ASCE, 2022), and NBC2015 (NRC, 2015) standardized procedures.

2.1 Description of the case study building

2.1.1 Building information

A 12-storey reinforced concrete office building located in Montreal on site Class D, has been selected with corresponding plan and elevation views as presented in Figure 2.1. This building was previously analyzed and designed in chapter 11 of the 4th edition of concrete design handbook (CHD, 2016). The lateral load resisting system consists of a central elevator core composed two C-shaped 400 mm thick concrete shear walls connected by 400 mm wide x 1000 mm deep coupling beam at the ceiling level of each floor and surrounded by the same size 550x550 mm columns and 200 mm thick slabs at each floor as the gravity load bearing system. The core walls extend from the top floor level and make an elevator penthouse at the level of 48.65m. The height of ground floor is 4.85m and the height of all the above floors equals to 3.65m. The total area of each floor is 900 square meters (Figure 2.1).

The seismic force resisting system (SFRS) in X-direction is ductile coupled wall, which implies that a minimum of two-thirds of the base overturning moment, which is resisted by the wall system, must be carried by axial tension and compression within the coupled walls. Shear cracking and bar buckling must not occur in coupling beams and their moderately ductile

detailing make them capable of flexural hinging or effectively withstanding loads through diagonal reinforcement. The walls must exhibit sufficient resistance to enable the achievement of the nominal strength in the coupling beams, as well as meet the required minimum level of ductility. While the SRFS in Y-direction is ductile shear walls in which walls should demonstrate the ability to undergo flexural yielding without experiencing local instability, shear failure, or bar buckling. Additionally, the walls must meet the criteria for ductile detailing (CDH, 2016).

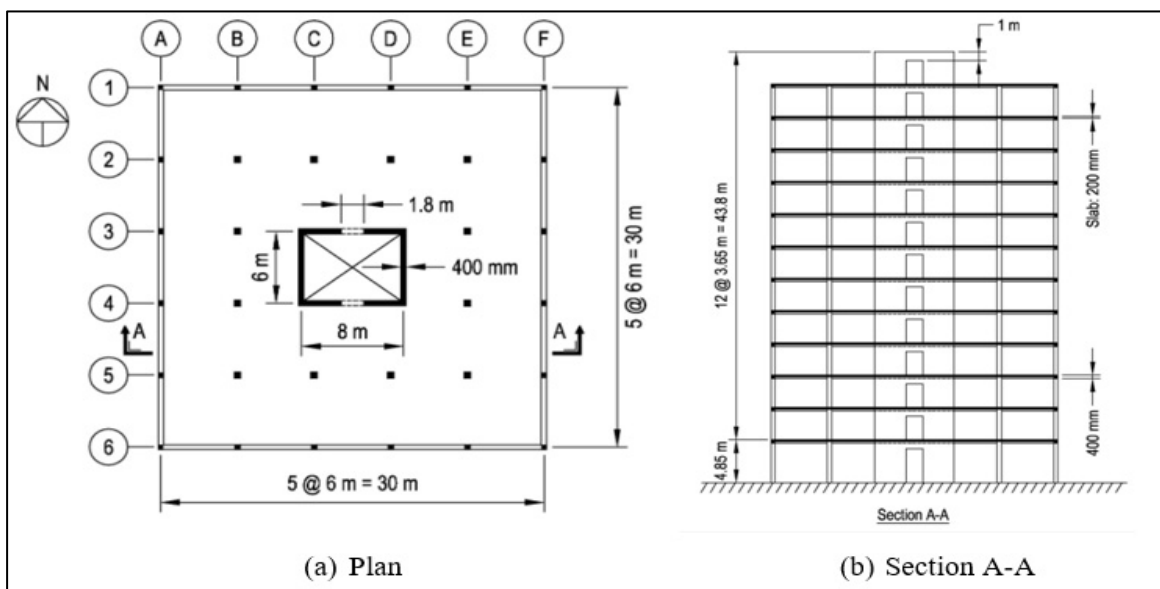


Figure 2.1 Plan and elevation of the 12-storey office building
Taken from Concrete design handbook (2016)

2.1.2 Description of input ground motions

This study incorporated ground motion input for structural analysis by utilizing the 5% damped response spectra of Montreal, based on site class D. These response spectra were obtained from the National building Code of Canada seismic hazard calculation tool (NRC, 2015) to be able to compare the predicted EDPs with previous studies conducted on the same building. The following response spectrum have been used for seismic analysis of this structure under three return periods of 40% in the 50 years (frequent earthquake), 10% in the 50 years (occasional earthquake), and 2% in the 50 years (very rare earthquake) which is the current NBC seismic

design intensity level (Figure 2.2). Furthermore, the spectral values are represented in Table 2.1.

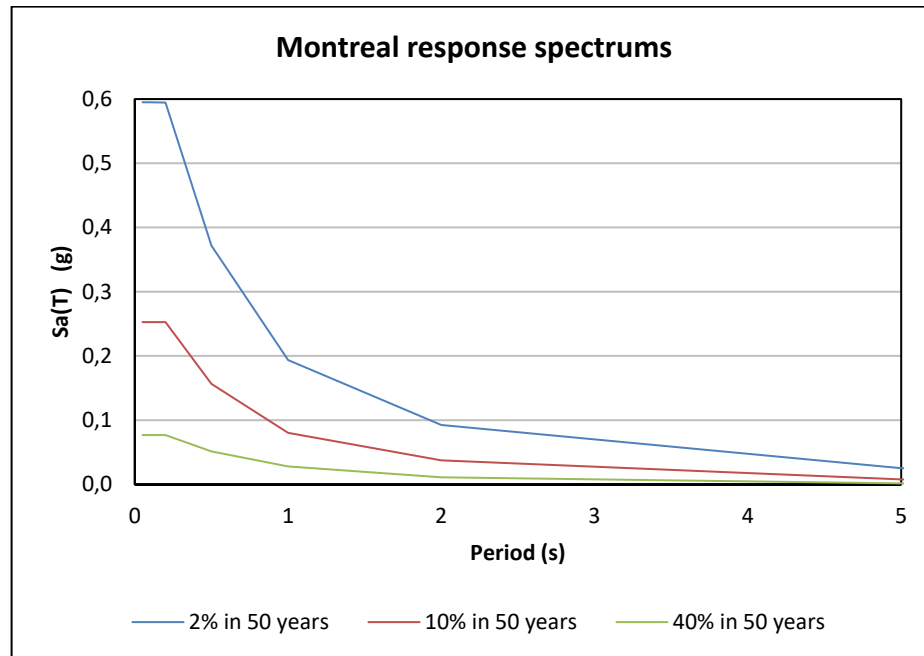


Figure 2.2 Montreal 5% damped response spectrum used in this section based on the NBC 2015 seismic hazard values

Table 2.1 Spectral values associated with 5% damped response spectra

probability	Modified Sa(T)		
	2% in 50 years	10% in 50 years	40% in 50 years
MAFE	0.000404	0.0021	0.01
$S_a(0.05)$	0.595	0.253	0.077
$S_a(0.1)$	0.595	0.253	0.077
$S_a(0.2)$	0.594	0.253	0.077
$S_a(0.5)$	0.372	0.156	0.051
$S_a(1.0)$	0.194	0.080	0.028
$S_a(2.0)$	0.092	0.038	0.011
$S_a(5.0)$	0.025	0.008	0.002
$S_a(10.0)$	0.008	0.003	0.001

2.1.3 Selected architectural components

The selected architectural components to conduct this study are partition walls (PW), suspended ceilings (SC), and curtain walls (CS), because they are typically found in most of the commercial buildings. PWs are non-load-bearing interior walls used to divide vast open rooms into smaller and more functional and usable spaces. Cold-framed steel framing with gypsum sheathing is most frequently used in the construction of commercial structures because of lower weight and constant moisture compared to wood framing PW (FEMA P-58/BD-3.9.2, 2011).

Ceiling systems are considered as highly susceptible to damages in contemporary buildings when it comes to seismic events (Dhakal, 2010). Suspended ceilings are composed of four main components: hanger rods, main beams, cross beams, and acoustical tiles. The hanger rods and wires hang from the floor slab above, providing support (vertically, diagonally, or both) for the main and cross beams. The ceiling tiles are simply placed on top of the beams and are not affixed permanently (Davidson et al., 2019). Previous research revealed that the principal concerns associated with the failure of SCs include dropping acoustical tiles, perimeter damage, separation of runners and cross runners, and the potential hazard of falling grid and lights, especially in case of heavy SCs (FEMA E-74, 2012).

Building facades are typically divided into two categories: heavy and light facades. The failure of facades can endanger life safety, as well as imposing serious financial losses in terms of repair cost (Biard et al., 2011). Curtain walls (CW) are a specific type of facade system that is typically composed of lightweight non-structural glass or metal panels that are attached to the building's structural frame (Kubba, 2012).

In this study, the quantity of architectural components on each floor has been estimated using Normative Quantity Estimation tool presented in the appendix D of FEMA P-58-2 user manual (FEMA, 2018). This tool is an Excel spreadsheet which requires building information, including the number, area, and occupancy of floors in order to calculate the quantity of each NSC on a gross square foot (gsf) basis. Table 2.2 presents the quantities utilized in this study, considering a consistent distribution of architectural components across all floors.

Table 2.2 Estimated quantity for selected architectural components based on FEAM P-58- Normative quantity estimation tool

Architectural components	Assumed Quantity per component	Quantity		Fragility Quantity Disperssion
		Directional	Non-directional	
Partition Wall	100 LF	9.688	--	0.2
Suspended Ceiling	1800 SF	--	4.844	0.0
Curtain Wall	30 SF	96.880	--	0.6

PWs and CWs are drift-sensitive, and they are generally aligned with principal orthogonal axes of building, therefore, their performance calculation is influenced by directionality. On the other hand, the failure of acceleration-sensitive components like SCs are not usually sensitive to the direction of the applied demand (PFA) and the estimated quantity can be considered as non-directional (FEMA P-58, 2018).

The assumed quantity per component in the normative quantity estimation tool represents the unit measure for each performance group. For instance, the unit measure for PW is 100 linear feet (LF), and the calculated quantity is 9.688. Consequently, the actual total quantity of partition walls on each floor is calculated as $100 \times 9.688 = 968.8$ LF. Similarly, the actual quantities for SC and CW are determined to be 8719.2 and 2906.4 square feet (SF), respectively.

The dispersions presented in Table 2.2 illustrate the level of uncertainty in approximating the quantity of architectural components. The estimated quantities of partition walls and curtain walls strongly depend on architectural drawings and can vary based on the specific architectural design. Conversely, the quantity of suspended ceilings is primarily determined by the area of the slab, enabling a more precise calculation with zero associated dispersion.

2.1.4 Estimated repair costs

The repair cost is defined as sum of all the costs which are required to restore a pre-earthquake condition of a building. In case of total loss, this cost will be equivalent with total replacement cost of the building (FEMA P-58, 2018). Based on the building information and the estimated quantity for NSCs, the total replacement cost of the building and the maximum possible repair

cost of each NSC under study have been determined and presented in table 2.3. PACT does not directly provide the total replacement cost for the building which is considered as total repair cost in case of collapse. The total replacement cost of the building was estimated by scaling the calculated cost provided in the example given in FEMA P-58/SD-3.7.16 at a reference time (2011). The estimation was adjusted proportionally based on the total area of the buildings (number of stories multiplied by the area of each story), taking into consideration the currency exchange rate (1.33) and inflation rate (1.18, data source: data.worldbank.org). Furthermore, while considering the same exchange rate and inflation rate, the maximum possible repair cost of each NSC is calculated by imposing significantly large EDPs in the PACT software. This is done to simulate the collapse of the building, resulting in a complete loss of all components. Once structural collapse occurs, further increases in intensity will not affect the repair cost. Consequently, the corresponding repair cost for each component would be equal to its maximum possible repair cost (Figure 2.3). It should be noted that to determine a more precise amount and establish the collapse threshold, a nonlinear static pushover and time history analyses would be required. However, conducting such analysis is beyond the scope of this study.

Table 2.3 Assumed total replacement costs of building and selected components

Item	Cost explanation	Cost (Can \$)
Building	total replacement cost	51 million
Partition Walls	maximum possible repair cost	3,56 million (6.9%)
Suspended Ceilings	maximum possible repair cost	4,05 million (7.9%)
Curtain Walls	maximum possible repair cost	6,03 million (11.7%)

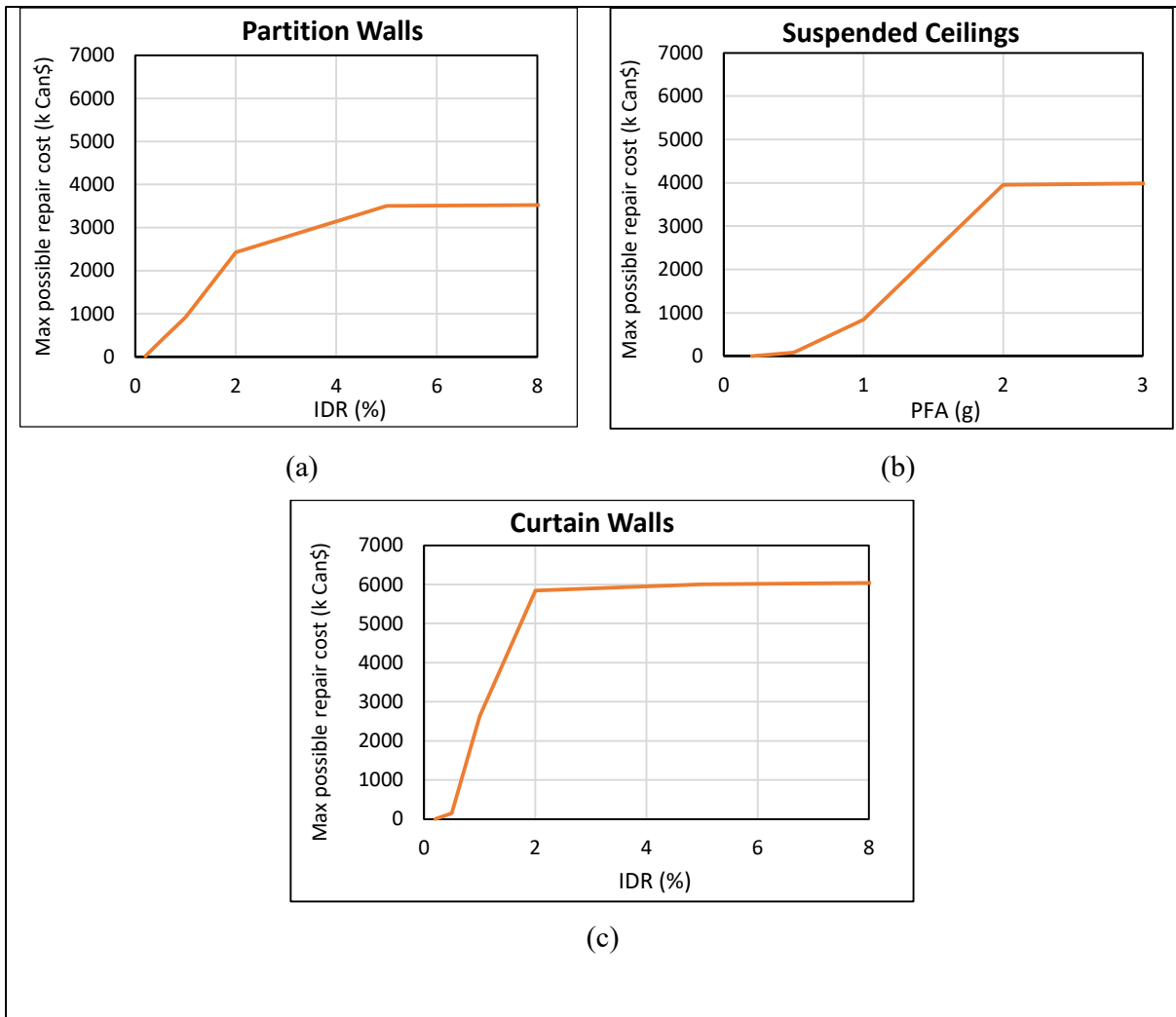


Figure 2.3 Maximum possible repair cost: a) Partition Walls; b) Suspended Ceilings; c) Curtain Walls

2.2 Finite element modelling of the building

As it is illustrated in chapter one, estimating the IDR with all introduced methods requires the development of a linear static model. Therefore, a 3D finite element model of the shear wall core of the building is created using SAP 2000 (CSI-SAP2000, V 21.1.0). The model is developed based on the assumptions outlined in 4th edition of the concrete design handbook CDH published by Cement Association of Canada (2016).

To consider cracked concrete sections allowance, the effect of cracking is simulated by defining stiffness modification factors, the coupling beams are assumed to have an effective

stiffness of 0.25 times the gross moment of inertia ($0.25I_g$) and 0.45 times the gross shear area ($0.45A_g$). In addition, the shear walls are considered to have an effective flexural stiffness of 0.5 times the flexural rigidity ($0.5EI_g$) and an effective axial stiffness of 0.5 times the axial rigidity ($0.5EA_g$). Normal density concrete with a characteristic strength of $f'_c=30\text{MPa}$ and reinforcement with yield strength of $F_y=400\text{ MPa}$ are utilized in this analysis.

For the verification of the finite element model (FEM), the periods of vibrations $T(\text{s})$ (Figure 2.4) and modal mass participation ratios $U_x\%$ and $U_y\%$ are compared with the results of the concrete design handbook (CDH, 2016). As it is shown in Table 2.4, the maximum difference observed in the periods is about 10%.

Table 2.4 Comparison of the periods obtained from FEM model with the values in the CDH (2016)

mode	Concrete Design Handbook			SAP 2000			Difference %		
	T(s)	$U_x\%$	$U_y\%$	T(s)	$U_x\%$	$U_y\%$	T(s)	$U_x\%$	$U_y\%$
1	2.169	0.000	0.670	2.151	0.000	0.649	-0.81	0.00	-3.14
2	1.935	0.710	0.000	1.852	0.699	0.000	-4.27	-1.61	0.00
3	0.485	0.180	0.000	0.455	0.184	0.000	-6.20	2.03	0.00
4	0.402	0.000	0.220	0.387	0.000	0.208	-3.83	0.00	-5.68
5	0.233	0.050	0.000	0.208	0.048	0.000	-10.55	-4.60	0.00
6	0.170	0.000	0.070	0.158	0.000	0.069	-6.77	0.00	-1.43

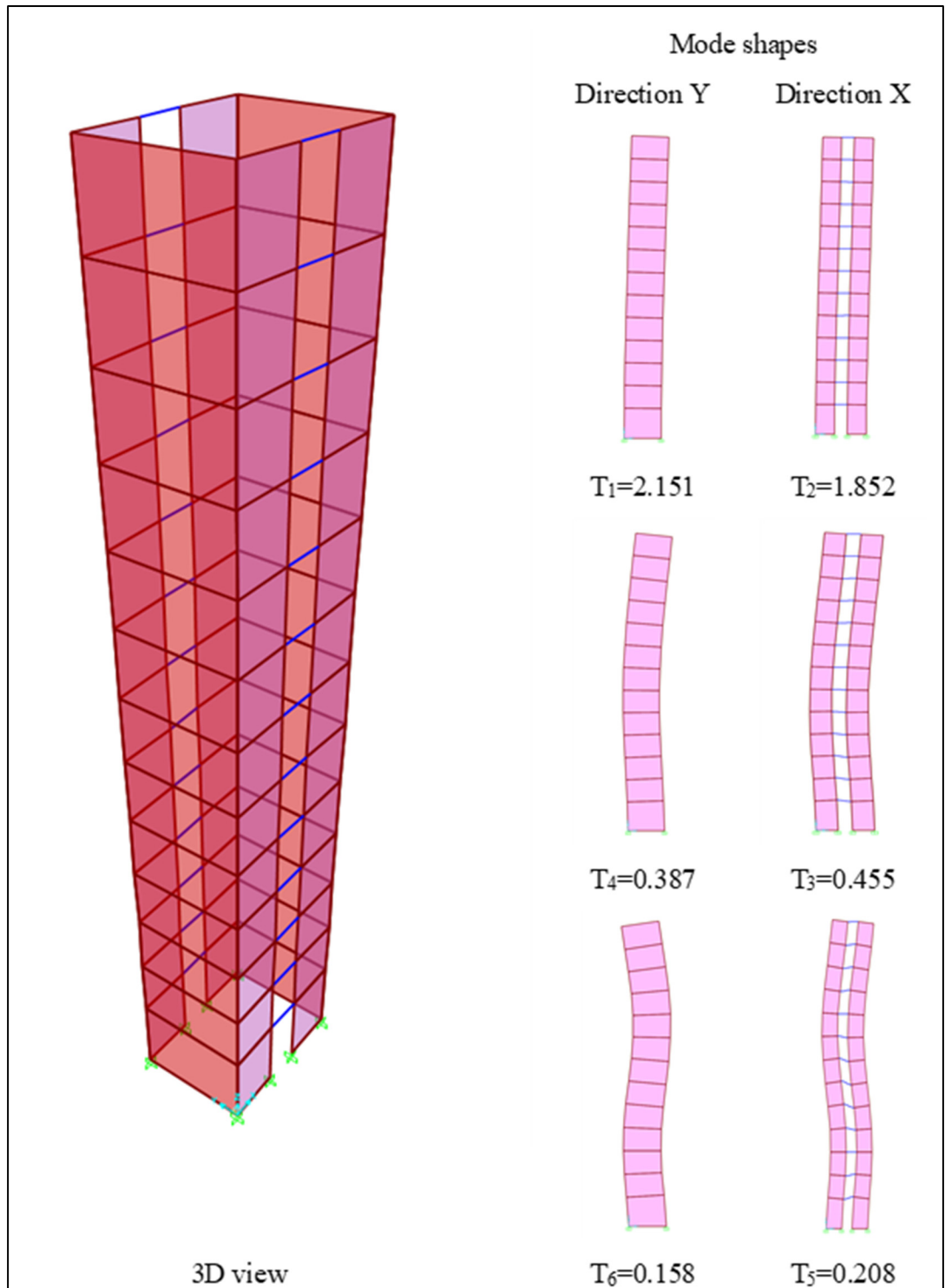


Figure 2.4 Obtained mode shapes and corresponding lateral periods of vibrations from SAP 2000 model

The second step for verification is to control the base shear with the calculated amount in the reference. The values are compatible, especially in the Y-direction (Table 2.5).

Table 2.5 Comparison of base shears obtained from FEM model and the values provided in CDH (2016) in both principal directions

Direction	Base Shear (kN) 2% in 50 years		
	SAP2000	handbook	Difference (%)
X-direction	1472	1365	7.87
Y-direction	1920	1936	-0.82

2.3 EDPs comparison

2.3.1 IDR comparison

2.3.1.1 Comparison of IDR obtained from different methods

Figure 2.5 depicts the estimated IDR due to earthquakes with the 40%, 10%, and 2% probability of exceedance, as the response spectra are presented in section 2.1.2., using different methods, namely FEMA-P58 simplified analysis, ASCE 7-22 equivalent lateral force procedure, and NBC-2015 equivalent static procedure. The details related to the procedures and equations used in these methods are presented in Appendices I, II and III.

As observed in Figure 2.5, the values of IDR associated with FEMA P-58 methodology are lower than other methods. Equivalent static analysis, whether based on NBC or ASCE7 standards, are often designed to be more conservative to ensure margin of safety. These methods overestimate the seismic forces and resulting drifts compared to more advanced analysis methods. FEMA P-58, even in simplified analysis, better captures the nonlinearity effect by taking it into account in both calculation of lateral force and drift modification factor by incorporating adjusting factors for inelastic response and cycling degradation and first mode response estimated yield strength. FEMA P-58 equations are based on statistical regression of hundreds of nonlinear dynamic analyses of building models and therefore expected to produce improved prediction of EDPs. Even in FEMA P-58 simplified analysis the EDPs are adjusted

by uncertainties in ground motion intensity, modeling, and computed displacement and acceleration.

As the seismic intensity increases, there is a notable upward trend in the calculated IDR. Furthermore, evaluating the IDR along building height reveals its variation is usually increasing except a slight decrease in upper floors, particularly in direction X. The extent of EDPs in the Y direction is greater than in the X direction, as expected due to the lower response modification coefficient for ductile shear walls compared to ductile coupled walls.

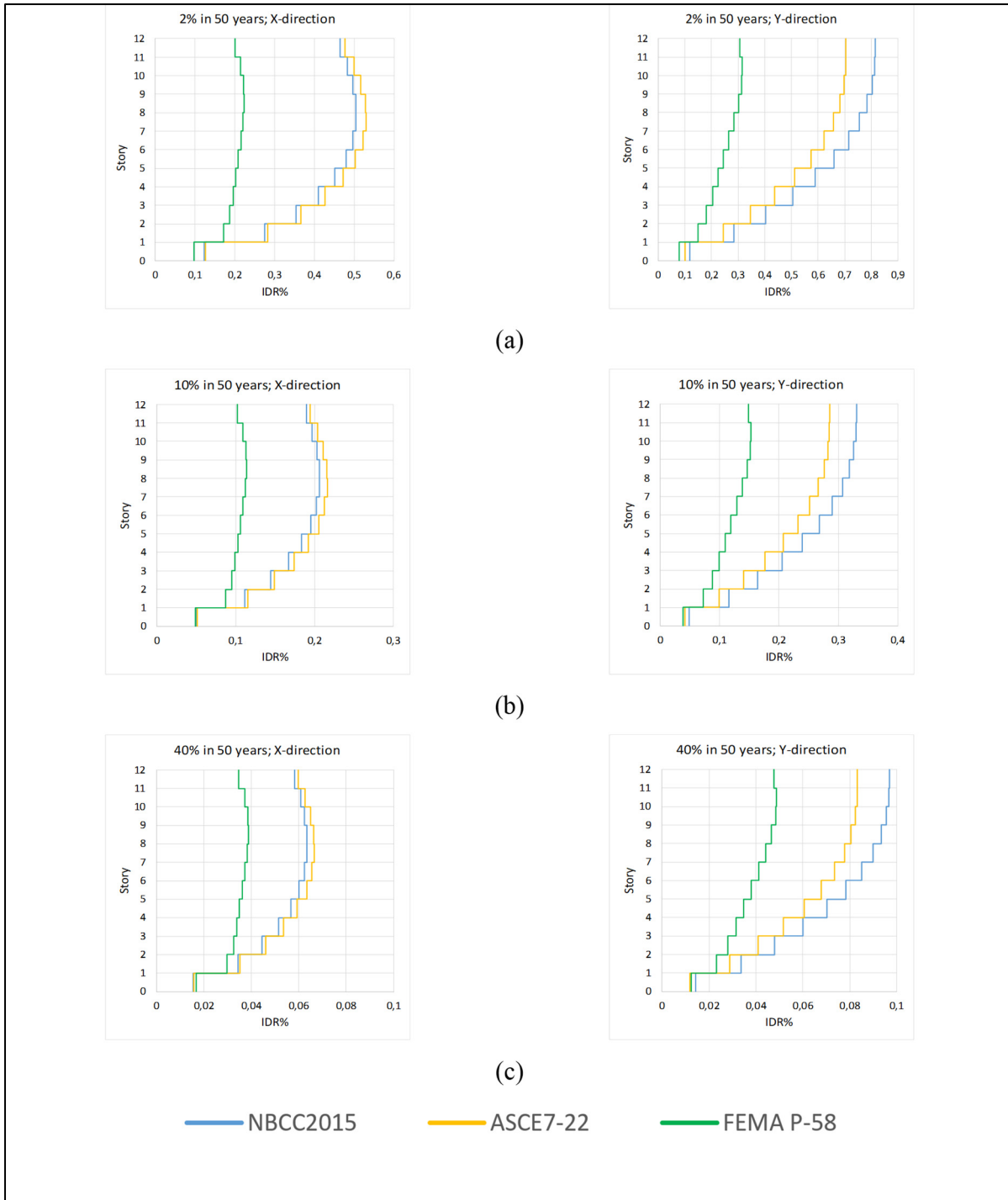


Figure 2.5 Estimated IDR using three different methods due to increasing earthquakes intensities

2.3.1.2 Validation of IDR results with previous studies

To validate the above calculation, the study conducted by Boivin (2006) has been used, as it is shown in Figure 2.6, the IDR results from FEMA P-58 simplified analysis and the inelastic time-history analysis provided by Boivin on a 2D cantilever shear wall model are almost close, and the IDR demand with these methods are considerably lower than the design IDR calculated by other utilised methods. As it is shown in appendix III, in the FEMA P-58 simplified analysis, the effect of inelastic behavior of structure has been taken into account in the calculation of both lateral force and the drift modification factor, for this reason the results are closer to the former conducted nonlinear analysis (Boivin, 2006).

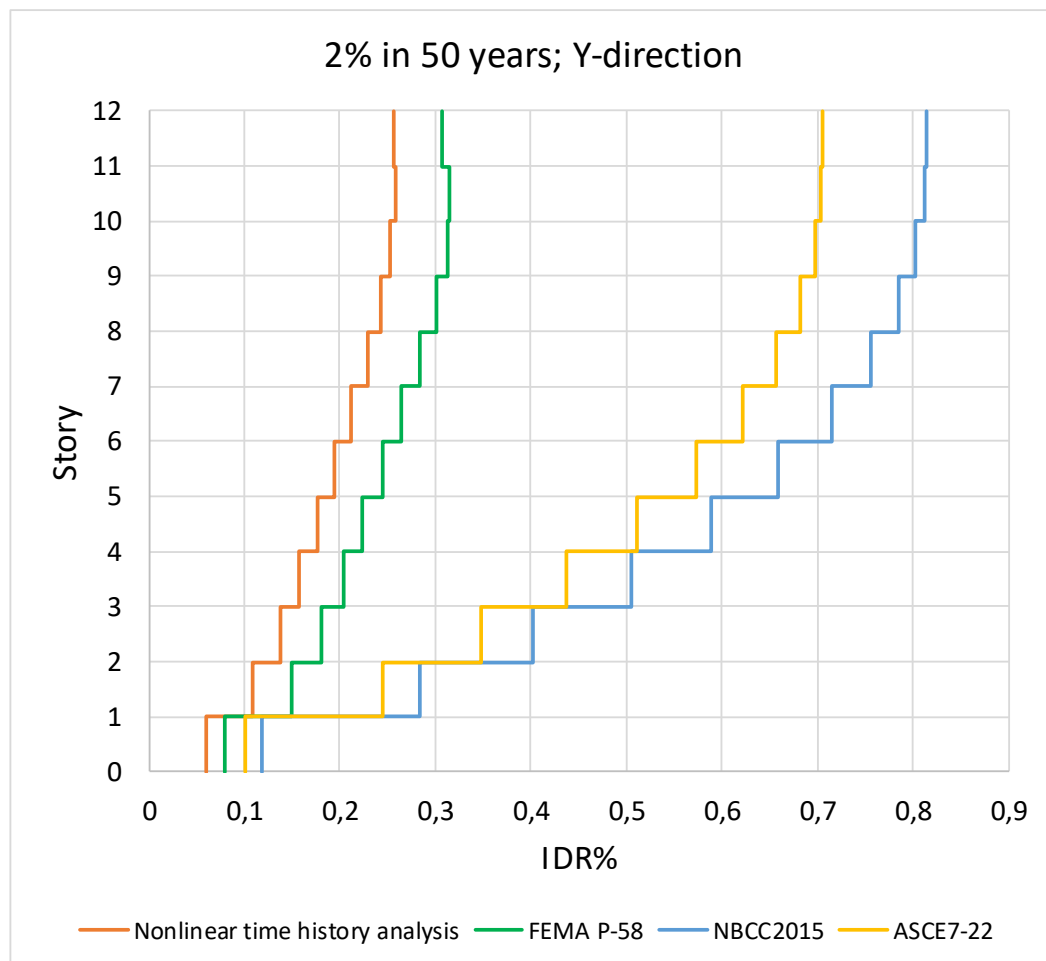


Figure 2.6 Verification of calculated IDR with previous study

In order to validate the prediction of the NBC2015 method, the maximum IDR reported in the concrete design handbook for the 2% in 50 years ground motion intensity were compared with the analyses conducted in this study. The maximum IDR calculated in concrete design handbook, 4th edition, for the directions X and Y are 0.54%, and 0.67%, respectively. These values have been calculated in this study by NBC 2015 method and are equal to 0.50% and 0.81%, respectively. And all these anticipated maximum IDRs are less than NBC limit of 2.5%. The difference between results for the direction X is 7.4% and for the direction Y is 17.2%. Table 2.6 compares the maximum IDR of the building in Y-direction predicted by each four utilised methods in this study with the computed inelastic seismic responses obtained from nonlinear analysis provided by Boivin (2006). It is assumed that nonlinear time history results can be considered as a reference for accuracy. Therefore, the results demonstrated that for this case study building, the FEMA P58 predicted the lowest deviation compared to nonlinear dynamic analysis.

Table 2.6 Comparison and validation of maximum IDR predicted by the three selected methods

Method	Maximum IDR (%) 2% in 50 years	Difference (%) compared to nonlinear analysis
NBC 2015	0.81	68.09
ASCE7-22	0.70	63.09
FEMA P-58	0.31	17.38
Dynamic analysis Boivin (2006)	0.26	0.00

2.3.2 PFA comparison:

2.3.2.1 Comparison of PFA obtained from different methods

Figure 2.7 plots the value of PFA/PGA ratio over height of the building. This value varies in each method differently, it is a straight line in NBC2015, which corresponds to the value of the height factor (A_x), which varies from 1 to 3. For the ASCE7-22, PFA changes as a function of the force amplification factor (H_f) which depends to the lowest fundamental period of

structures in the principal direction as well as height. For structures with the period less than 0.4, it would be straight line which varies between 1 to 3.5, and for the higher periods it would follow a non-linear equation that allows (z/H) to be exponents by the order of 10. The other factor that is effective in the calculation of PFA by ASCE 7-22 is structure ductility reduction factor (R_μ), which depends on building response modification factor (R) and building overstrength factor (Ω_0) and take into account, in approximate manner, the nonlinear response of the structure.

Moreover, the values obtained from FEMA P-58 follow an S-shaped pattern. These values are lower than the PFA calculated by the linear acceleration profile of NBC, especially for higher intensities and upper stories. They are closer to the results of the ASCE 7-22 inelastic profile, and the non-linear analysis provided in previous studies.

In the case study building, the S-shaped acceleration pattern indicates lower PFA at the floors located in the middle third of the building height, as opposed to the lower and upper thirds.

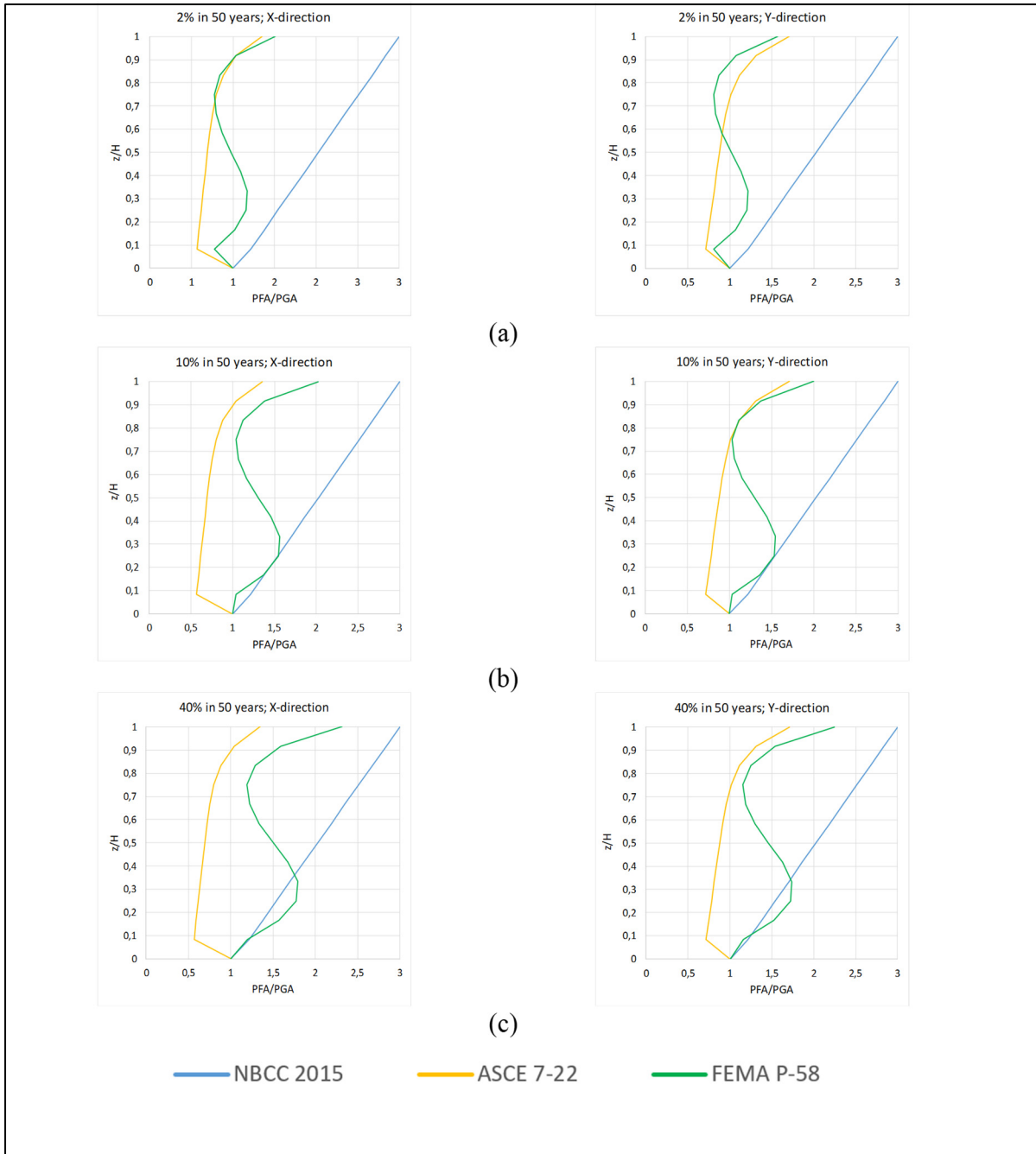


Figure 2.7 Estimated PFA/PGA ratio using three different methods due to increasing earthquakes intensities

2.3.2.2. Validation of PFA results with previous studies

Fathali and Lizundia (2011) conducted research to evaluate the current seismic design equations for non-structural components using strong motion records. They found out the relation between PFA/PGA versus (z/h) can be well fitted by a linear or non-linear regression analysis. And reviewing actual building recorded responses shows the relation is not straight line as is specified in the building codes and can follow the below non-linear equation. (Equation 2.1)

$$\frac{PFA}{PGA} = 1 + \alpha \left(\frac{z}{H}\right)^\beta \quad (2.1)$$

Where:

z: floor height on which NSCs is attached

H: total building height

Figure 2.8 shows that by considering the $\alpha=2$ and $\beta=1$, the equation (2.1) will be the same as proposed equation in NBC 2015 to estimate PFA. While the $\alpha=1.50$ and $\beta=3.15$, the result of equation (2.1) can be fitted to the elastic PFA calculated by simplified equations proposed in ASCE7-22 using a linear regression model with $R^2=0.97$ (Table 2.7). The details of linear regression model are provided in Appendix VI.

Table 2.7 Comparison of code defined height factors and the equation provided by Fathali and Lizundia (2011)

Code	Fathali ans Lizundia (2011)	R ²
NBC 2015	$\frac{PFA}{PGA} = 1 + 2\left(\frac{z}{H}\right)$	1
ASCE 7-22	$\frac{PFA}{PGA} = 1 + 0.59\left(\frac{z}{H}\right) + 0.94\left(\frac{z}{H}\right)^{10}$	0.97

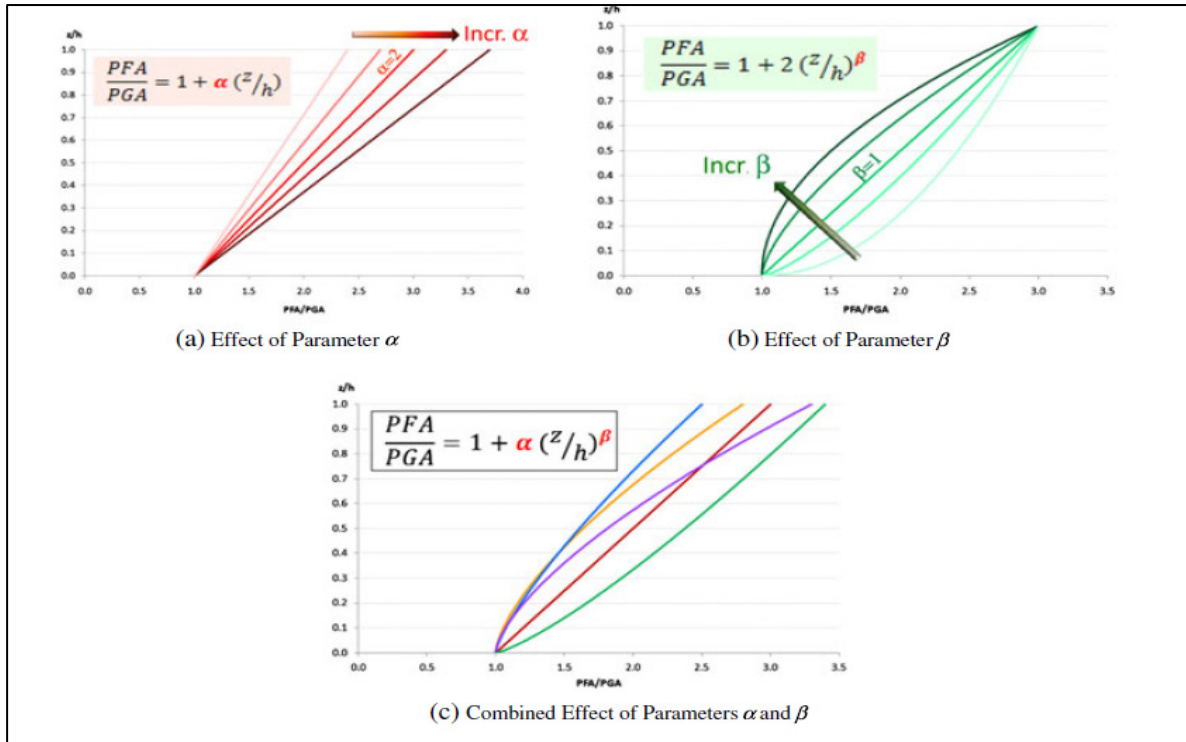


Figure 2.8 General non-linear relation between PFA/PGA and z/h
 Taken from Fathali & Lizundia (2011)

The case study shear wall building has been previously studied by Abouda (2022) to evaluate the effect of nonlinearity of the structure on the height amplification factors for floor acceleration. In this study, the PFA demands were extracted from a linear and elastic model prepared in SAP 2000 (CSI, 2019) and a non-linear model prepared in Perform 3D (CSI, 2019). In the linear model, the median variation of A_x (PFA/PGA) takes on an "S" shape. For 2% in 50 years earthquake, A_x values were always close to 1, ranging from 1.7 at the top floor to 0.6 at the 10th floor. The A_x values calculated considering nonlinearity were found to reduce progressively to a minimum amount of 0.3 at the 10th floor, then the amplification factor starts to increase. The non-linear behavior of structures has a significant influence on PFA responses. Figure 2.9 compares the results provided by Abouda (2022) with the acceleration amplification profiles obtained from FEMA P-58 simplified method, ASCE 7-22 inelastic profile and NBC elastic profile at the earthquake with 2% probability of occurrence in 50 years. NBC profile doesn't include inelasticity and the predicted PFA with this method is overestimated in comparison with other methods. The ASCE 7-22 inelastic profiles modify the floor

acceleration by considering the ductility of building, which depends on the seismic force resistance system. Although the profile shape is not exactly similar to nonlinear analysis and the acceleration increases from first story up to top floor level, but the acceleration values are more realistic in comparison with elastic acceleration profiles of ASCE 7-22 or NBC 2015. The simplified procedure of FEMA P-58 considers the effect of inelastic behavior in calculation of seismic demands; however, it provided overestimation of the PFA/PGA ratio compared to the results from Abouda (2022) based on inelastic response analysis.

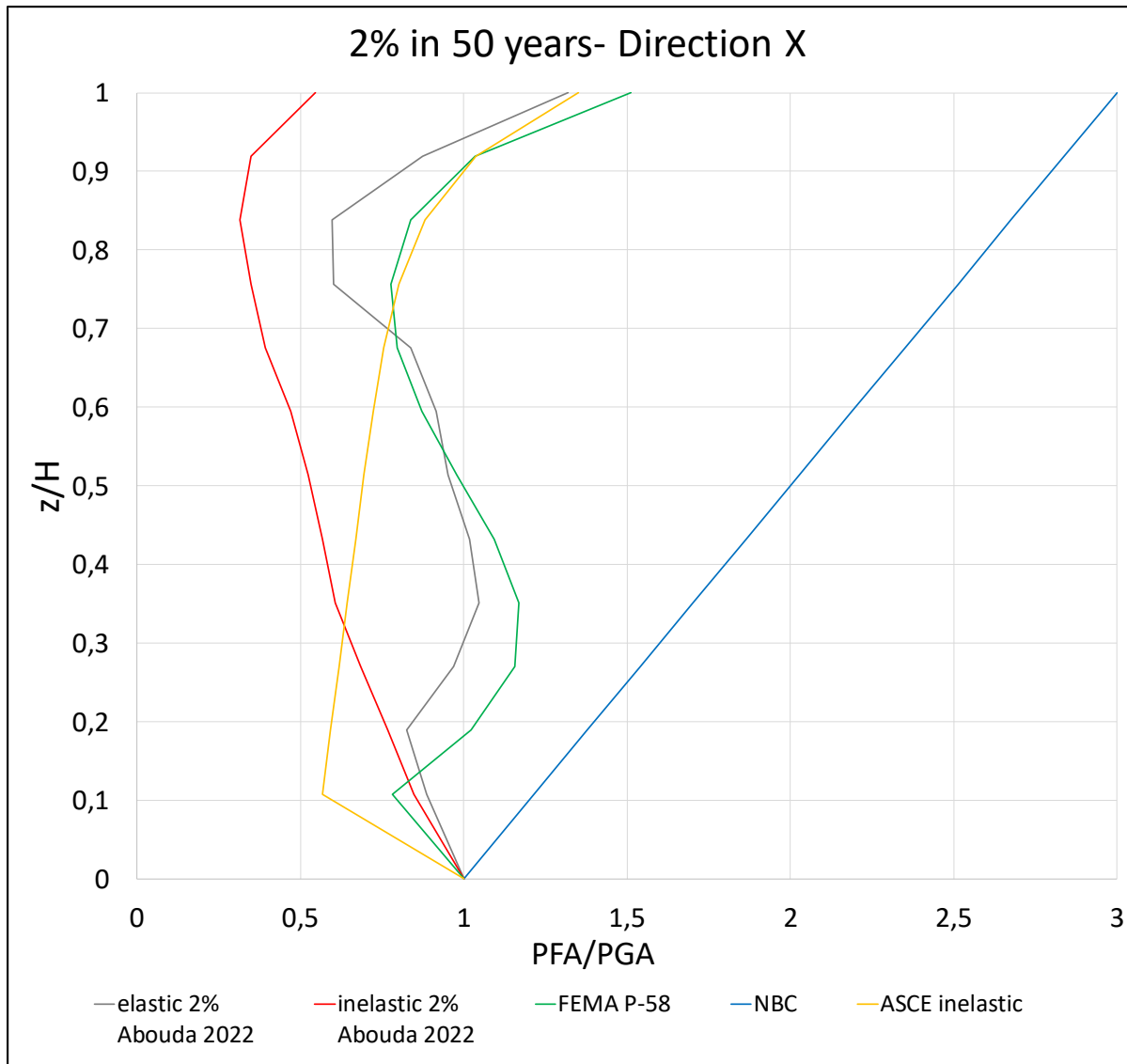


Figure 2.9 Validation of PFA calculated by different methods with previous studies considering 2% in 50 years earthquake

Table 2.8 presents a comparison between the PFA calculated using the FEMA P-58 simplified analysis, ASCE 7-22 inelastic acceleration profile, NBC 2015 elastic acceleration profile, and the deviations from the results obtained from Abouda's nonlinear analysis (2022). In general, the disparities between the inelastic profile of Abouda (2022) and the PFA values derived from FEMA P-58 and ASCE 7 inelastic profile are smaller when compared to PFA calculated using NBC 2015. Notably, there is a discernible trend in the results of FEMA P-58 simplified

method, wherein the discrepancies in estimated accelerations are more prominent in the top third of the building's height, as opposed to the middle and lower thirds.

Table 2.8 Comparison and verification of FEMA P-58, ASCE7-22, and NBC2015 methods with previous studies

floor	FEMA P-58			NBC 2015			ASCE 7-22			inelastic Abouda	
	PFA (g)	PFA/PGA	Deviation (%)	PFA (g)	PFA/PGA	Deviation (%)	PFA (g)	PFA/PGA	Deviation (%)	PFA (g)	PFA/PGA
12	0,570	1,511	63,9	1,131	3,000	81,8	0,509	1,351	59,6	0,206	0,546
11	0,390	1,034	66,2	1,070	2,838	87,7	0,391	1,038	66,4	0,132	0,349
10	0,316	0,839	62,6	1,009	2,676	88,3	0,333	0,882	64,4	0,119	0,314
9	0,293	0,778	55,1	0,948	2,513	86,1	0,302	0,802	56,5	0,132	0,349
8	0,301	0,797	50,7	0,886	2,351	83,3	0,285	0,755	47,9	0,148	0,393
7	0,328	0,871	45,8	0,825	2,189	78,4	0,272	0,723	34,7	0,178	0,472
6	0,369	0,979	46,5	0,764	2,027	74,1	0,262	0,695	24,6	0,198	0,524
5	0,412	1,092	48,0	0,703	1,864	69,5	0,252	0,669	15,1	0,214	0,568
4	0,441	1,169	48,1	0,642	1,702	64,3	0,243	0,643	5,6	0,229	0,607
3	0,436	1,158	40,8	0,581	1,540	55,5	0,233	0,618	-11,0	0,258	0,686
2	0,386	1,024	24,9	0,519	1,378	44,2	0,223	0,592	-29,9	0,290	0,769
1	0,294	0,781	-8,5	0,458	1,216	30,3	0,214	0,567	-49,4	0,319	0,847
0	0,377	1,000	0,0	0,377	1,000	0,0	0,377	1,000	0,0	0,377	1,000

2.4 Sensitivity of estimated loss to the EDPs calculation method

This section presents the results of loss analysis in terms of repair cost and other parameters such as loss ratio, defined as repair cost of each component divided by total replacement cost of building, and repair ratio, defined as repair cost of each component divided by maximum possible repair cost of that component. The results are provided for three mainly used architectural components in office building, considering 3 previously defined methods to estimate EDPs, in three different earthquake intensities, frequent, moderate, and rare earthquake corresponding to 40%, 10%, and 2% probability of exceedance in 50 years.

2.4.1. Assumed fragility curves and replacement costs

Table 2.9 shows the fragility curves that are selected for this part of study. The connection condition of selected fragilities are the standard connections.

Table 2.9 Selected fragilities for architectural components
Taken from FEMA P-58 Fragility Specification (FEMA, 2018)

Architectural components	Selected fragility	DS1		DS2		DS3	
		Median	Dispersion	Median	Dispersion	Median	Dispersion
Partition Wall	C1011.001a	0.005	0.40	0.01	0.30	0.021	0.20
Suspended Ceiling	C3032.001c	0.70	0.25	1.2	0.25	1.43	0.25
Curtain Wall	B2022.032	0.0088	0.25	0.0108	0.25		
<p>C1011.001a: Wall Partition, Type: Gypsum with metal studs, Full Height, Fixed Below, Fixed Above C3032.001c: Suspended Ceiling, SDC A, B, C, Area (A): $1000 < A < 2500$, Vert support only B2022.032: Midrise stick-built curtain wall, Config: Monolithic, Lamination: Not laminated, Glass Type: Annealed, Details: 1/4 in. (6 mm) AN monolithic; glass-frame clearance = 0 in. (0 mm); aspect ratio = 6:5 sealant = dry</p>							

2.4.2. Comparison of calculated repair costs

Figure 2.10 illustrates the total repair costs of the selected NSCs due to varying earthquake intensities. As expected, a clear correlation exists between the magnitude of EDPs and the resulting repair costs. This correlation becomes especially evident as earthquake intensity increases. Notably, for the design-based earthquake (2% in 50 years), the repair costs estimated from EDPs calculated using NBC 2015 equations significantly surpass those derived from other methods. This discrepancy highlights the conservative nature of this codes in estimating building responses.

Comparing the calculated repair costs for rare and moderate earthquake intensity (2% and 10% in 50 years, respectively), a striking similarity is observed among various methods, with negligible differences between them rather than design-based earthquake (2% in 50 years),

which is mostly because of the fact that building responses are still in the elastic range in lower intensities.

It's worth noting that the repair cost based on EDPs obtained from the simplified analysis, using the simplified method from FEMA P-58, leads to lower repair costs. This outcome aligns with the lower values of EDPs estimated through this method.

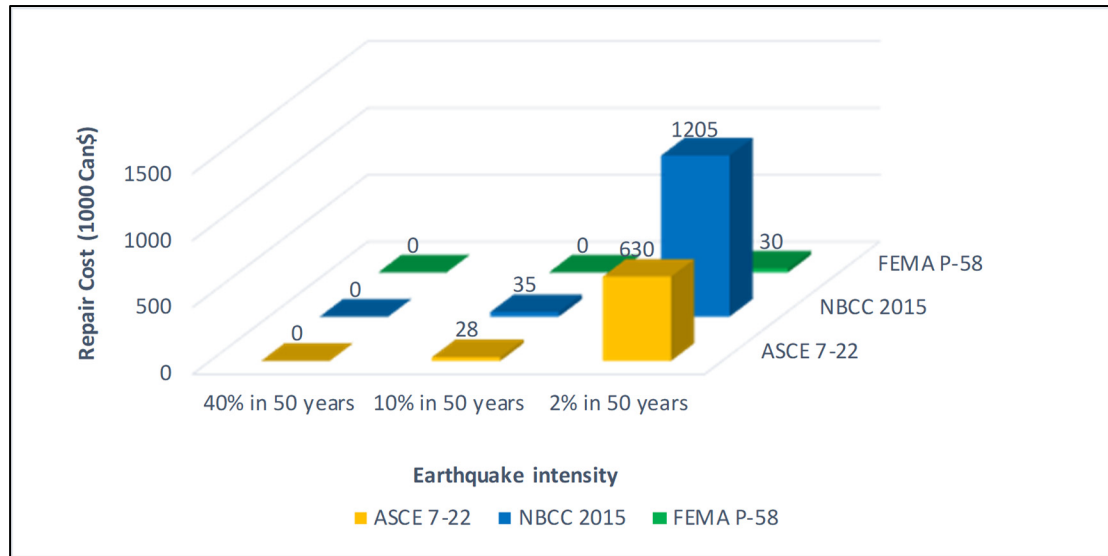


Figure 2.10 Sensitivity of the repair cost of architectural components to the EDPs estimation method

2.4.3. Contribution of selected architectural components and effect of their location along building height in the repair cost

Figure 2.11 illustrates the loss ratios attributed to three selected NSCs and their contributions across varying earthquake intensities. Additionally, in this figure the impact of different EDP calculation methods on repair cost becomes apparent. The loss ratio, defined as the calculated repair cost divided by the estimated total building replacement cost.

Partition walls consistently emerge as major contributors to the estimated repair costs, outpacing other NSCs in most scenarios. An exception arises in Figure 2.11-a, where EDPs are calculated using NBC2015. In this case, the IDR surges to nearly 0.1%. This IDR induced a 70% probability of DS1 occurrence and 38% probability of DS2 occurrence in the curtain walls. Consequently, curtain walls' contribution in this condition rises significantly. Moreover,

the Figures 2.11-b and 2.11-c reveal the negligible contribution of suspended ceilings to estimated repair cost. This stems from significantly lower PFA calculated by FEMA P-58 and ASCE 7-22 methods in comparison to NBC 2015 method due to considering the effect of nonlinearity.

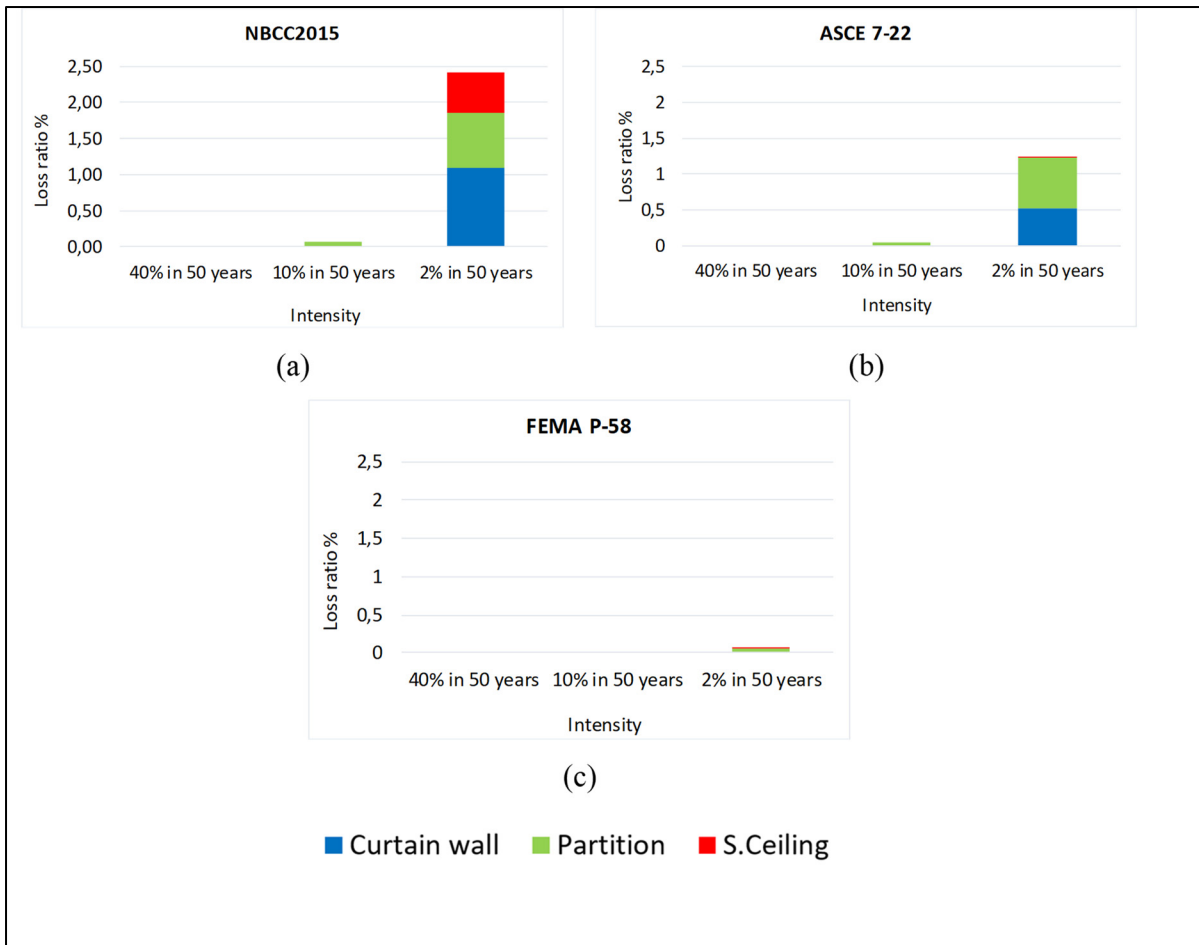


Figure 2.11 Contribution of each NSC in estimated loss ratio due to different calculated EDP method

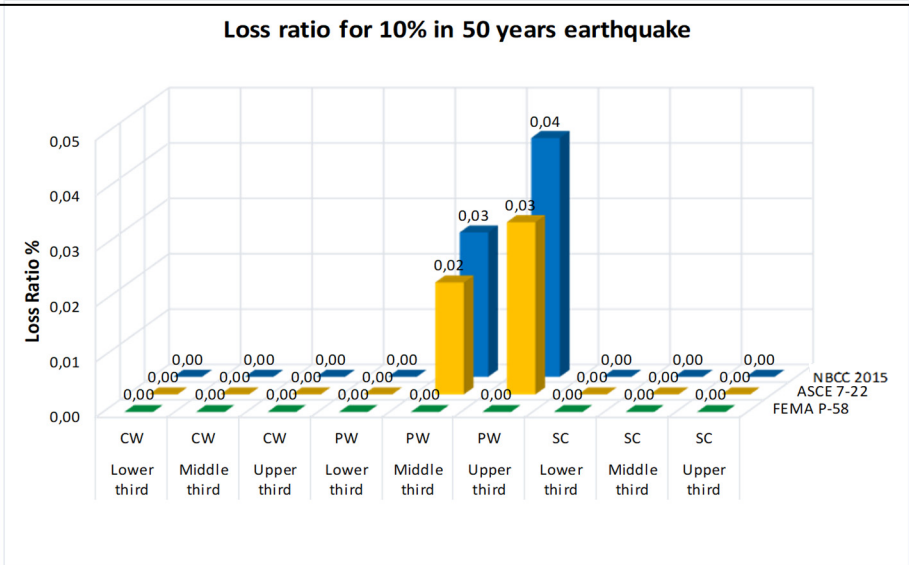
Figure 2.12 presents a comprehensive view of how repair costs of different architectural components are distributed along the building height. By showing the loss ratio (the calculated repair cost divided by the estimated total building replacement cost). This analysis takes into account various methods for estimating EDPs and considers earthquakes with probabilities of occurrence at 10% and 2% within a 50-year period.

Particularly noteworthy is the role of partition walls as the primary source of repair costs for a 10% in 50 years earthquake. Because of their sensitivity to drift, partition walls experience a higher contribution in the upper third of the building. The correlation between the calculated loss ratio and EDPs is evident. For instance, in the presented scenario, the calculated IDR using the NBC method surpasses that obtained from the ACSE7 method, consequently resulting in higher repair costs.

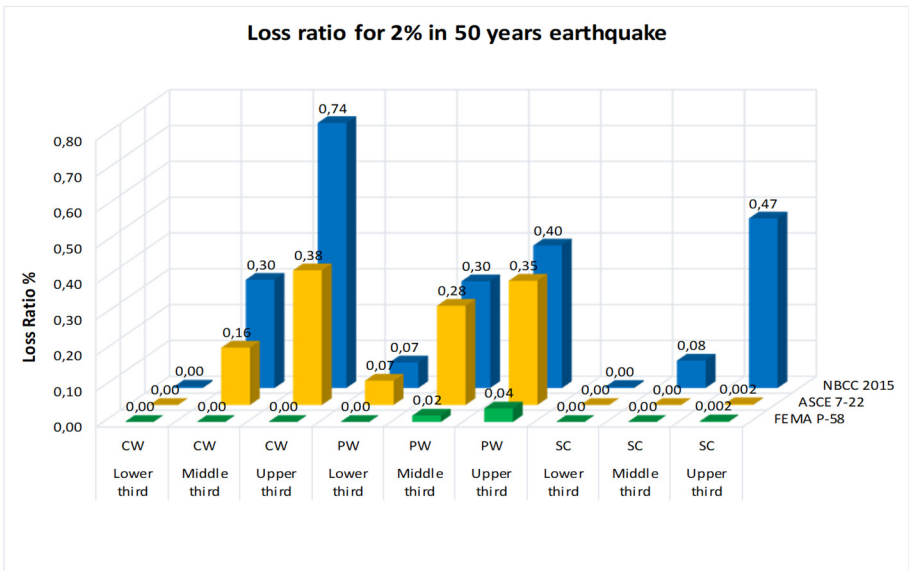
When earthquake intensity increases to 2% in 50 years, both suspended ceilings and curtain walls start affecting repair costs. Notably, a significant portion of repair costs concentrates in the upper third. This outcome is tied to the higher estimated EDPs.

Overestimated cost associated with EDPs calculated through NBC2015 can be observed in both 10% and 2% in 50 years earthquakes. The FEMA P-58 and ASCE 7-22 methods yield lower accelerations, resulting in negligible repair costs for suspended ceilings. However, it is foreseeable that with considering stronger ground motions, resulting larger accelerations from the FEMA P-58 method might affect the middle third's contribution to repair costs less than the lower and upper thirds due to the S-shaped pattern of floor acceleration variation.

Figure 2.13 reflects the repair cost distribution of each architectural component across the building height using a repair ratio (the repair cost of each architectural component divided by total replacement cost that architectural component). This representation reaffirms the findings in Figure 2.12.



(a)



(b)

Figure 2.12 Variation of loss ratio of each architectural components along building height considering different methods for EDPs calculation

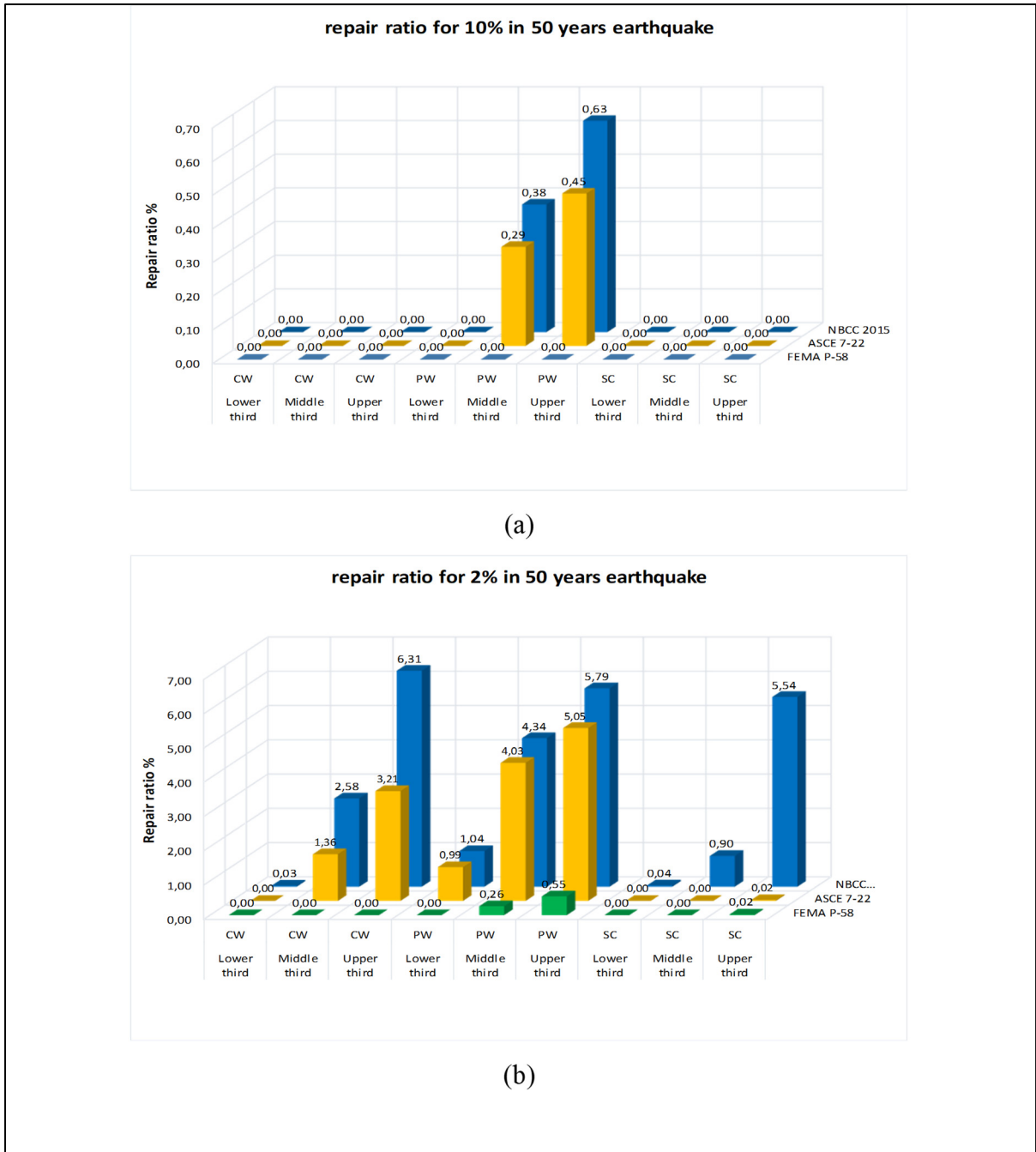


Figure 2.13 Variation of repair ratio of each architectural components along building height considering different methods for EDPs calculation

2.4.4 Synthesizing the results of loss estimation

Figure 2.14 summarised the findings of this chapter, displaying the repair costs of selected architectural components. The intensity measure utilized in this figure is $S_a(T1)$, representative of the geometric mean of spectral accelerations at the first mode's period within each principal direction. This metric is calculated based on the Montreal spectrum, sourced from the seismic hazard tool calculator (NBC 2015). Specifically, $S_a(T1)$ corresponds to 0.012g, 0.040g, and 0.098g for seismic events with probabilities of occurrence at 40%, 10%, and 2% in 50 years, respectively.

As evident from the figure 2.14, there is a trend of increasing repair costs as the intensity of seismic activity increases. It is noteworthy that repair costs resulting from EDPs computed through NBC 2015 surpass those from ASCE 7-22 and FEMA P-58 methods. Except for the predicted repair cost for the curtain walls with the NBC 2015 method at the intensity level of 2% in 50 years earthquake, partition walls notably emerge as significant contributors to repair costs among the selected architectural components. Conversely, the impact on suspended ceilings is comparatively minor, with no repair cost for all considered methods during 40% and 10% probability earthquakes in 50 years. In addition, for the 2% probability of occurrence in 50 years, ASCE7-22 and FEMA P-58 methods estimate around 1000 Can\$ expenditure. Which is significantly lower than the repair cost based on the PFA obtained from NBC 2015. As it is explained in the validation of calculated EDPs, it becomes evident that the EDPs derived from simplified analysis method of FEMA P-58 better align with nonlinear response analysis for IDR prediction from previous studies (with deviation of 16.5% at maximum IDR). For PFA, however, it provided a deviation of 64% increase at the maximum PFA compared to nonlinear analysis but still this method is with the lowest overall deviation.

Upon closer examination, disparities in predicted repair cost are more pronounced at higher seismic intensities, particularly during seismic events with a 2% probability of occurrence in 50 years. In this intensity, the differences become significantly amplified, especially for EDPs predicted with the NBC2015 method.

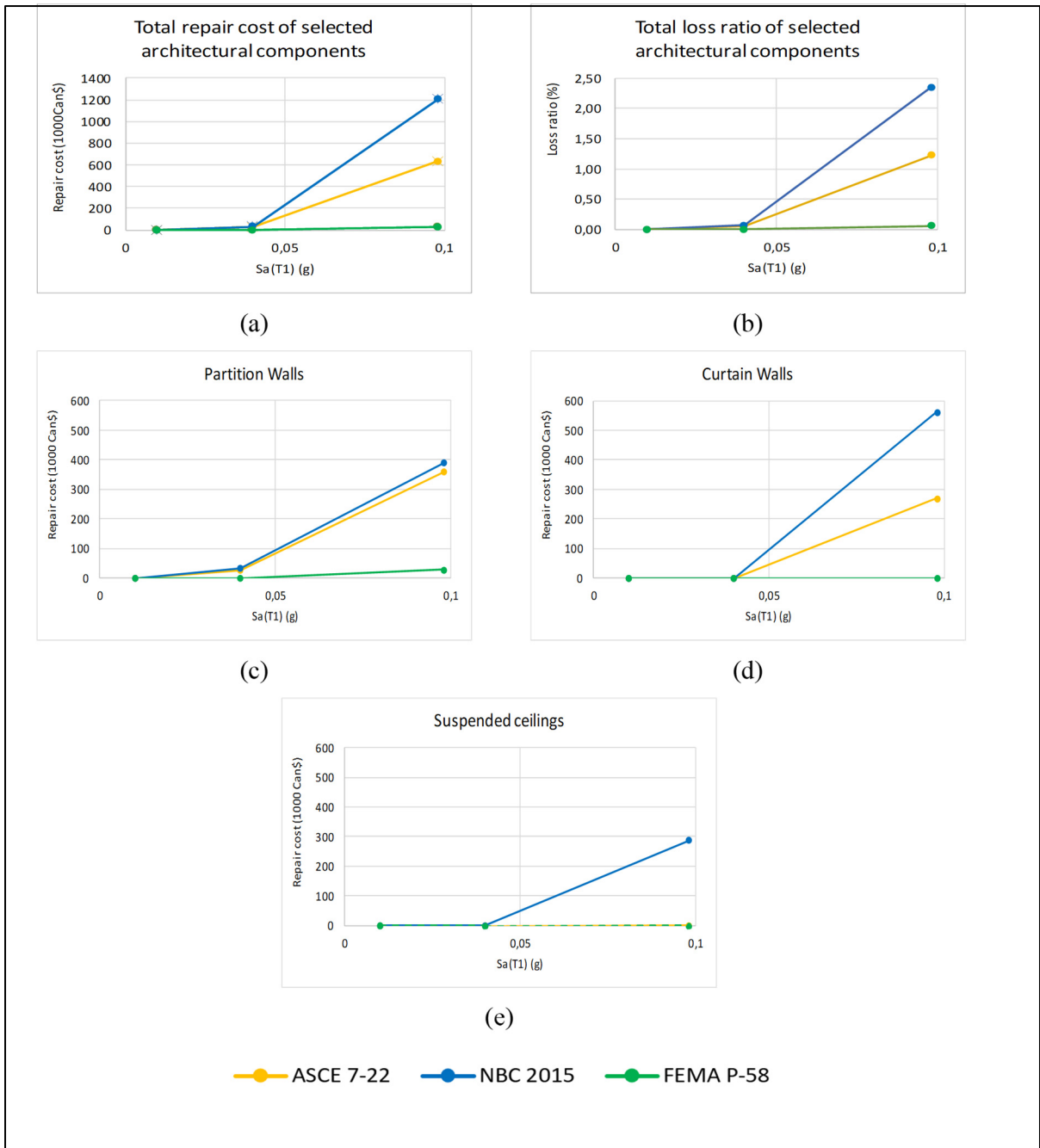


Figure 2.14 a) Total repair cost; b) Loss ratio of three selected NSCs; (c), (d), (e) Repair cost associated with each selected NSCs

CHAPTER 3

INFLUENCE OF CONNECTION DETAILS ON THE SEISMIC RESPONSE OF ARCHITECTURAL COMPONENTS AND INDUCED REPAIR COST IN REINFORCED CONCRETE SHEAR WALL BUILDINGS

S. R. Daregholi ^a, R. Assi ^b and A. Abo-El-Ezz ^c,

^{a,b,c} Department of Construction Engineering, École de Technologie Supérieure,
1100 Notre-Dame West, Montréal, Quebec, Canada, H3C 1K3

Paper submitted for ASCE Journal of Architectural Engineering, August 2023

3.1 Abstract

Losses associated with Non-Structural Components (NSCs) failure during earthquakes are the most significant contributor to overall building economic loss. Consequently, recent studies focused on proposing modifications to connection details to enhance their seismic performance. This study quantitatively investigates the repair cost and benefits of improving the connection details for three commonly used architectural NSCs: partition walls, suspended ceilings, and curtain walls. Additionally, it examines the distribution of repair costs of NSCs along the building height. The FEMA-P58 building-specific loss estimation methodology has been applied to a 12-story reinforced concrete office building located in Montreal, to estimate the economic loss in terms of the repair cost. The results demonstrate that enhancing connection detailing reduces repair costs of the selected NSCs, by more than 30% at design-level earthquake. Moreover, the estimated loss due to the failure of selected NSCs is mainly concentrated in the upper third of the building's height.

Keywords: architectural non-structural component, loss estimation, repair cost, FEMA P-58, fragility curves, damage states, consequences functions

3.2 Introduction

NSCs in buildings typically constitute approximately 70% or more of the total investment cost of a typical building (Rojas et al., 2023). These components can be categorized as (1)

architectural components, such as exterior cladding, partition walls, and suspended ceilings; (2) mechanical and electrical components, such as heating and ventilation piping systems, and (3) building contents such as office equipment's, and furniture (CSA S-832, 2014; Assi et al., 2016). NSCs are susceptible to damage mainly due to excessive displacement in the case of drift-sensitive components or excessive acceleration in the case of acceleration-sensitive components (FEMA P-58, 2018; Pardalopoulos et al., 2015). Damage to NSCs and their failure can pose life safety risks for occupants and passers-by, impede safe evacuation and hinder rescuers from reaching the building's interior, and significantly impair the post-earthquake functionality and operation of the building (D'Amore et al., 2023; Perrone et al., 2019; Villaverde R, 2004). As highlighted consistently in the reconnaissance reports and post-earthquake surveys from past events such as the 1994 Northridge earthquake in United States and the 2010 Maule earthquake in Chile, damage to NSCs often occurs at significantly lower earthquake intensities compared to those required to induce structural damage (Filiatrault et al., 2001; Miranda et al., 2012). NSCs contribute remarkably to building loss, even in a modern code-compliant building (Goulet et al., 2007). For example, Bradley et al. (2009) evaluated the seismic performance of a 10-story code-conforming reinforced concrete building in New Zealand, which showed that 26% of predicted building loss was due to drift-sensitive NSCs like partitions and facades, and 49% of the predicted loss was caused by acceleration-sensitive NSCs like ceilings, mechanical equipment, and contents. Another study by Zeng et al. (2016) focused on a regional loss prediction on the campus of Tsinghua University in China, including buildings with different occupancies and structural systems. This study indicated a significant portion of losses were arising from damage to architectural NSCs like exterior walls, partitions, and ceiling systems with a predicted loss ratio of 35% (defined as repair cost to replacement cost ratio) for maximum credible earthquake shaking. In another research conducted by Ni et al. (2018), two tall buildings, situated in high and moderate seismic zones in Manila and Bangkok were investigated to assess their performance at service, design-based, and maximum credible earthquake levels. For the first building, the damage ratio of architectural NSCs defined as the number of damaged components divided by the total number of components in a performance group ranged from 3.5% to 11%. In the case of the second building, the damage ratio for architectural NSCs was found to be between 2.7% and 4.7%. The associated damage

was observed even at service-level earthquake. Consequently, there has been a significant rise in community expectations for seismic mitigation of NSCs (Fierro et al., 2011; Achour et al., 2011; Filiatrault et al., 2018).

Furthermore, failures of NSCs in recent earthquakes were frequently caused by a lack of or insufficient anchoring and bracing (Miranda et al., 2012). Several numerical and experimental studies have evaluated the potential influence of anchorage type and its behavior on the expected seismic demands and subsequent performance of NSCs and their connections within buildings. These studies consistently demonstrated the positive effect of mitigation measures. These measures can play a crucial role in ensuring the protection of both NSCs and the anchorage system even under severe earthquakes by minimizing damage to either vertical architectural NSCs like facades, partitions, or horizontal ones like ceilings (Rojas et al., 2023; Purgstaller et al., 2020; Quintana Gallo et al., 2018; Ciurlanti et al., 2022).

These mitigation solutions in previous studies evaluated the effect of connection detailing on the fragility curves of partition walls (Retamales et al., 2013; Sousa & Monteiro, 2018; Preti & Bolis, 2017; Hasani & Ryan, 2022), suspended ceilings (Ryu & Reinhorn, 2019; Brandolese et al., 2019; Dhakal et al., 2016), and curtain walls (Biard et al., 2011). Parameters considered in these studies include adequate bracing, internal and lateral gaps, and the energy dissipation mechanism of connections (Bianchi et al., 2021). All these solutions concentrate on better understanding of the seismic performance and damage mechanisms of NSCs, aiming to propose effective measures to reduce the risk of components' damage (Bianchi et al., 2019). Nevertheless, previous studies have not specifically determined the exact extent of loss reduction resulting from the implementation of seismically improved connections, and there is limited research work done to evaluate quantitatively the potential impact of optimizing the improved seismic connection detailing of NSCs on reducing seismic loss in code-conforming buildings.

Therefore, the objective of this study is to quantify the impact of improving the connection details of partition walls, suspended ceilings, and curtain walls on the expected repair cost in code-conforming buildings subjected to 8 various levels of ground motion intensities, ranging from 40% to 2 % probability of occurrence in 50 years, by comparing two standard and improved connection detailing conditions. In addition, this research aims to evaluate the

distribution of repair cost caused by the failure of NSCs along the building height, which can help in planning for post-earthquake repair sequences.

The methodology employed to achieve this objective is based on the FEMA-P58-1 loss modeling approach (FEMA, 2018) as illustrated in Figure 3.1, using Performance Assessment Calculation Tool (PACT 3.1.2, 2012). This approach provides a more tangible measure for stakeholders and decision-makers, as it focuses on the financial aspects of repairs rather than solely relying on engineering demand parameters (EDPs), which are normally used by engineers in their calculations to evaluate buildings behaviors (FEMA P-58-1, 2012). While this study focuses on assessing the repair costs associated with the failure of architectural NSCs of the building, it is important to acknowledge that other indirect losses, such as business interruption during the repair period and the potential loss of building functionality, can significantly impact the overall economic loss. However, these factors are out of the scope of this study.

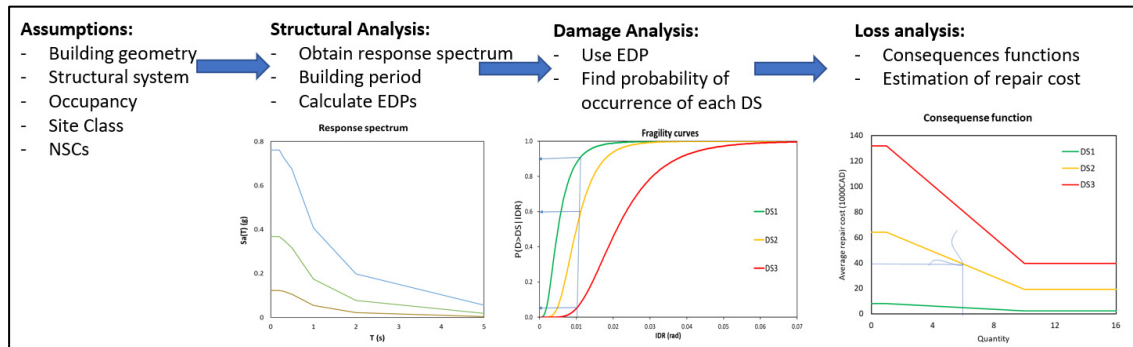


Figure 3.1 Framework of FEMA P-58 loss estimation methodology used in this study

3.3 Description of the studied building and NSCs

3.3.1 Building information

A 12-story reinforced concrete office building located in Montreal on site Class-D (stiff soil with shear wave velocity between 180 and 360 m/s) has been selected. The lateral load-resisting system consists of an elevator core composed of two C-shaped 400 mm thick concrete shear walls connected by 400mm wide x 1000mm deep coupling beam on the ceiling level of each floor. It is surrounded by the same size 550x550mm columns and 200mm thick slabs on

each floor as the gravity load-bearing system. The core walls extend from the rooftop level and create an elevator penthouse. (Figure 3.2)

In X-direction, the seismic force-resisting system (SFERS) consists of reinforced concrete ductile coupled walls, while it consists of ductile reinforced concrete shear walls in the Y-direction (CDH, 2016).

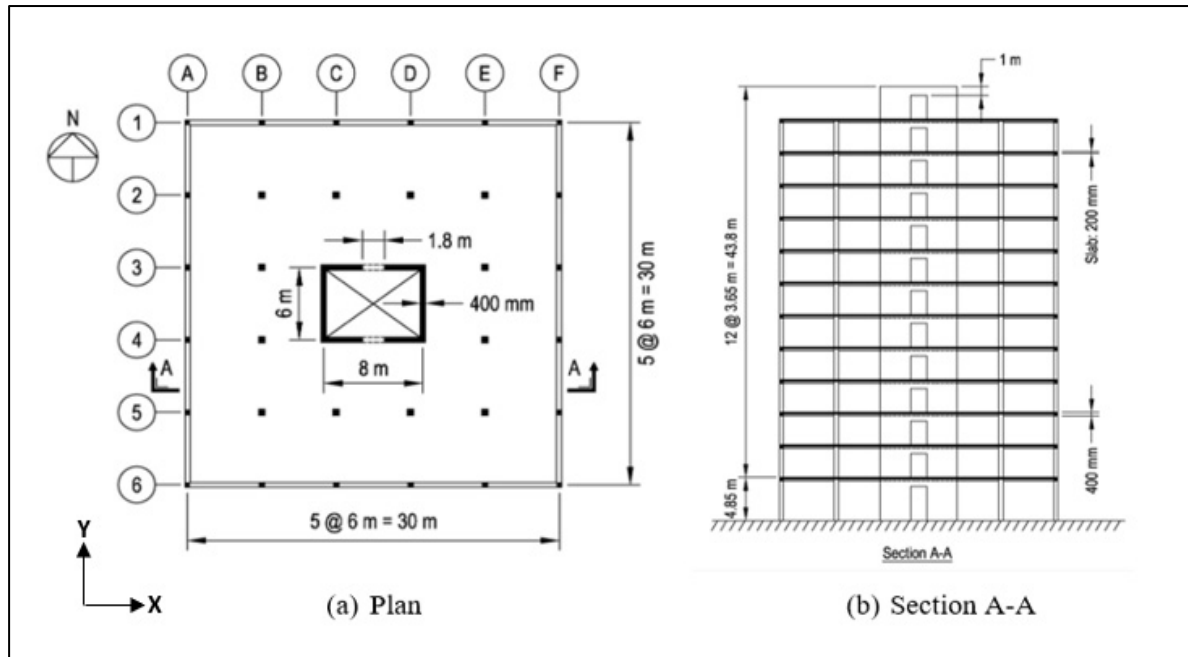


Figure 3.2 Plan and elevation views of the 12-story office building
Taken from Concrete design handbook (2016)

3.3.2 Selected architectural components and their estimated replacement cost

Partition walls (PW), suspended ceilings (SC), and curtain walls (CS) are selected in this study as they are typically found in commercial buildings. Bradley et al. (2009) revealed that these components contribute about 40% of the expected loss of a mid-rise code-conforming building in New Zealand subjected at an earthquake with 2% in 50 years probability of exceedance.

The NSC quantities per floor were estimated using the Normative Quantity Estimation tool presented in FEMA P-58-2 (FEMA, 2012). This tool utilizes building details, including the number, area, and occupancy of floors as well as the NSC fragilities to calculate the quantities per gross square foot basis. Table 3.1 presents the quantities used in this study, considering a

consistent distribution of NSCs across all floors. PWs and CWs are drift-sensitive, and their performance varies according to the building's principal directions. Conversely, SCs are acceleration-sensitive and are typically unaffected by the direction of the applied load. Thus, the estimated quantity of SCs is considered as non-directional (FEMA P-58-1, 2018). The dispersion quantities in Table 3.1 represent the uncertainty in estimating the quantity of NSCs. The quantity of PWs and CWs relies on architectural drawings, which can vary in buildings even with the same occupancy. Conversely, the ceiling area determines the quantity of SCs, allowing a precise estimation with zero dispersion. The building's total replacement cost was evaluated by adjusting the calculated cost from FEMA P-58/SD-3.7.16 example based on the building's total area and occupancy. The lateral force resistance system of the example building consists of reinforced masonry shear walls, whose behavior is similar to the reinforced concrete shear wall building. The currency exchange rate (1.33) and inflation rate (1.18, source: data.worldbank.org) were taken into account to reflect current expenses in Canada, since the reference time of the example is 2011. The estimated total replacement cost of the building is around 51 million Can\$. Furthermore, the maximum possible repair cost of each NSC is calculated by subjecting them to significantly large peak floor acceleration (PFA) and inter-story drift ratio (IDR), using the PACT software. After the building collapse, the corresponding repair cost remains unchanged even for larger EDPs (Figure 3.3), because this state indicates a complete loss of the NSCs.

Table 3.1 Estimated quantity and maximum possible repair cost for each NSCs based on FEAM P-58 Normative quantity estimation tool

NSC	Assumed Quantity of components	Quantity		Fragility Quantity Dispersion	Maximum possible repair cost (Can\$)
		Directional	Non- directional		
Partition Wall (PW)	100 LF	9.688	--	0.2	3,529,625
Suspended Ceiling (SC)	1800 SF	--	4.844	0.0	4,050,782
Curtain Wall (CW)	30 SF	96.880	--	0.6	6,027,822

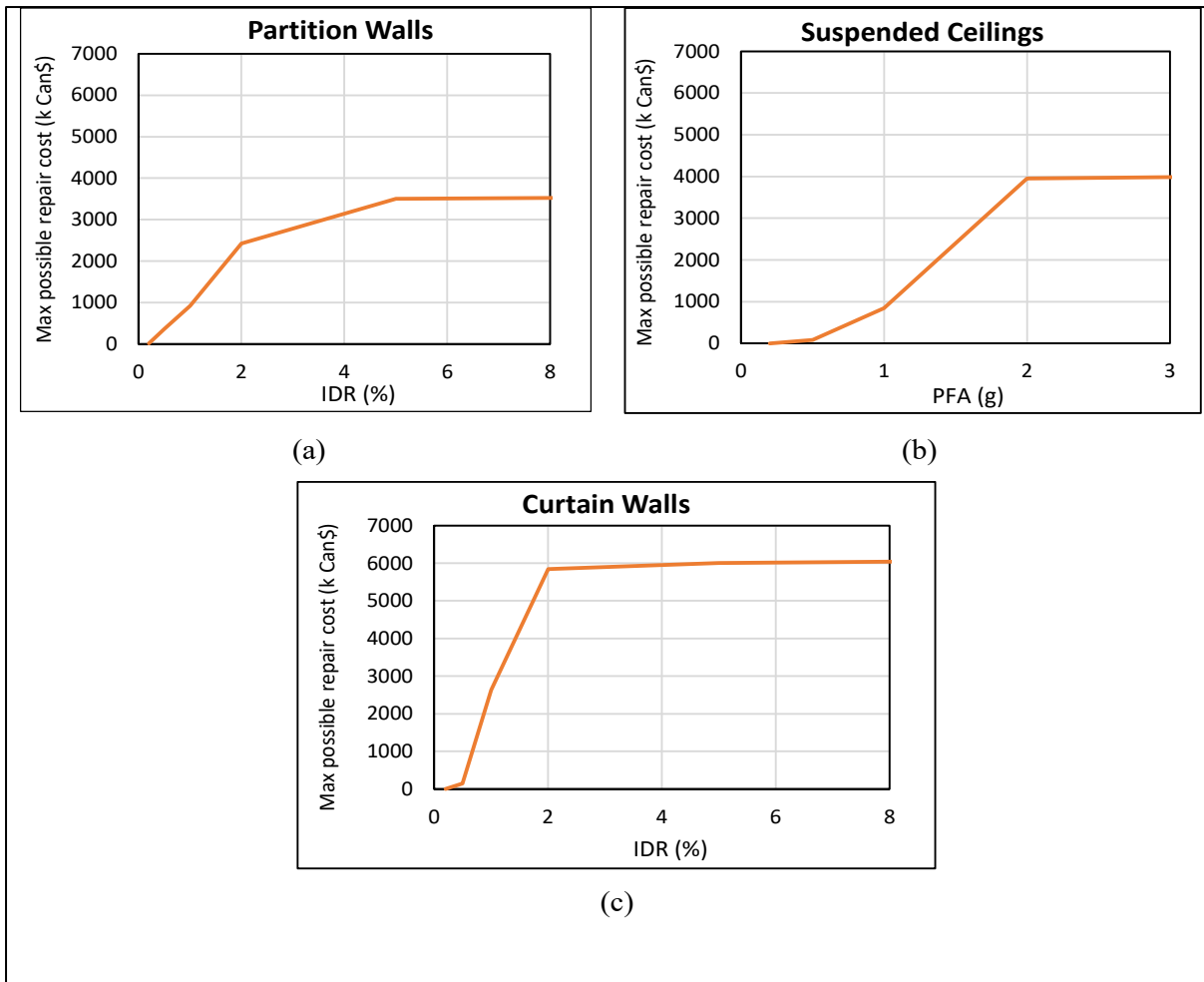


Figure 3.3 Maximum possible repair cost: a) Partition Walls; b) Suspended Ceilings; c) Curtain Walls

3.3.3 Seismic intensities

5% damped response spectra of Montreal (Figure 3.4), considering site class-D with 8 different return periods ranging from frequent (40% in 50 years) to rare (2% in 50 years) were used in this study (NBC, 2020). The reason for selecting intensities below the design level is that NSCs sustain damage not only during severe earthquakes but also in more frequent ones. Intensities exceeding the design-based earthquake are not considered because they could lead to structural damage or building collapse.

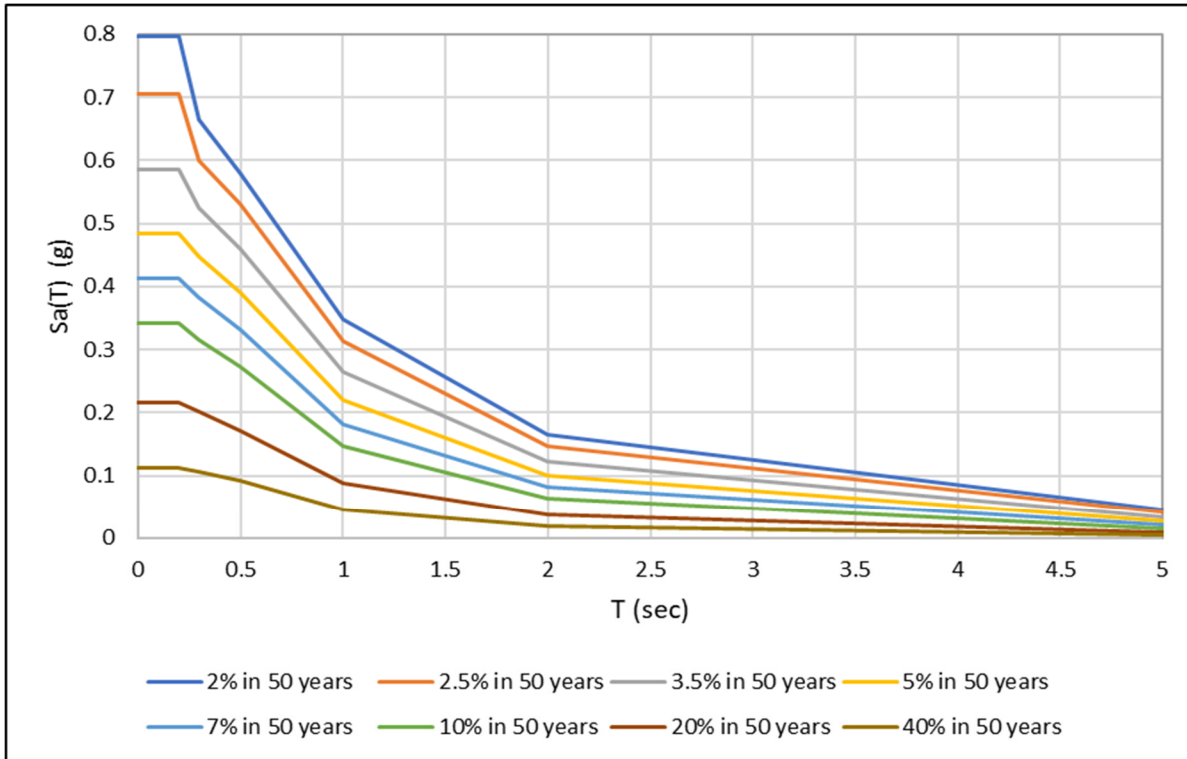


Figure 3.4 Utilized response spectra - Montreal (site class-D) based on the NBC 2020 hazard values

3.4 Structural analysis

EDPs could be utilized to assess damage to both structural and non-structural elements (FEAM P-58-1, 2018). The desired EDPs in this study are IDR and PFA which are obtained through the simplified analysis method provided in FEMA P-58 (Figure 3.5). PFA is calculated by multiplying peak ground acceleration (PGA) with the height modification factor (H_{ai}). IDR is calculated by multiplying the obtained story drift ratio from the building elastic model implemented in SAP2000 (CSI-SAP2000, V 21.1.0) by the drift modification factor ($H_{\Delta i}$). These modification factors take into account the first modal period of building, story heights, and the influence of building nonlinearity.

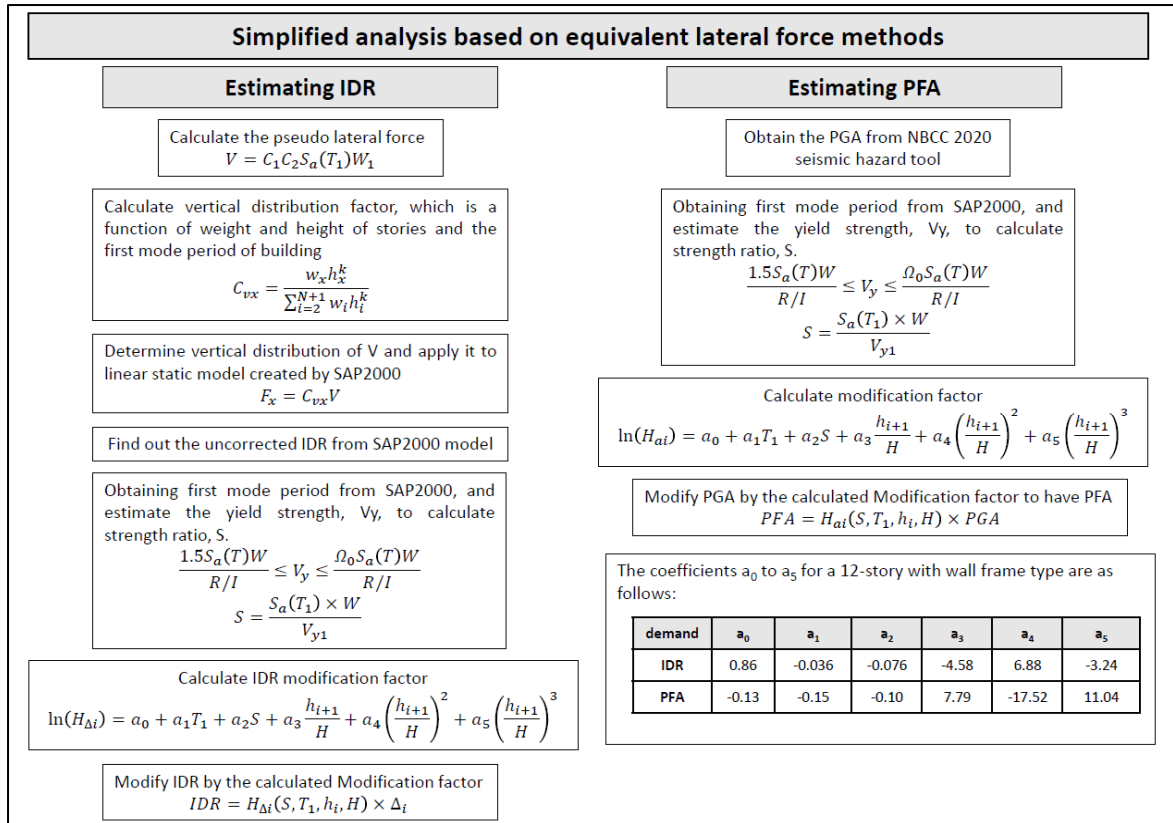


Figure 3.5 Calculation of IDR and PFA based on the simplified linear method presented in FEMA P-58-1 (FEMA, 2018)

Figure 3.5 illustrates factors C1 and C2 accounting for inelastic response and cyclic degradation. $S_a(T_1)$ represents the 5% damped spectral acceleration at the fundamental period. W denotes the total seismic weight, while w_i represents the lumped weight on each floor. W_1 corresponds to the first modal effective weight in the considered direction. The h_i (or h_x) refers to the above-base height for level i (or x). The constant k depends on the period of the first mode. V_{y1} is the estimated yield strength based on the first mode response, with values of 4370 kN/m² for the X-direction and 5780 kN/m² for the Y-direction. These values are based on assumed coefficients R=8.0, $\Omega_0=2.5$, and I=1.0 for X-direction, and R=5.0, $\Omega_0=2.5$, and I=1.0 for Y-direction (ASCE7, 2022). The results from the simplified analysis have been adjusted to account for uncertainties in ground motion intensity, modeling, and computed EDPs. These dispersions depend on the first modal period and strength ratio and have been calculated for IDR and PFA in each principal direction and intensity separately. (FEMA, 2018). A simplified elastic 3D model of the shear wall core using SAP2000 (CSI, V 21.1.0) was developed to

calculate the IDR. Material properties and concrete cracking assumptions followed the Concrete Design Handbook (Cement Association of Canada, 2016). The model was validated by comparing vibration periods with handbook results, showing a maximum difference of 10%. It was found that median PFA and IDR increase with seismic intensity in both X- and Y-directions. PFA exhibits an S-shaped pattern along the building height, with values increasing in the lower third, decreasing in the middle third, and surpassing 0.8g at the rooftop (approximately 1.7 times PGA) for the design-based earthquake. Generally, IDR increase along the building height, except for a slight reduction on upper floors. For the design-based earthquake, IDR reaches 0.43% and 0.6% in X- and Y-directions, respectively.

3.5 Selection of component fragility curves and repair cost consequences functions

The fragility curves and consequences functions of standard and improved conditions of selected NSCs are selected from the Fragility database of FEMA P-58. Fragility curves are represented using parameters of a lognormal distribution, which consist of the median of the EDPs and a dispersion factor. This factor considers uncertainties associated with the design accuracy of failure demand, material strength variations, and construction quality (FEMA, 2018).

3.5.1. Partition Walls

Three distinct damage states for PWs (Table 3.1), along with corresponding fragility analysis demand levels were identified in Laboratory experiments by Retmales et al. (2013). These damage states are determined based on observed damage and repair operation features, as outlined in Table 3.1 (MCEER-11-0005, 2011). PWs, primarily influenced by IDR, are susceptible to visible damage even during slight to moderate earthquakes when the IDR reaches 0.1-0.2% (Bersofsky, 2004). Notably, when drift levels reach 2%, repair costs equate to the original construction cost (Lee et al. in 2007.) One potential approach to enhance the seismic performance of PWs is isolating them from the building lateral deformation by using

friction/sliding connections (Araya-Letelier et al., 2019). The connection details between partition walls and surrounding elements significantly impact PWs' seismic performance (Fiorino et al., 2018). This study compares the conventional full height and full restraint PW (standard condition) with the improved connection of a full height PW with fixed bottom and slip track without return at the top (Table 3.2). Previous studies (Magliulo et al., 2014; Petrone et al., 2017) support this selection, comparing the seismic performance of conventional and improved PWs.

According to FEMA P-58/BD-3.9.2 a slip track, located at the top of a partition wall (PW), allows the top track to slide in-plane. This friction connection prevents direct conveyance of lateral deformation to the PW, as the studs are not attached to the top track. The top row of screws, connecting the gypsum to the stud, is positioned below the top track flange (FEMA, 2018). These improved connections enable PWs to withstand up to 1% IDR without damage. (Araya-Letelier et al., 2019). The obtained fragility curves for PWs are shown in Figure 3.6. With an IDR range of less than 0.6% (based on structural analysis), the occurrence of DS1 is more likely to happen (62% in the standard condition, 82% in the improved condition) compared to DS2 and DS3. Improved connection details effectively prevent DS3 in PWs. Yet, considering this IDR range, DS3 occurrence in the standard condition is negligible. The consequences functions reveal significantly lower repair costs in the improved condition, so that maximum repair costs (associated with lower repair action quantities) for DS1 decreased from approximately 4202 Can\$ to 2801 Can\$, while that for DS2 decreased from 10711 Can\$ to 7147 Can\$, representing a 33% reduction. The minimum repair costs (associated with the upper repair action quantities) are reduced by about 62% for both DS1 (from 2241 Can\$ to 840 Can\$) and DS2 (from 5713 Can\$ to 2142 Can\$). Additionally, the improved connection eliminates DS3, resulting in zero associated repair costs (Figure 3.7).

3.5.2. Suspended Ceilings

Referring to FEMA P-58/BD-3.9.4, three damage states are defined for SCs (Table 3.2). The collapsed ceiling panels relative to the total number of panels during an earthquake, specifically percentages of 5%, 30%, and 50%, are frequently used as criteria to determine the

damage levels corresponding to slight, moderate, and extensive damage (Bianchi & Pampanin, 2022). In this study, the standard connection for SCs has only a vertical support, while the improved condition includes both vertical and diagonal supports. Fragility curves shown in Figure 3.6 demonstrate that improving the connection condition reduces damage probability at the same PFA. For instance, at the maximum PFA of 0.8g obtained from structural analysis, the probabilities of occurrence for DS1, DS2, and DS3 in the improved condition are 11.9%, 8.7%, and 14.8% in case of the standard condition, respectively. Additionally, the fragility curves exhibit a gentle slope in the improved condition indicating higher dispersion consistent with the values in Table 3.3. This means that, for the same increase in PFA, the improved condition experiences a smaller increase in the probability of exceeding each damage state compared to the standard condition. For example, increasing earthquake intensity from 10% to 2% in 50 years raises PFA at the rooftop in from 0.45g to 0.80g. This results in a 66% increase for DS1, 5% for DS2, and 1% for DS3 in the standard condition, while in the improved condition, it causes an 8% increase for DS1, 0.45% for DS2, and 0.15% for DS3.

The consequences functions of the improved condition indicate a 67% increase in repair cost for quantities of damaged components in the lower parts of the buildings, mainly due to the higher cost of the improved attachments. However, for larger quantities of damage, there is a potential reduction of 25% in the repair cost under the improved condition. This reduction can be attributed to possible economies of scale. Therefore, improving connection details may decrease physical damage; but it may not result in a directly proportional decrease in repair costs, and the repair cost may vary depending on the quantity of damaged components. In this study, the computed maximum PFA is equal to 0.8g. As a result, the probability of the occurrence of DS2 and DS3, and their corresponding high repair costs of improved condition is negligible.

3.5.3. Curtain Walls

CWs are predominantly sensitive to in-plane IDR but may be damaged from out-of-plane large accelerations (Bianchi & Pampanin, 2022). Glazed exterior wall systems are classified based on glass types, assembly, and the installation method (ASCE 41, 2013). The glazing can

experience various DSs depending on its construction details and the imposed IDR (Table 3.3). Aside from external stresses, forces transmitted from the metal frame at the corners and edges can partially or completely damage the glass. Providing clearances on all four sides of the glass panel helps mitigate earthquake-induced rotations and displacements (Djuric-Mijovic et al., 2018). This study compares a standard connection (no clearance to the support frame) to an improved condition with an anticipated gap between the glass panel and the frame. Fragility curves (Figure 3.6) indicate that when CWs experience the same IDR, the probability of damage significantly decreases with the inclusion of a sufficient gap. For instance, at the maximum IDR= 0.006 rad, the probabilities of occurrence for DS1 and DS2 decrease from 6% and 1% in the standard condition to nearly zero in the improved condition. This implies that providing an 11mm gap effectively protects the glazing from damage. Furthermore, the repair costs for DS1 and DS2 remain identical due to the similarity in the required repair actions, with the only difference being the presence of an installation gap (Figure 3.7). Consequently, the repair cost for both conditions is nearly equivalent to the cost of replacing the glass.

Table 3.2 Definition of Damage States for PWs, SCs, and CWs based on FEMA P-58
Fragility Specification (FEMA, 2018)

NSC	Damage State	Description	Consequences	Repair Description
Partition Walls (PW)	DS1	Superficial damage to the walls	Screw pop-out, cracking of wall board, warping or cracking of tape, slight crushing of wall panel at corners.	Retape joints, paste and repaint. May require cutting and replacing corner sections of board. Repair 5% wallboard, 10% retape, 25% repaint.
	DS2	Significant local damage of the walls	Moderate cracking or crushing of gypsum wall boards (typically in corners). Moderate corner gap openings, bending of boundary studs.	Remove and replace 10% of wall board (both sides), retape and paste 25% of wall, paint 50% of wall. Replace boundary studs of approximately 5 intersections per 100 ft of wall length.
	DS3	Severe damage to the walls	Buckling of studs and tearing of tracks. Tearing or bending of top track, tearing at corners with transverse walls, large gap openings, walls displaced.	Remove and replace 50% of length of metal stud wall, 50% of both sides of the gypsum, and any embedded utilities. Retape and paste as required. Repaint 100%.
Suspended ceilings (SC)	DS1	Slight damage	5 % of ceiling grid and tile damage	Reinstall, repair, or replace 5% of the ceiling area.
	DS2	Moderate damage	30% of ceiling grid and tile damage.	Replace 30% of the ceiling area.
	DS3	Extensive damage	50% of ceiling grid and tile damage.	Replace the entire ceiling
Curtain Walls (CW)	DS1	Glass cracking	Serviceability failures	Replace cracked glass panel.
	DS2	Glass fallout	Life safety hazard	Replace cracked glass panel; cover exposure in meantime.
	DS3	Gasket seal failure.	Serviceability failures	Remove glass panel and replace damaged gaskets.

Table 3.3 Selected fragilities for PWs, SCs, and CWs
Taken from FEMA P-58 Fragility Specification (FEMA, 2018)

NSCs	Condition	Selected fragility	DS1		DS2		DS3	
			Median	Dispersion	Median	Dispersion	Median	Dispersion
Partition Walls (PWs)	Standard condition	C1011.001a	0.005	0.40	0.01	0.30	0.021	0.20
	Improved condition	C1011.001d	0.0035	0.6	0.0095	0.45	--	--
Suspended ceilings (SCs)	Standard condition	C3032.001c	0.70	0.25	1.2	0.25	1.43	0.25
	Improved condition	C3032.003c	1.21	0.30	1.75	0.30	1.95	0.30
Curtain Walls (CWs)	Standard condition	B2022.032	0.0088	0.25	0.0108	0.25	--	--
	Improved condition	B2022.031	0.0138	0.25	0.0219	0.30	--	--
<p>C1011.001a: Wall Partition, Type: Gypsum with metal studs, Full Height, Fixed Below, Fixed Above</p> <p>C1011.001d: Wall Partition, Type: Gypsum with metal studs, Full Height, Fixed Below, Slip Track Above without returns</p> <p>C3032.001c: Suspended Ceiling, SDC A, B, C, Area (A): $1000 < A < 2500$, Vert support only</p> <p>C3032.003c: Suspended Ceiling, SDC D, E ($I_p=1.0$). Area (A): $1000 < A < 2500$, Vert & Lat support only</p> <p>B2022.031: Midrise stick-built curtain wall, Config: Monolithic, Lamination: Not laminated, Glass Type: Annealed, Details: 1/4 in. (6 mm) AN monolithic; glass-frame clearance = 0.43 in. (11 mm); aspect ratio = 6:5 sealant = dry</p> <p>B2022.032: Midrise stick-built curtain wall, Config: Monolithic, Lamination: Not laminated, Glass Type: Annealed, Details: 1/4 in. (6 mm) AN monolithic; glass-frame clearance = 0 in. (0 mm); aspect ratio = 6:5 sealant = dry</p>								

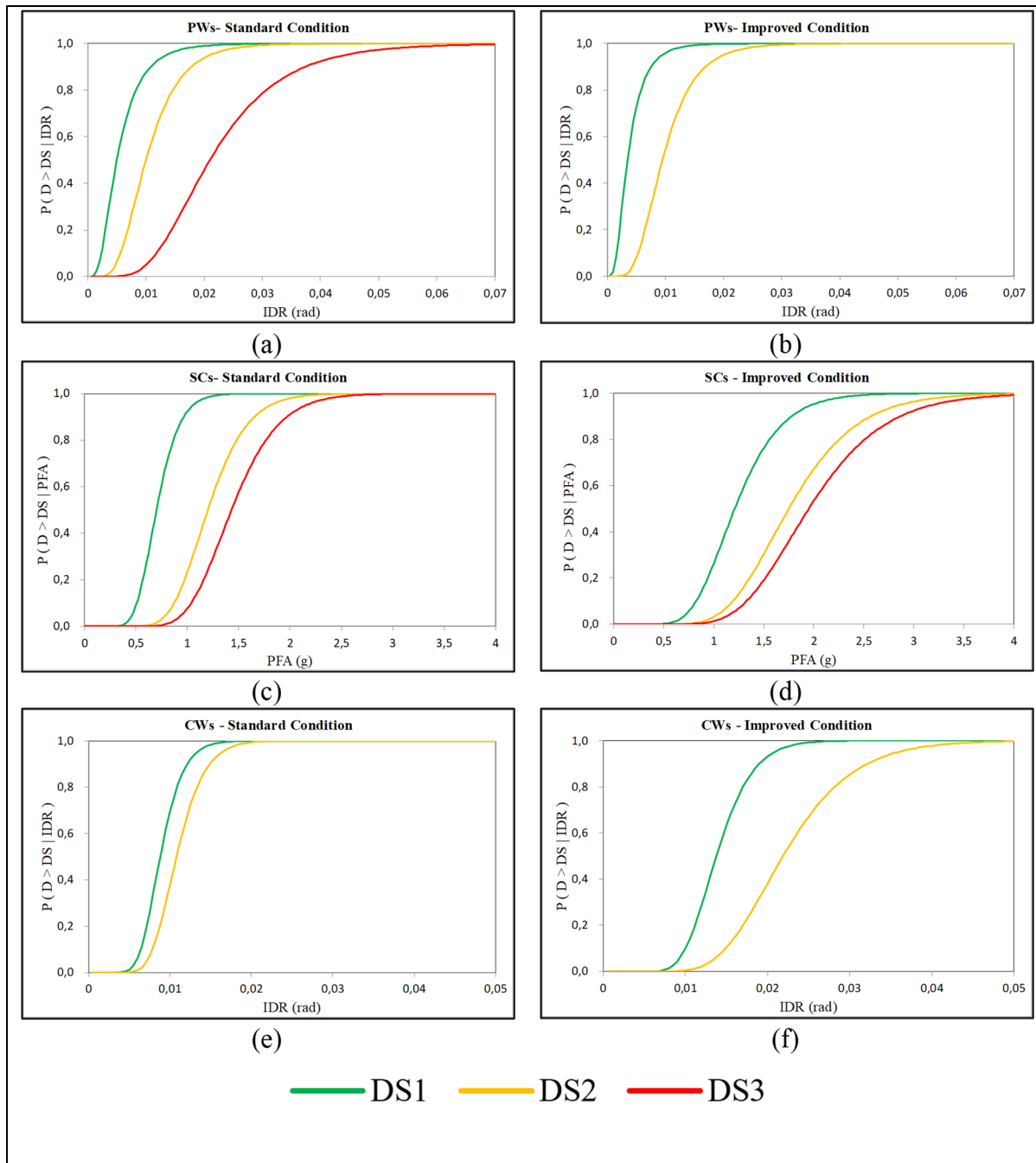


Figure 3.6 Fragility curves for standard and improved conditions of selected PWs (a) and (b); SCs (c) and (d); CWs (e) and (f)
Taken from Fragility Specification Manager of FEMA P-58 (2011)

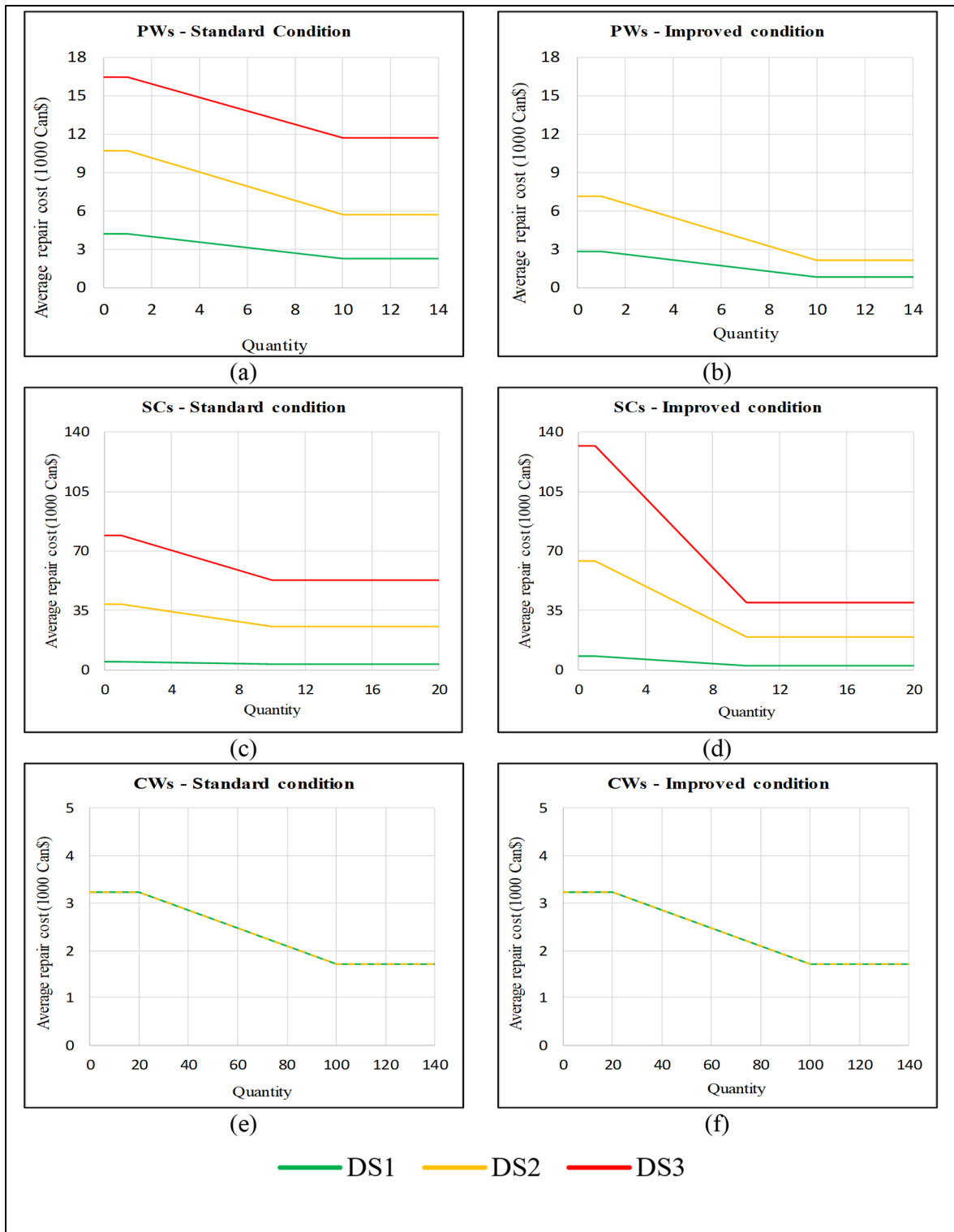


Figure 3.7 Consequences functions for standard and improved conditions of selected PWs, SCs, and CWs
 Taken from Fragility Specification Manager of FEMA P-58 (2011)

3.6 Results of loss estimation before and after improving the connection details

In this section, the impact of connection details on repair costs for PWs, SCs, and CWs is examined using the performance assessment calculation tool (PACT). Furthermore, an evaluation of the distribution of repair costs along the building height is conducted. Through PACT, loss estimation results can be categorized and exported by floors, directions, and performance groups. Figure 3.8 illustrates the impact of connection detail improvement on the total repair costs (including all floors and directions) for each selected architectural components, considering various earthquake intensities. To capture a comprehensive intensity measure in both building directions, the geometric mean of spectral acceleration of the two principal directions at the building's first mode period is utilized (Equation 3.1).

$$S_a(T_1) = \sqrt{S_a^X(T_1) \times S_a^Y(T_1)} \quad (3.1)$$

Where: $S_a^X(T_1), S_a^Y(T_1)$: Spectral acceleration at the 1st modal period of building in each of the principal directions. ($T_1^X = 1.935s$ and $T_1^Y = 2.169s$)

PWs contribute more to the repair costs compared to SCs and CWs, because of the high susceptibility of PWs to damage even at relatively small earthquakes, (20% probability of occurrence in 50 years), while SCs and CWs experience slight damages at earthquakes with moderate earthquakes 10% and 5% probabilities of occurrence in 50 years, (Figure 3.8-a, b, and c). DS1 in PWs occurs at an IDR of 0.1% to 0.2%, while DS2 occurs at approximately 0.35% IDR (in standard condition). For CWs, DS1 is triggered within the range of 0.35% to 0.4% IDR. The median for the lognormal distribution of damage states is higher for CWs than PWs (Table 3.3). Furthermore, consequences functions show that the average repair cost for PWs is notably higher than that for CWs, especially in the standard condition. Improved connection details generally reduce repair costs, except for PWs at low and moderate earthquake intensities. Results show that for IDR values below 0.35% in X-direction and 0.47% in Y-direction, the standard condition sustained fewer repair cost compared to the improved condition. Nevertheless, as the earthquake intensity increases, the repair cost in the improved condition decreases. For the specified design ground motion intensity (2% probability of occurrence in 50 years), the repair cost is reduced by 30% for PWs, 84% for

SCs, and 100% for CWs compared to standard connections. Figures 3.8-d, 3.8-e, and 3.8-f present the impact of connection details on the loss ratio (the repair cost of each NSC divided by the total replacement cost of the building), showing a decrease for PWs, SCs, and CWs when connection details are improved. The loss ratio decreases from 0.46% to 0.32% for PWs, from 0.31% to 0.05% for SCs, and from 0.19% to 0.00% for CWs at design-based earthquake ($S_a(T1) = 0.175g$).

Figures 3.8-g, 3.8-h, and 3.8-i depict the architectural components repair ratio (the repair cost of each component relative to its maximum probable repair cost), indicating a decrease when using improved condition. The ratios decrease from 6.63% to 4.72% for PWs, from 3.92% to 0.61% for SCs, and from 1.66% to 0.00% for CWs at design-based earthquake ($S_a(T1) = 0.175g$).

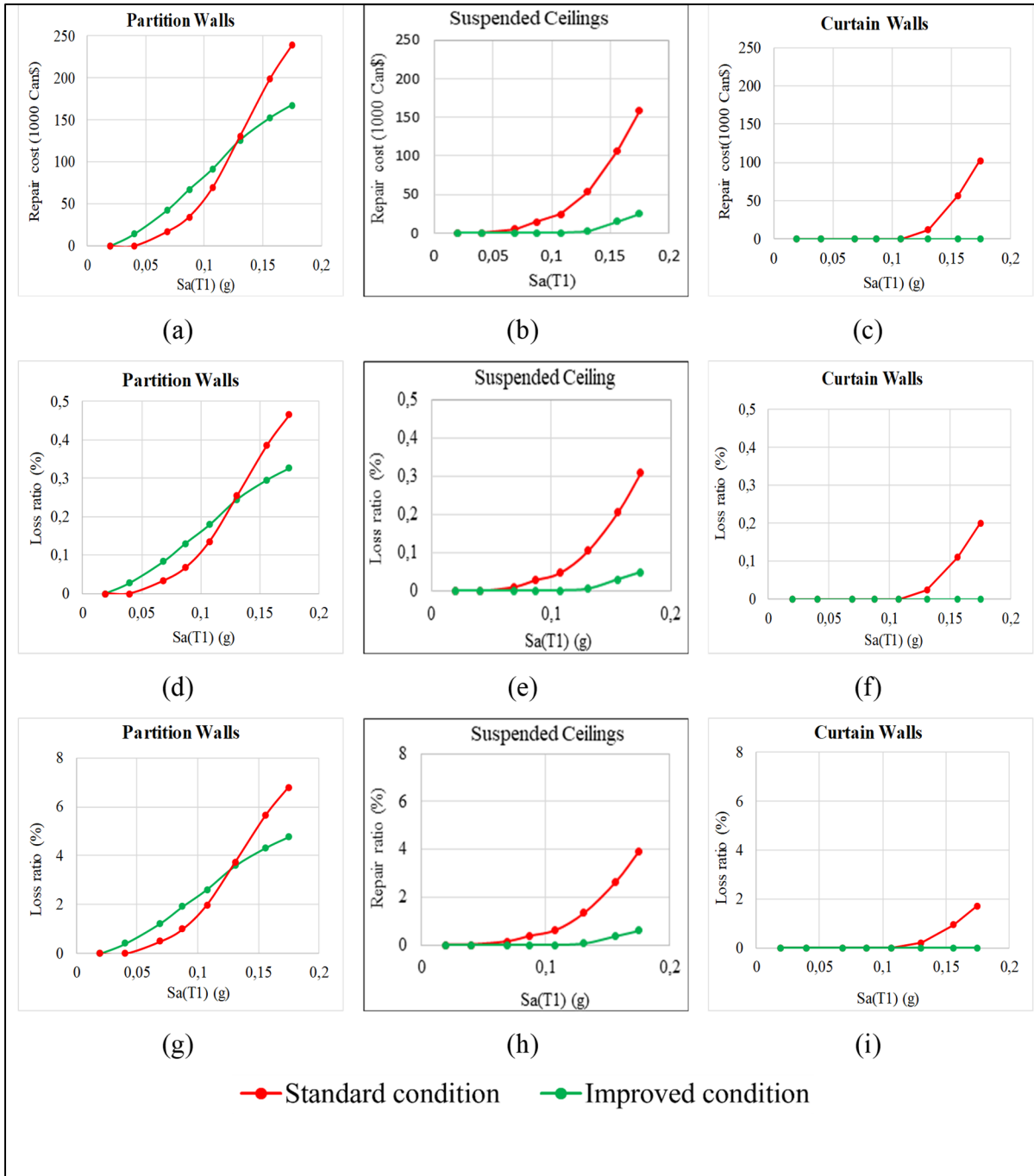


Figure 3.8 Total Repair cost: a) PWs; b) SCs; c) CWs; Loss ratio: c) PWs; d) SCs; e) CWs; Repair ratio: f) PWs; g) SCs; h) CWs; based on spectral acceleration at the fundamental period of the building

Figure 3.9 displays the distribution of repair costs along the building's height for the selected architectural components. As previously mentioned, PWs and CWs are primarily sensitive to

IDR. Therefore, they exhibit higher repair costs on the upper floors. Conversely, SCs are sensitive to PFA. Consequently, lower repair costs for SCs were observed in the middle floors compared to the lower and upper thirds. Repair costs are mainly concentrated in the upper third of the building, contributing to at least 52% of the total loss resulting from the failure of the three selected architectural components during a design-based earthquake (2%/50 years). As the earthquake intensity decreases, the contribution of the upper part to NSC repair costs becomes more pronounced, except for CWs, which show no losses for lower intensities. For the design-based earthquake (2% in 50 years, $S_a(T1)=0.175g$), PWs located in the upper third account for 52% of repair costs, while the middle third contributes 36%, and the lower third accounts for 12%. SCs attribute 16% to the middle third, 25% to the lower third, and 59% to the upper floors. CWs exhibit 82% of repair costs in the upper third and 18% in the middle third.

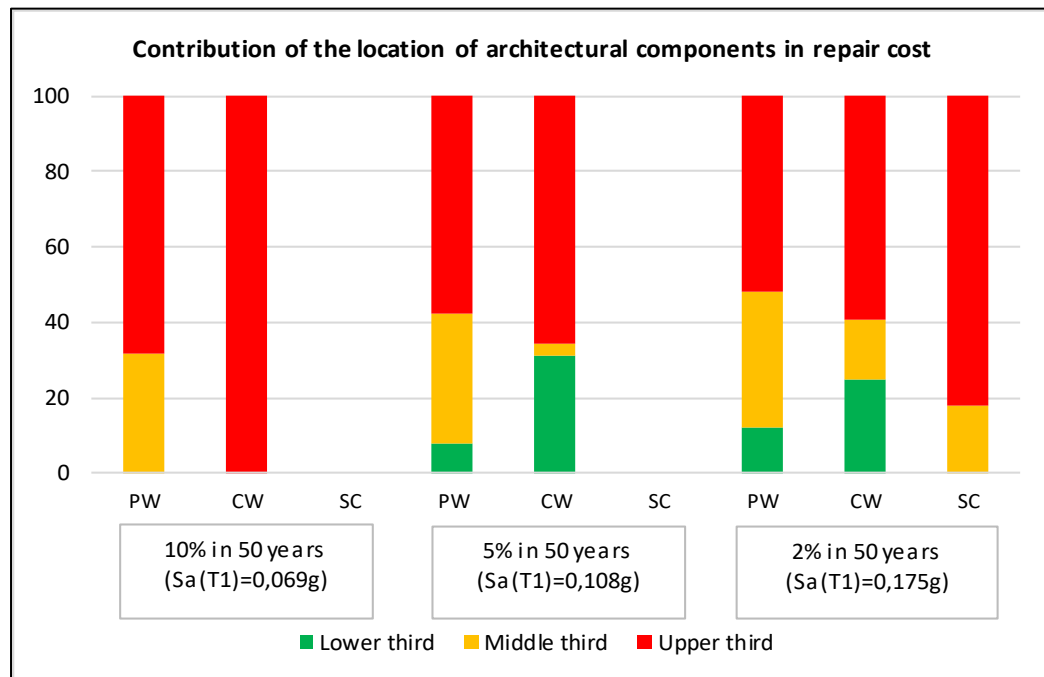


Figure 3.9 Effect of Location of architectural components on their contribution to repair cost

3.7 Conclusion

This paper assesses the impact of connection details on building repair costs in a 12-story code-compliant building located in Montreal on site class-D for three commonly used architectural components: PWs, SCs, and CWs. The study focuses on the reduction in repair costs resulting from improved connection conditions. Additionally, it examines the vertical distribution of repair cost along the building's height using the FEMA P-58 methodology.

Among the selected architectural components, PWs experience the highest repair costs due to their vulnerability even in code-conforming buildings at low to moderate earthquakes. Damage requiring repair in PWs is observed at a maximum IDR of 0.13% in the X-direction and 0.16% in the Y-direction, induced by an earthquake event with $S_a(T1) = 0.040g$ (20% probability of occurrence in 50 years). The provided quantitative loss estimation shows that improving connection details decreases repair costs by up to 30% for PWs, 84% for SCs, and 100% for CWs at design-based earthquake level. Loss distribution along the building height directly correlates with the building response parameters. Therefore, higher estimated losses in drift-sensitive NSCs occur in the upper third, while acceleration-sensitive NSCs exhibit lower losses in the middle third due to the S-shaped variation in PFA. In general, the upper third sustains the most significant portion of the loss at design-based earthquakes level ($S_a(T1) = 0.175g$), as it constitutes over 50% of the repair cost for PWs, approximately 60% for SCs, and 82% for CWs. Additionally, among the selected architectural components, within the lower third, the most vulnerable component is the SCs, which incurs more than 20% of its total replacement cost.

This study investigated only one mid-rise building with a specific structural system and located in a particular soil class condition. To enhance the study's applicability, further research should consider different building heights, lateral load-resisting systems, site class, and evaluate the impact of connection improvement on other NSCs such as electrical and mechanical NSCs, and building contents, using the performance-based approach to see if similar observations can be drawn.

CONCLUSIONS

This project examined the effect of EDPs estimation method on the building repair cost as well as the impact of connection details of three commonly used architectural components on building repair costs in a 12-story code-compliant building located on site class D in Montreal. The main focus of this study is to assess the reduction in repair costs associated with the improved connection condition of partition walls, suspended ceilings, and curtain walls in the building. Additionally, the study highlighted the vertical distribution of repair cost along the building's height as a fraction of the overall repair costs computed based on FEMA P-58 methodology. The objectives are achieved by analysing the quantity of damaged components, caused by the building's response to a range of seismic excitations, using selected component fragility curves, and estimating the repair cost associated with such damage through consequence functions. The conclusions are limited to the selected case study building and the mentioned assumptions.

Based on the numerical investigations in chapter 2 related to the comparative analysis of EDP prediction methods and corresponding losses, the following conclusions can be made:

- There is a direct correlation between the calculated EDPs and their corresponding repair cost. While increasing the earthquake intensity, the value of EDPs will be larger, therefore, the building will experience more damages. Consequently, it is logical to have more repair cost. The relation of earthquake intensity and repair cost is not proportional and linear. By increasing EDPs the repair cost increases exponentially.
- At design based earthquake with 2% probability of occurrence in 50 years with $S_a(T1)=0.098g$ (NBC, 2015), the repair cost due to the EDPs calculated through code NBC 2015 is more conservative compared to other methods, and the FEMA P-58 leads to the lowest repair cost.
- Considering the effect of nonlinearity significantly impacts on the predicted EDPs, especially PFA, it is concluded that the EDPs obtained from the simplified analysis utilizing the simplified method outlined in FEMA P-58 better align with nonlinear response analysis conducted in previous studies (Abouda, 2022; Boivin 2006). The

maximum variation of IDR and PFA from nonlinear analyses are 27% and 66%, respectively.

- While the PFA estimated using ASCE 7-22 properly considers the effects of non-linearity and closely aligns with the results of previous non-linear analyses, but the estimated IDR by this method is still more conservative compared to the IDR obtained from non-linear analysis. Consequently, the estimated repair cost of drift-sensitive architectural components using the IDR from ASCE 7-22 is higher than the resulting repair cost from the FEMA P-58 method.
- It is observed that variations in estimated repair costs between different methods become more evident at higher seismic intensities, particularly during seismic events with a 2% probability of occurrence in 50 years. At this intensity, the predicted repair cost using EDPs from FEMA P-58 is 29.9k Can\$, however this value increases to 630k Can\$, and 1205.1k Can\$ while using EDPs calculated by the ASCE 7-22, and NBC 2015 methods, respectively.

Based on the analysis of connection details impacts on the predicted losses presented in chapter 3, the following conclusions can be made:

- Among the selected architectural components, partition walls incurred the highest repair costs. This is due to the fact that even in buildings designed and constructed according to code requirements, partition walls can sustain damage in relatively low to moderate earthquakes. In this study, it is observed that the damage requiring repair in partition walls was initiated at a maximum IDR of 0.13% in the X direction and 0.16% in the Y direction. These IDR values are induced by an earthquake event with $S_a(T1) = 0.040g$ (NBC, 2020), which is associated with a 20% probability of occurrence within a 50-year
- The provided quantitative loss estimation demonstrated that improving the connections leads to a decrease in repair costs for partition walls, suspended ceilings, and curtain walls by up to 30%, 84%, and 100% (at design-based earthquake), respectively.

Based on the assessment of the loss distribution along the height in chapter 3, the following conclusions can be made:

- In this study, due to the increasing IDR along the building height, the estimated repair cost in drift-sensitive architectural components is higher in the upper third of the building (59% of total repair cost of these components) compared to the middle (34%) and lower (7%) thirds, respectively.
- The contribution of the middle third to the resulting repair cost of acceleration-sensitive architectural components is lower than that of the lower third as a result of the S-shaped variation in PFA along the building height. The upper third experiences the most significant part of the repair cost.
- In design-based earthquakes ($S_a(T1) = 0.175g$ according to NBC 2020 hazard curves), the upper third portion of a building contributes more than 50% of the repair cost for partition walls, approximately 60% of the repair cost for suspended ceilings, and over 80% of the repair cost for curtain walls.
- Within the lower third of the building's height, the most vulnerable component among the selected architectural components is the suspended ceiling, which incurs more than 20% of its total repair cost.
- The findings underscore the critical importance of achieving more accurate predictions for EDP. Such accuracy significantly impacts the realistic estimation of repair cost distribution along building height. This estimation, in turn, offers invaluable guidance and serves as a benchmark for developing repair sequence models and strategic planning of repair operations.

RECOMMENDATIONS

This study investigated only one mid-rise building with a specific structural system and located in a particular soil class condition. To enhance the study's applicability the following items are recommended for further research:

- Further research should consider different building heights. Although changing the building height may not change the pattern of variation of EDPs, but it impacts on the values of EDPs, then the same NSCs can experience more or less damages, especially at top floors.
- Different lateral load-resisting systems can be considered in the future. Because lateral load-resisting system can significantly impact on building response, therefore the repair cost varies by considering different structural systems.
- Soil condition will affect directly on seismic intensity and hazard analysis. So, considering different site class will change building responses, damages in NSCs, and the corresponding repair cost.
- This study focuses on three typically used architectural components. This approach can be used to quantify the impact of mitigation actions and connection improvements on the repair cost reduction of other NSCs such as electrical and mechanical components, as well as building contents. Using different NSCs with different fragility curves and repair cost consequences functions can lead to more comprehensive results.
- It would be important to focus on different occupancies and population models in the further studies. Because the types of NSCs and their quantities are related to the building occupancy. Obviously changing the type and quantity of a NSCs can impact significantly on the estimated repair cost.
- Indirect economic loss which are expressed by factors such as repair time and business interruption can significantly impact on the economic loss which worth to be studied to investigate if similar observations can be drawn.

APPENDIX I

CALCULATION OF EDPs USING SIMPLIFIED ANALYSIS BASED ON ASCE 7 METHOD

This Appendix shows the steps of calculation of IDR and PFA using ASCE 7 method explained in the literature review. The following spectrum has been used in the analysis. This is Montreal site class D spectrum based on NBC 2015 hazard calculation tool.

IDR prediction :

To estimate the displacement and drift, the distributed lateral forces should be calculated using the equivalent lateral force procedure outlined in ASCE7-22. These forces can then be applied to a linear static model to obtain the floor displacement and story drift ratio, denoted as Δ_i .

The equivalent lateral force is the product of the spectral acceleration at the design period (T_a) multiplied by the building seismic weight (W). In addition, the capacity of the system to resist against earthquake is taken into account by dividing applicable force by response modification coefficient and multiplying it by the importance factor (I_e). (Equation AI.1)

To calculate the design earthquake force, V , superior limits are specified for building's fundamental period. These depend on the structural system and are in place to prevent the selection of non-conservative seismic forces resulting from long periods. However, considering seismic forces based on these upper period limits could result in excessive lateral displacements. Therefore, to compute lateral displacement and story drift, it is permissible to use lateral force with relaxed upper limits for the building period.

$$V = \frac{S_a W}{\left(\frac{R}{I_e}\right)} \quad (\text{A I-1})$$

The calculated equivalent static seismic force is distributed throughout the height of the building using Equation AI.2.

$$F_x = V \times \frac{W_x h_x^k}{\sum_{i=1}^n W_i h_i^k} \quad (\text{A I-2})$$

Where:

F_x : seismic load at level x

W_x and W_i : effective seismic weight at level x and i

h_x and h_i : elevation of level x and i from the ground level

For the structures with a period of 0.5 s or less, $k=1$, and for the ones with a period of 2.5 s or more, $k=2$. In case of having a period between 0.5 s and 2.5 s, k could be 2 or be determined by linear interpolation between 1 and 2. (ASCE 7-22)

Finally, to account for inelastic effects, the displacement obtained from the equivalent lateral force procedure is modified by multiplying it with the deflection amplification factor (C_d) and dividing it by the importance factor (I_e).

PFA prediction :

According to Article 13.3.1 of ASCE7-22, non-structural components, with some exceptions based on the seismic design category (SDC), are required to withstand the effects of horizontal seismic design forces, F_p , in the most vulnerable direction. The calculation for this force is provided in Equation AI.3.

$$0.3S_{DS}I_pW_p \leq F_p = 0.4S_{DS}I_pW_p \left(\frac{H_f}{R_\mu} \right) \left(\frac{C_{AR}}{R_{po}} \right) \leq 1.6S_{DS}I_pW_p \quad (\text{A I-3})$$

Where:

F_p : Seismic design force

S_{DS} : 5% damped site-specific spectral acceleration at short period

I_p : Component importance factor (1.0 or 1.5)

W_p : Component operating weight

H_f : Force amplification factor, calculated in equation AI.4.

R_μ : Structure ductility reduction factor, calculated in equation AI.8.

C_{AR} : Component resonance ductility factor, which converts PFA or PGA into the peak component acceleration

R_{po} : Component strength factor

$$H_f = 1 + a_1 \frac{z}{H} + a_2 \left(\frac{z}{H} \right)^{10} \quad (\text{A I-4})$$

Where:

$$a_1 = 1/T_a \leq 2.5 \quad (\text{A I-5})$$

$$a_2 = \left(1 - \left(0.4/T_a\right)^2\right) \geq 0 \quad (\text{A I-6})$$

z: Height of the point of the attachment of the component above the base of the structure

H: Average roof height of structure from the base

T_a: Lowest fundamental period of the supporting building in either orthogonal direction. It can be calculated through Equation AI.7.

$$T_a = C_t h_n^x \quad (\text{A I-7})$$

Where the values of C_t and x are depended to the structure type. For concrete shear wall structures are equal to 0.0488 and 0.75, respectively.

$$R_\mu = \left(\frac{1.1R}{I_e \Omega_0}\right)^{1/2} \geq 1.3 \quad (\text{A I-8})$$

Where:

I_e: building importance factor

R: Building response modification factor

Ω₀: building overstrength factor

In the Equation AI.3, the product of 0.4S_{DS}H_f can be regarded as estimated elastic peak floor acceleration at the point of attachment of the NSC. And 0.4 S_{DS} represents the design peak ground horizontal acceleration. To take into account the effect of nonlinearity and to have inelastic PFA, 0.4S_{DS}H_f shall be divided by structure ductility reduction factor R_μ.

Table A I-1 Montreal site class D spectral accelerations (g) based on NBC 2015 seismic hazard values

Spec. Acc.	Modified Sa(T)		
	2% in 50 years	10% in 50 years	40% in 50 years
S _a (0.05)	0.595	0.253	0.077
S _a (0.1)	0.595	0.253	0.077
S _a (0.2)	0.594	0.253	0.077
S _a (0.5)	0.372	0.156	0.051
S _a (1.0)	0.194	0.080	0.028
S _a (2.0)	0.092	0.038	0.011
S _a (5.0)	0.025	0.008	0.002
S _a (10.0)	0.008	0.003	0.001
S _a (T _{1x})	0.108	0.044	0.014
S _a (T _{1y})	0.089	0.036	0.011

Table A I-2 Lateral distribution of shear force along building height using ASCE 7 equivalent static procedure

floor	h _i (m)	W _i (kN)	X		Y		2%in 50years		10%in 50years		40%in 50years	
			W _i .h _i ^k (kN.m)	W _i .h _i ^k / Σ W _i .h _i ^k	W _i .h _i ^k (kN.m)	W _i .h _i ^k / Σ W _i .h _i ^k	F _x	F _y	F _x	F _y	F _x	F _y
12	45	8264	4856476	0,211	8596133	0,222	258,6	359,2	105,6	145,4	32,5	42,4
11	41,35	7489	3819621	0,166	6675621	0,172	203,4	278,9	83,0	112,9	25,6	32,9
10	37,7	7489	3271867	0,142	5639580	0,145	174,2	235,6	71,1	95,4	21,9	27,8
9	34,05	7489	2758799	0,120	4683145	0,121	146,9	195,7	60,0	79,2	18,5	23,1
8	30,4	7489	2281587	0,099	3807747	0,098	121,5	159,1	49,6	64,4	15,3	18,8
7	26,75	7489	1841582	0,080	3015017	0,078	98,1	126,0	40,0	51,0	12,3	14,9
6	23,1	7489	1440369	0,063	2306831	0,059	76,7	96,4	31,3	39,0	9,6	11,4
5	19,45	7489	1079852	0,047	1685397	0,043	57,5	70,4	23,5	28,5	7,2	8,3
4	15,8	7489	762385	0,033	1153382	0,030	40,6	48,2	16,6	19,5	5,1	5,7
3	12,15	7489	491009	0,021	714127	0,018	26,1	29,8	10,7	12,1	3,3	3,5
2	8,5	7489	269899	0,012	372060	0,010	14,4	15,5	5,9	6,3	1,8	1,8
1	4,85	7817	110067	0,005	139482	0,004	5,9	5,8	2,4	2,4	0,7	0,7
sum	45	90971	22983513	1	38788522	1	1223,9	1620,7	499,6	655,9	153,8	191,4

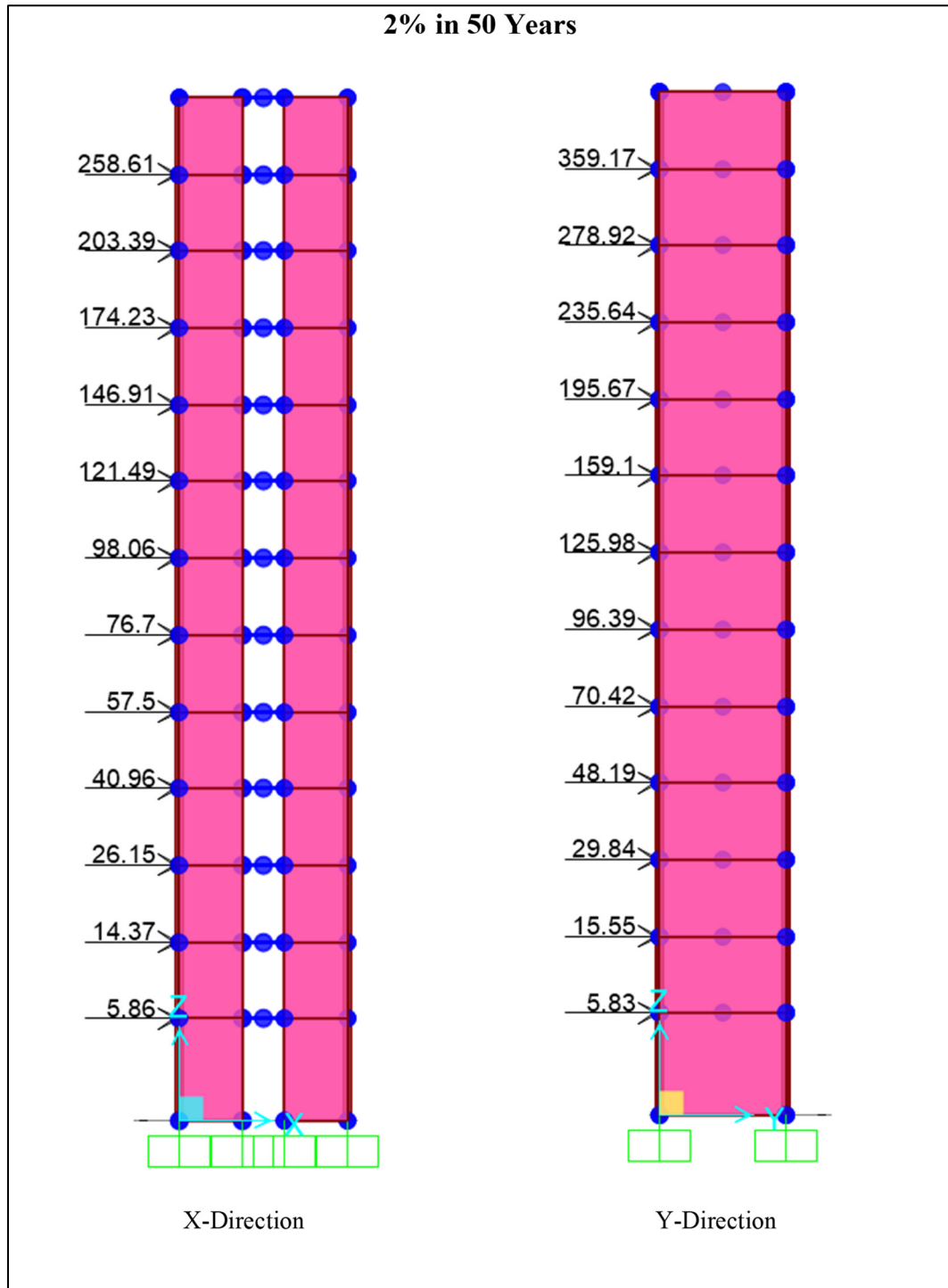


Figure A I-1 Applied lateral distributed shear force due to 2% in 50 years earthquake in SAP2000 to calculate corresponding IDR

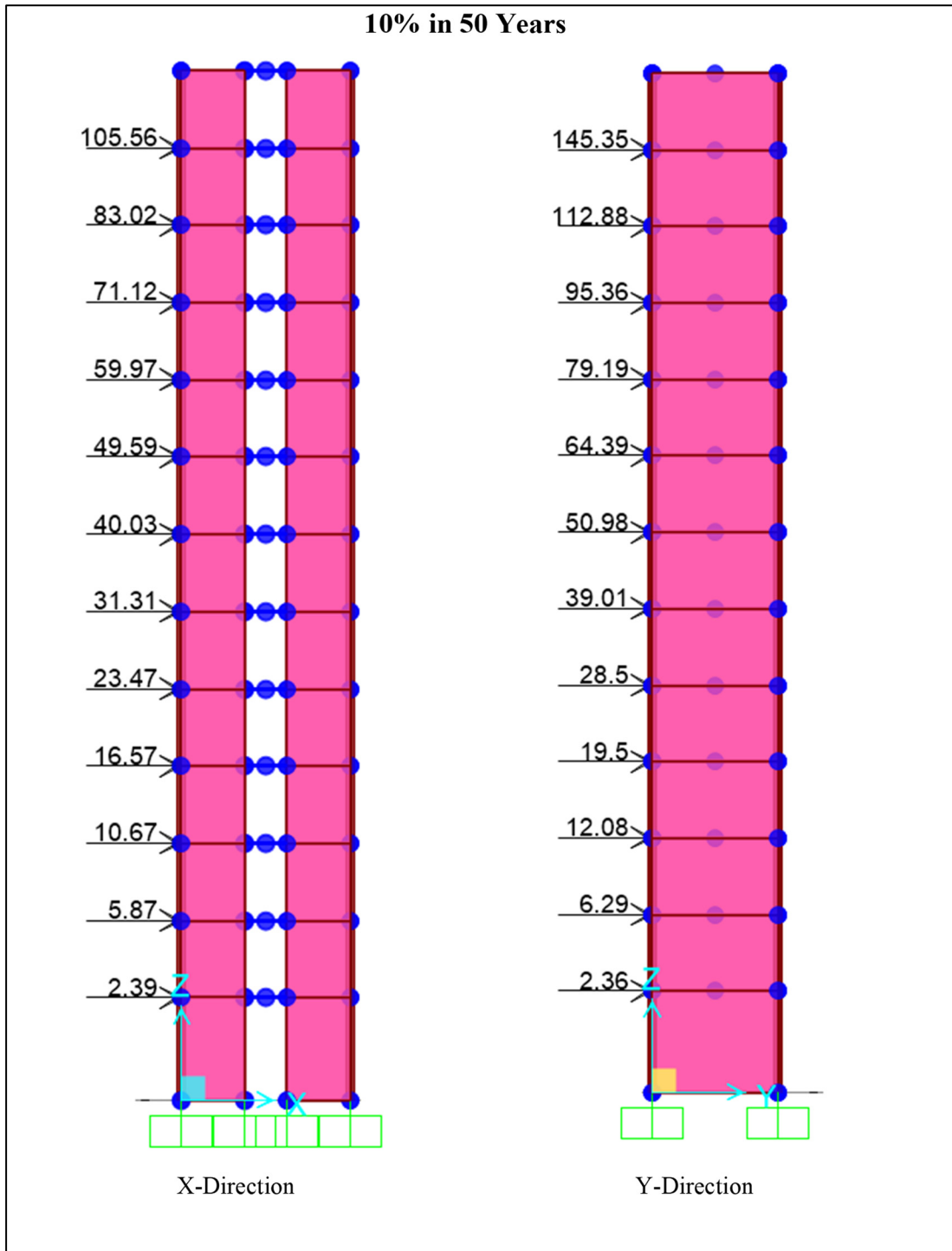


Figure A I-2 Applied lateral distributed shear force due to 10% in 50 years earthquake in SAP2000 to calculate corresponding IDR

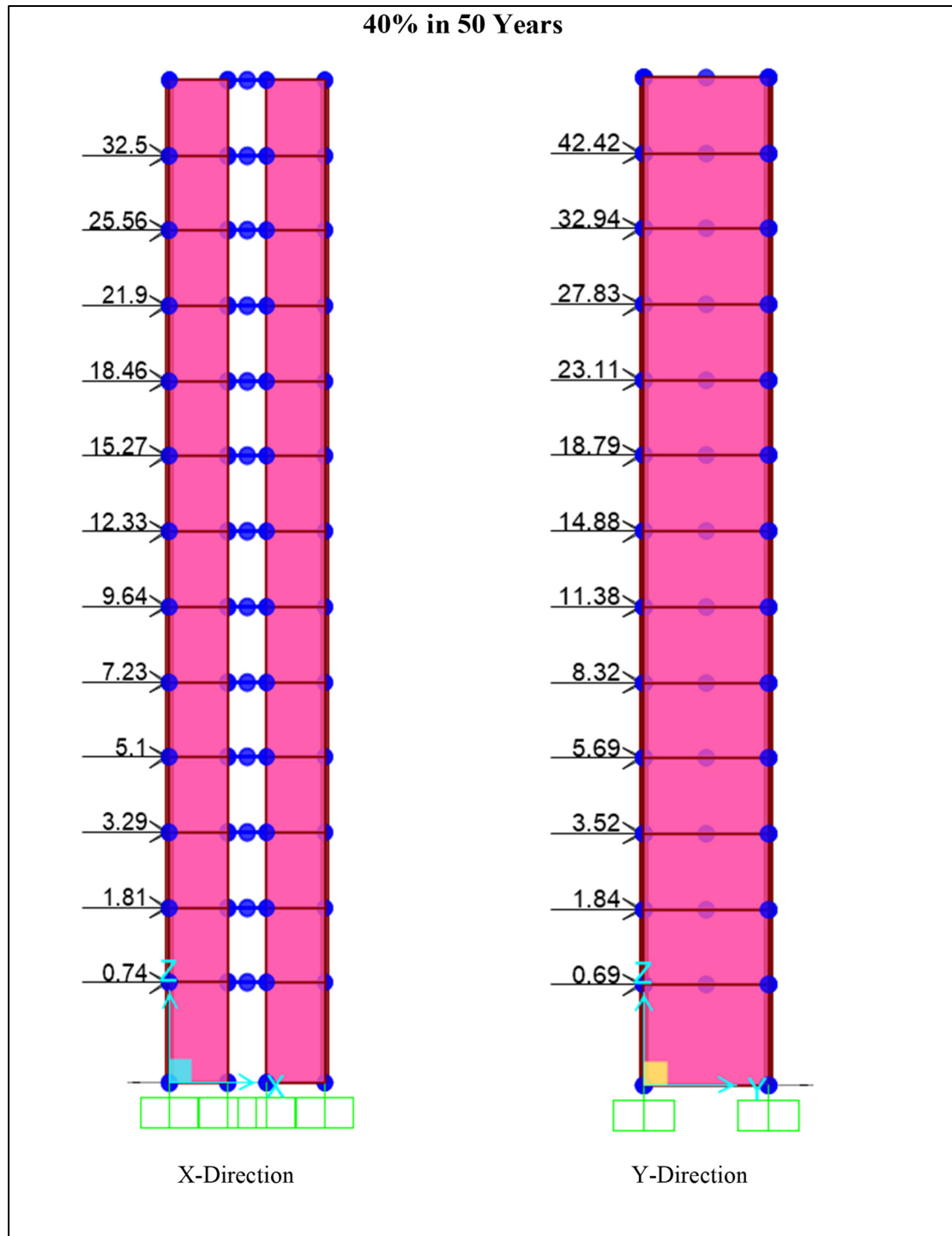


Figure A I-3 Applied lateral distributed shear force due to 40% in 50 years earthquake in SAP2000 to calculate corresponding IDR

Table A I-3 IDR obtained from linear static model created in SAP2000

SAP2000 results						
IDR	2%in 50years		10%in 50years		40%in 50years	
	Drift x	Drift y	Drift x	Drift y	Drift x	Drift y
12	0.0047	0.0070	0.0019	0.0028	0.0005	0.0008
11	0.0049	0.0070	0.0020	0.0028	0.0006	0.0008
10	0.0051	0.0069	0.0021	0.0028	0.0006	0.0008
9	0.0052	0.0068	0.0021	0.0027	0.0006	0.0008
8	0.0052	0.0065	0.0021	0.0026	0.0006	0.0007
7	0.0052	0.0062	0.0021	0.0025	0.0006	0.0007
6	0.0050	0.0057	0.0020	0.0023	0.0006	0.0006
5	0.0047	0.0051	0.0019	0.0020	0.0005	0.0006
4	0.0042	0.0043	0.0017	0.0017	0.0005	0.0005
3	0.0036	0.0034	0.0014	0.0014	0.0004	0.0004
2	0.0028	0.0024	0.0011	0.0009	0.0003	0.0002
1	0.0012	0.0010	0.0005	0.0004	0.0001	0.00012

Table A I-4 PFA (g) considering the height modification factor defined in ASCE 7-22

h _x (m)	H _f	acceleration(g)		
		40%in50	10%in50	2%in50
45	2.963	1.117	0.388	0.109
41.35	2.746	1.035	0.359	0.101
37.7	2.540	0.957	0.332	0.093
34.05	2.343	0.883	0.307	0.086
30.4	2.157	0.813	0.282	0.079
26.75	1.980	0.746	0.259	0.073
23.1	1.814	0.684	0.237	0.067
19.45	1.659	0.625	0.217	0.061
15.8	1.513	0.570	0.198	0.056
12.15	1.377	0.519	0.180	0.051
8.5	1.252	0.472	0.164	0.046
4.85	1.137	0.428	0.148	0.042
0	1	0.377	0.131	0.037

APPENDIX II

CALCULATION OF EDPs USING SIMPLIFIED ANALYSIS BASED ON METHOD OF NBC 2015

This Appendix shows the steps of calculation of IDR and PFA using NBC 2015 method explained in the literature review.

IDR prediction :

According to the equivalent static procedure, the design earthquake force, V , depends on seismic force demand which is a product of the design spectrum at the design period (T_a) multiplied by the building seismic weight (W). Additionally, the capacity of the system to resist earthquakes is considered. This is achieved by dividing the applicable force by the ductility-related (R_d) and overstrength-related (R_o) force modification factors, and then multiplying by the importance factor (I_E) and higher mode factor (M_v) as it is indicated in Equation A II.1. The values of R_d , R_o , and I_E are presented at Table A II-1.

Table A II-1 Ductility- and overstrength-related force modification factors, Importance factor, and seismic weight of building

	X	Y
R_d	4	3.5
R_o	1.7	1.6
I_E	1	
Weight	90975 kN	

To calculate the design earthquake force, V , upper limits are specified for the building's fundamental period. These limits depend on the structural system and aim to prevent the selection of non-conservative seismic forces resulting from long periods. However, using seismic forces based on these upper period limits may lead to excessive lateral displacements. Therefore, for computing lateral displacement and story drift, it is permissible to employ lateral forces with relaxed superior limits for the building period.

Calculated seismic force, V , need not to exceed $\frac{2}{3}$ of the value calculated at $T=0.2$ s, and calculated value at $T=0.5$ s. Also, it must not be less than the value calculated at $T=2.0$ s.

$$V = \frac{S(T_a)M_v I_E W}{R_d R_o} \quad (\text{A II-1})$$

The calculated equivalent static seismic force is distributed over the height of the building by the Equation A II.2.

$$F_x = (V - F_t) \frac{W_x h_x}{\sum_{i=1}^n W_i h_i} \quad (\text{A II-2})$$

Where:

F_x : seismic load at level x

F_t : concentrated load at the top level to consider higher mode effects

If $T_a \geq 0.7$ s then $F_t = 0.07T_a V \leq 0.25V$

W_x and W_i : seismic weight at level x and i

h_x and h_i : elevation of level x and i from the ground level (NBC 2015)

Finally, to consider inelastic effects, the displacement obtained from equivalent static force procedure, shall be modified by multiplying it by ductility- and overstrength-related force modification factor ($R_d.R_o$), and dividing by importance factor (I_E).

PFA prediction

According to the section 5.3.3.1 of the CSA S832-14 (CSA, 2014), All the restraints and connections of operational and functional components (OFC or NSC) must be designed to withstand a minimum amount of lateral force, V_p , (equation AII.3) determined in accordance with NBC Article 4.1.8.18.

$$V_p = 0.3F_a S_a(0.2) I_E S_p W_p \quad (\text{A II-3})$$

Where:

F_a : acceleration-based site coefficient

$S_a(0.2)$: spectral response acceleration at period of 0.2 seconds

I_E : earthquake importance factor for the building

S_p : horizontal force factor for non-structural component, which can be calculated by equation AII.4.

W_p : weight of non-structural component

$$S_p = \frac{C_p A_r A_x}{R_p} \quad \text{with } 0.7 \leq S_p \leq 4.0 \quad (\text{A II-4})$$

Where:

C_p : non-structural component factor to take into consideration the likelihood of component failure.

A_r : dynamic amplification factor of non-structural component.

A_x : height factor which can be calculated by equation 13. It represents the amplification of acceleration at each level which NSC is attached, and it varies from 1.0 at the base to 3.0 at the rooftop.

R_p : response modification factor of non-structural component, which indicate energy dissipation of the component and its attachment.

$$A_x = 1 + 2 \frac{h_x}{h_n} \quad (\text{A II-5})$$

Where:

h_x : height above the base of the structure to level x

h_n : total height of the structure

In this method the product of $0.3F_a S_a(0.2)A_x$ can be regarded as the estimated peak floor horizontal acceleration at the point of attachment for NSC and the product of $0.3F_a S_a(0.2)$ represents design peak ground horizontal acceleration

Table A II-2 First vibration periods (s) in the X and Y principal directions

h_n	45 m
T_a	0.87 s
T_{1x} SAP	1.85 s
T_{1y} SAP	2.15 s
period limit ($2T_a$)	$2 \times 0.87 = 1.74$ s

The following spectrum has been used in the analysis. This is Montreal site class D spectrum based on NBC 2015 hazard calculation tool.

Table A II-1 Spectral accelerations (g)
and higher mode factor

Spec. Acc.	Modified Sa(T)		
	2% in 50	10% in 50	40% in 50
S _a (0.05)	0.595	0.253	0.077
S _a (0.1)	0.595	0.253	0.077
S _a (0.2)	0.594	0.253	0.077
S _a (0.5)	0.372	0.156	0.051
S _a (1.0)	0.194	0.080	0.028
S _a (2.0)	0.092	0.038	0.011
S _a (5.0)	0.025	0.008	0.002
S _a (10.0)	0.008	0.003	0.001
S(0.2)/S(5.0)	23.4	32.1	48.7
M _{v x}	1	1	1
M _{v y}	1.18	1.18	1.18
S(T _{1x})	0.108	0.044	0.014
S(T _{1y})	0.089	0.036	0.011

Table A II-2 Calculating base shear and controlling with the determined
limits at NBC 2015

	Base Shear	2% in 50	10% in 50	40% in 50
Calculated	V _x	1439.846	587.736	180.966
	V _y	1707.501	691.021	201.656
$max_1 = \frac{2}{3} \times \frac{S_a(0.2) \times M_v \times I_E}{R_d \times R_0} \times W$	V _x	5301.780	2254.075	832.637
	V _y	7596.694	3229.768	982.512
$max_2 = \frac{S_a(0.5) \times M_v \times I_E}{R_d \times R_0} \times W$	V _x	4972.886	2092.651	688.332
	V _y	7125.435	2998.47	986.282
$min = \frac{S_a(2.0) \times M_v \times I_E}{R_d \times R_0} \times W$	V _x	1236.532	502.104	147.031
	V _y	1771.774	719.444	210.675
Final	V _x	1439.846	587.736	180.966
	V _y	1771.774	719.444	210.675

Table A II-3 Calculating increased shear force of top floor due to higher mode effect and controlling with the specified limit of NBC 2015

Calculated	F_{tx}	175.115	71.480	22.009
	F_{ty}	215.484	87.499	25.622
max	$F_{tx\ max}$	359.961	146.934	45.241
	$F_{ty\ max}$	442.943	179.861	52.668
final	F_{tx}	175.115	71.480	22.009
	F_{ty}	215.484	87.499	25.622

Table A II- 4 Distributed shear forces along building height

floor	h_i (m)	W_i (kN)	$W_i \cdot h_i$ (kN.m)	$W_{ih_i} / \sum W_{ih_i}$	2%in 50years		10%in 50years		40%in 50years	
					F_x	F_y	F_x	F_y	F_x	F_y
12	45	8264	371880	0,163	381,72	469,72	155,82	190,73	47,98	55,85
11	41,35	7489	309670	0,136	172,05	211,71	70,23	85,97	21,62	25,17
10	37,7	7489	282335	0,124	156,86	193,02	64,03	78,38	19,71	22,95
9	34,05	7489	255000	0,112	141,67	174,33	57,83	70,79	17,81	20,73
8	30,4	7489	227666	0,100	126,49	155,64	51,63	63,20	15,90	18,51
7	26,75	7489	200331	0,088	111,30	136,96	45,43	55,61	13,99	16,29
6	23,1	7489	172996	0,076	96,11	118,27	39,23	48,02	12,08	14,06
5	19,45	7489	145661	0,064	80,93	99,58	33,03	40,44	10,17	11,84
4	15,8	7489	118326	0,052	65,74	80,89	26,83	32,85	8,26	9,62
3	12,15	7489	90991	0,040	50,55	62,21	20,64	25,26	6,35	7,40
2	8,5	7489	63657	0,028	35,37	43,52	14,44	17,67	4,44	5,17
1	4,85	7817	37912	0,017	21,06	25,92	8,60	10,52	2,65	3,08
sum	45	90971	2276426	1	1439,85	1771,77	587,74	719,44	180,97	210,68

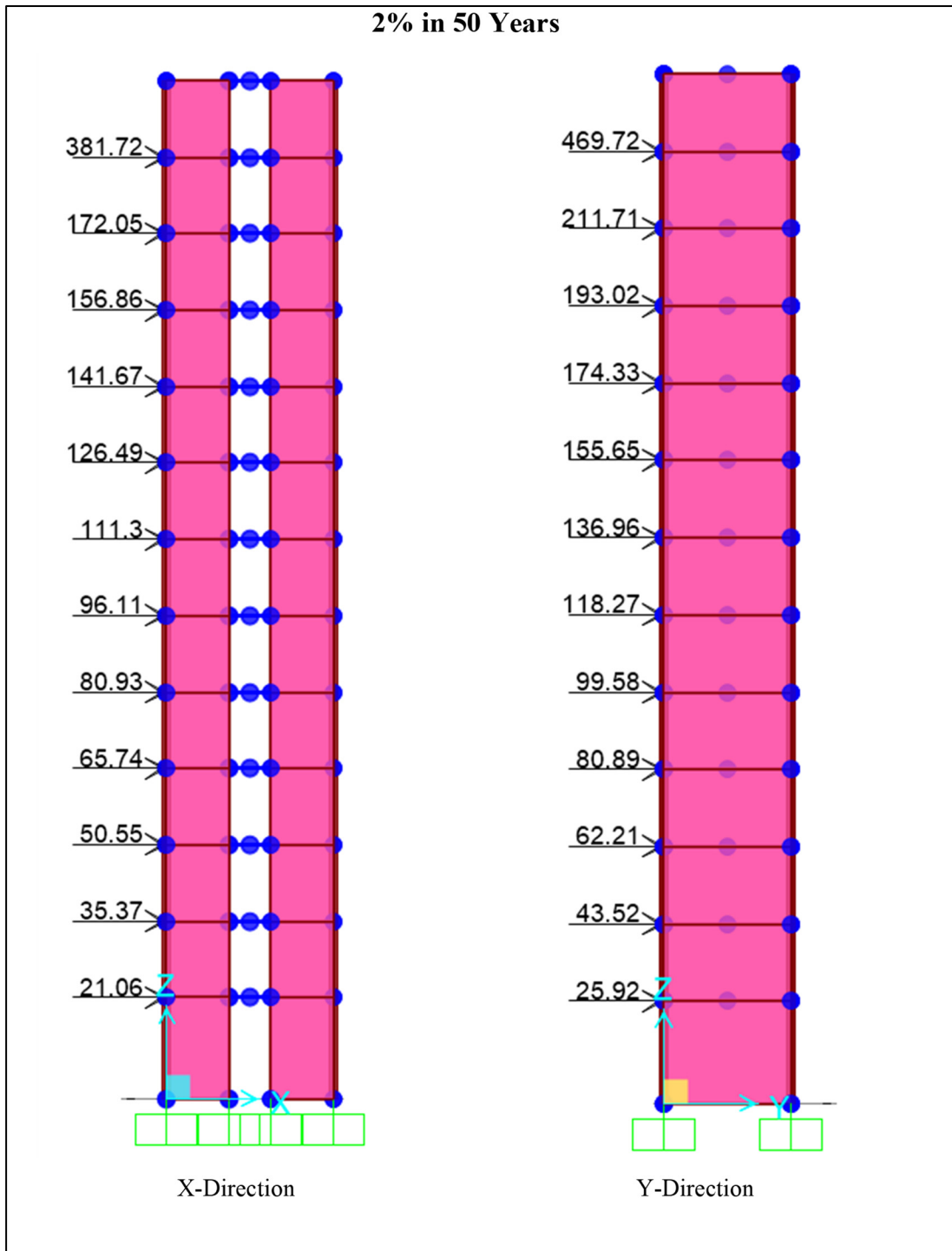


Figure A II-1 Applied lateral distributed shear force due to 2% in 50 years earthquake in SAP2000 to calculate corresponding IDR

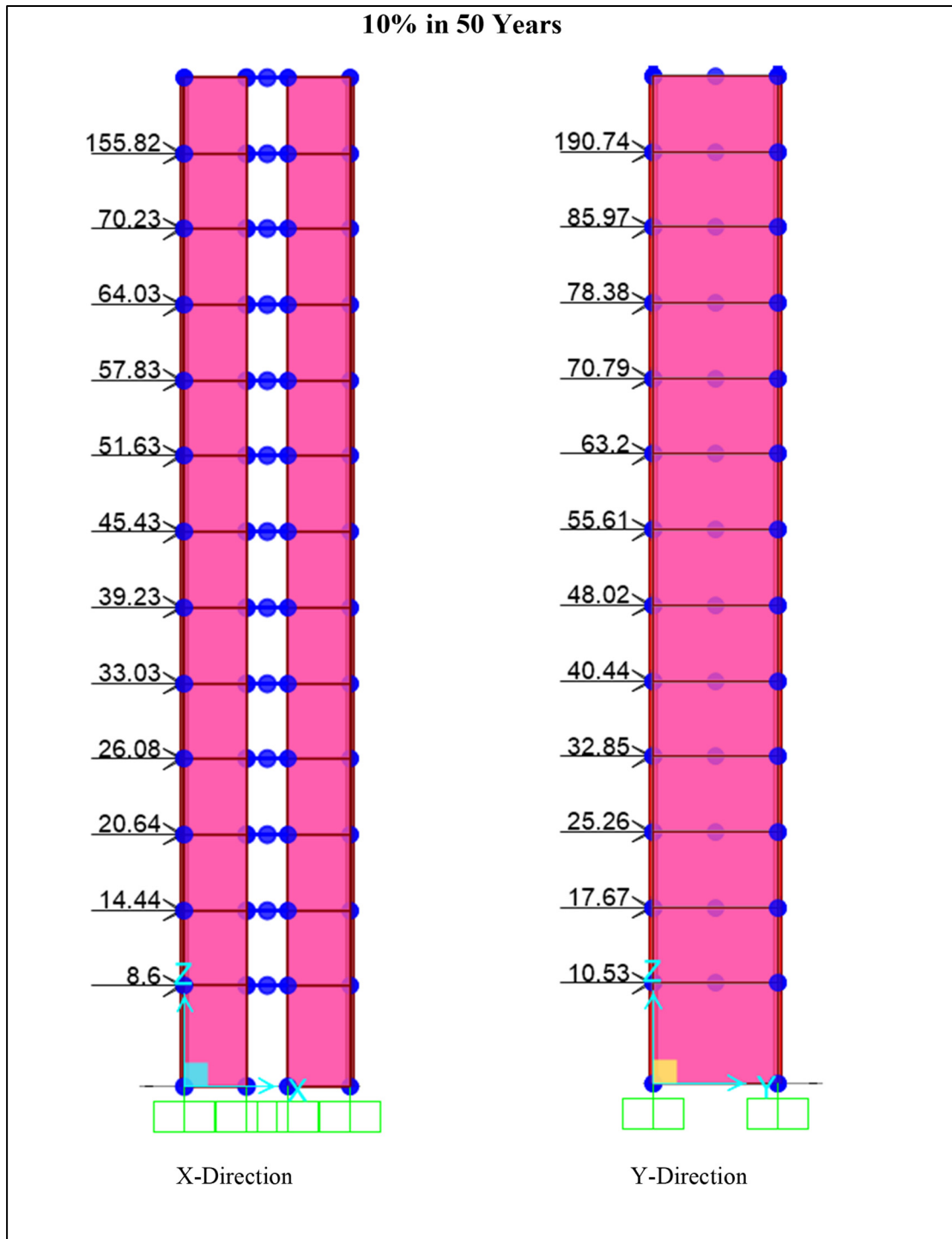


Figure A II-2 Applied lateral distributed shear force due to 10% in 50 years earthquake in SAP2000 to calculate corresponding IDR

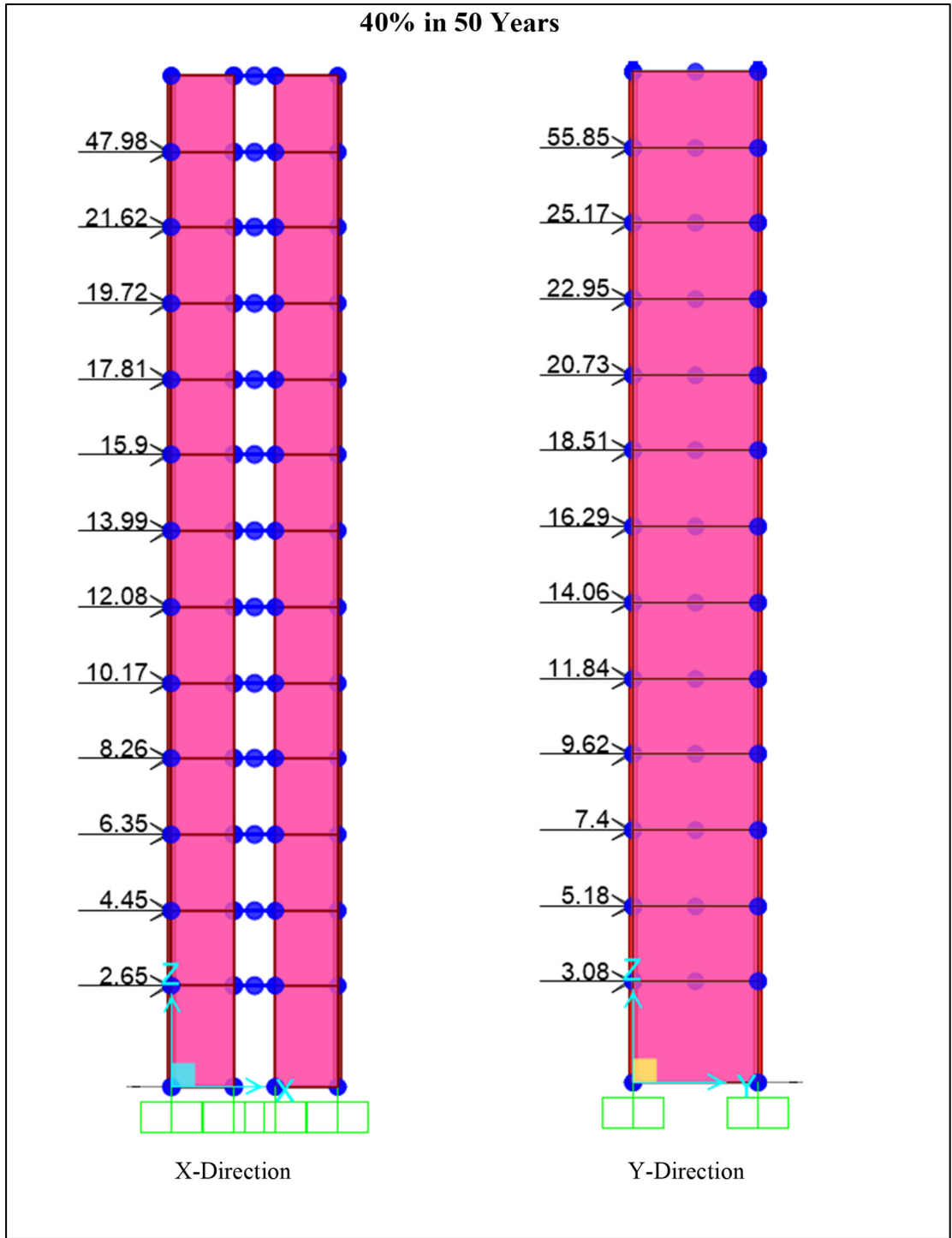


Figure A II-3 Applied lateral distributed shear force due to 40% in 50 years earthquake in SAP2000 to calculate corresponding IDR

Table A II-5 IDR obtained from linear static model created in SAP2000

SAP2000 results						
IDR	2%in 50years		10%in 50years		40%in 50years	
	Drift x	Drift y	Drift x	Drift y	Drift x	Drift y
12	0.0046	0.0081	0.0018	0.0033	0.0005	0.0009
11	0.0048	0.0081	0.0019	0.0032	0.0006	0.0009
10	0.0049	0.0080	0.0020	0.0032	0.0006	0.0009
9	0.0050	0.0078	0.0020	0.0031	0.0006	0.0009
8	0.0050	0.0075	0.0020	0.0030	0.0006	0.0008
7	0.0049	0.0071	0.0020	0.0029	0.0006	0.0008
6	0.0047	0.0065	0.0019	0.0026	0.0006	0.0007
5	0.0045	0.0058	0.0018	0.0023	0.0005	0.0007
4	0.0041	0.0050	0.0016	0.0020	0.0005	0.0006
3	0.0035	0.0040	0.0014	0.0016	0.0004	0.0004
2	0.0027	0.0028	0.0011	0.0011	0.0003	0.0003
1	0.0012	0.0012	0.0005	0.0004	0.0001	0.0001

Table A II-6 PFA (g) considering the height modification factor defined in NBC 2015

h _x (m)	A _x	acceleration(g)		
		40%in50	10%in50	2%in50
45	3.00	1.13	0.39	0.11
41.35	2.84	1.07	0.37	0.10
37.7	2.68	1.01	0.35	0.10
34.05	2.51	0.95	0.33	0.09
30.4	2.35	0.89	0.31	0.09
26.75	2.19	0.83	0.29	0.08
23.1	2.03	0.76	0.27	0.07
19.45	1.86	0.70	0.24	0.07
15.8	1.70	0.64	0.22	0.06
12.15	1.54	0.58	0.20	0.06
8.5	1.38	0.52	0.18	0.05
4.85	1.22	0.46	0.16	0.04
0	1.00	0.38	0.13	0.04

APPENDIX III

CALCULATION OF EDPs USING SIMPLIFIED ANALYSIS BASED ON EQUIVALENT LATERAL FORCE METHOD OF FEMA P-58

This Appendix shows the steps of calculation of IDR and PFA using equivalent lateral force method of FEMA P-58 explained in the literature review. The following spectrum has been used in the analysis. This is Montreal site class D spectrum based on NBC 2015 (for 1st specific objective of study) and NBC 2020 (for 2nd and 3rd objectives of study) hazard calculation tool.

IDR prediction :

In the first step the pseudo lateral force, V , is needed to be calculated using following equation:

$$V = C_1 C_2 S_a(T_1) W_1 \quad (\text{A III-1})$$

Where:

C_1 : adjustment factor for inelastic response, for $T_1 > 1.0$ sec is equal to 1.0.

C_2 : adjustment factor for cyclic degradation, for $T_1 > 0.7$ sec is equal to 1.0.

$S_a(T_1)$: 5% damped spectral acceleration at the fundamental period of the building.

W_1 : the first modal effective weight in the considered direction (not less than 80% of the total weight)

Next step is to determine the vertical distribution of pseudo lateral forces at each level x (F_x), by the following equation:

$$F_x = C_{vx} V \quad (\text{A III-2})$$

In which, C_{vx} is a vertical distribution factor.

$$C_{vx} = \frac{w_x h_x^k}{\sum_{i=2}^{N+1} w_i h_i^k} \quad (\text{A III-3})$$

Where:

w_i : lumped weight at each floor level i .

h_i (or h_x): height above the effective base of the building for level i (or x). Figure A III-1.

k: a constant equal to 2.0 for a first mode period greater than 2.5 s, or equal to 1.0 for a first mode period less than 0.5 s. and for other periods between 0.5 s and 2.5 s can be linearly interpolated.

In the next step, in order to compute modified story drift ratios by considering the inelastic behavior and higher mode effects, Δ_i^* , first the distributed lateral forces are applied to a linear static model to obtain floor displacement and uncorrected story drift ratio, Δ_i . Then Δ_i^* will be calculated by equation (A III-4).

$$\Delta_i^* = H_{\Delta i}(S, T_1, h_i, H) \times \Delta_i \quad (\text{A III-4})$$

Where:

$$\ln(H_{\Delta i}) = a_0 + a_1 T_1 + a_2 S + a_3 \frac{h_{i+1}}{H} + a_4 \left(\frac{h_{i+1}}{H}\right)^2 + a_5 \left(\frac{h_{i+1}}{H}\right)^3 \quad (\text{A III-5})$$

for $S \geq 1, i = 1 \text{ to } N$

And:

$$S = \frac{S_a(T_1) \times W}{V_{y1}} \quad (\text{A III-6})$$

Where:

S: Strength ratio

W: total weight

V_{y1} : first mode response estimated yield strength. The elastic design coefficients for structural system and occupancy of buildings, V_{y1} can be estimated using pushover analysis or can be considered by the inferior and superior limits indicated in (A III-7). In this study average of inferior and superior limits is considered.

$$\frac{1.5S_a(T)W}{R/I} \leq V_{y1} \leq \frac{\Omega_0 S_a(T)W}{R/I} \quad (\text{A III-7})$$

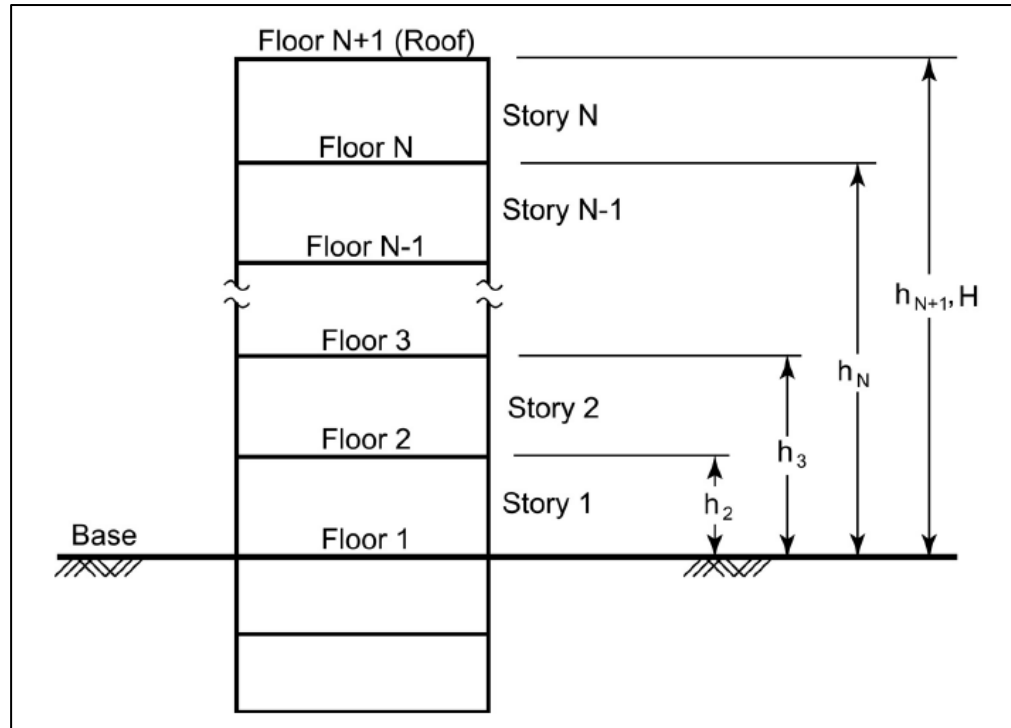


Figure A III-1 Definition of floor levels and heights, and storey numbers
Taken from FEMA P-58-1 (2018)

PFA prediction

Peak floor acceleration (PFA), a_i^* , can be derived from peak ground acceleration (PGA) by means of the following equation:

$$a_i^* = H_{\Delta i}(S, T_1, h_i, H) \times PGA \quad (\text{A III-8})$$

Where:

$$\ln(H_{\Delta i}) = a_0 + a_1 T_1 + a_2 S + a_3 \frac{h_{i+1}}{H} + a_4 \left(\frac{h_{i+1}}{H} \right)^2 + a_5 \left(\frac{h_{i+1}}{H} \right)^3 \quad (\text{A III-9})$$

for $S \geq 1, i = 2 \text{ to } N + 1$

The values of the coefficient a_0 to a_5 are chosen based on the number of stories and structural system of the frames in each direction and are indicated in the Table A III-1.

Table A III-1 Correction factors for story drift ratio and floor acceleration for 10-story to 15-story buildings with wall frame type (FEMA P58-1, 2018)

demand	a ₀	a ₁	a ₂	a ₃	a ₄	a ₅
Story drift ratio	0.86	-0.036	-0.076	-4.58	6.88	-3.24
Floor acceleration	-0.13	-0.15	-0.10	7.79	-17.52	11.04

To carry out performance evaluation using this procedure, the results obtained from simplified analysis need to be adjusted to account for uncertainties in ground motion intensity, β_{gm} , modeling, β_m , and computed displacement and acceleration (record to record variability), $\beta_{a\Delta}$ and β_{aa} . The values of these dispersions depend on the first modal period and strength ratio and can be obtained from table 5.6 of the FEMA P-58-1 (2018). The total dispersion values for drift, β_{SD} , and acceleration, β_{FA} , are calculated using the following equations. (FEMA P-58-1, 2018)

$$\beta_{SD} = \sqrt{\beta_{a\Delta}^2 + \beta_m^2} \quad (\text{A III-10})$$

$$\beta_{FA} = \sqrt{\beta_{aa}^2 + \beta_m^2} \quad (\text{A III-11})$$

Table A III-2 Utilized spectral accelerations based on NBC 2015 seismic hazard values

Spec. Acc.	Modified S _a (T)		
	2% in 50 years	10% in 50 years	40% in 50 years
S _a (0.05)	0.595	0.253	0.077
S _a (0.1)	0.595	0.253	0.077
S _a (0.2)	0.594	0.253	0.077
S _a (0.5)	0.372	0.156	0.051
S _a (1.0)	0.194	0.080	0.028
S _a (2.0)	0.092	0.038	0.011
S _a (5.0)	0.025	0.008	0.002
S _a (10.0)	0.008	0.003	0.001
PGA [g]	0.377	0.131	0.037
S _a (T _{1x})	0.108	0.044	0.014
S _a (T _{1y})	0.089	0.036	0.011

Table A III-3 Calculating lateral force distribution coefficient

floor	h_i (m)	W_i (kN)	$W_i h_i^k$ (x)	$W_i h_i^k$ (y)	C_{vx}	C_{vy}
12	45	8264	163872576	633993531,4	0,17	0,17
11	41,35	7489	127683691	486742204,5	0,13	0,13
10	37,7	7489	116412942	443777052,2	0,12	0,12
9	34,05	7489	105142193	400811899,9	0,11	0,11
8	30,4	7489	93871444	357846747,7	0,10	0,10
7	26,75	7489	82600695	314881595,4	0,09	0,09
6	23,1	7489	71329946	271916443,1	0,08	0,07
5	19,45	7489	60059197	228951290,9	0,06	0,06
4	15,8	7489	48788448	185986138,6	0,05	0,05
3	12,15	7489	37517699	143020986,3	0,04	0,04
2	8,5	7489	26246950	100055834,1	0,03	0,03
1	4,85	7817	16091033	61736206,93	0,02	0,02
0	0		0	0	0	0
sum	45	90971	949616816	3629719931	1	1

Table A III-4 Distributed lateral force along building height

floor	2%		10%		40%	
	F_x	F_y	F_x	F_y	F_x	F_y
12	1351,677	1132,318	551,746	458,247	169,885	133,727
11	1053,178	869,3262	429,901	351,814	132,369	102,668
10	960,214	792,590	391,953	320,759	120,684	93,605
9	867,249	715,854	354,005	289,704	108,999	84,542
8	774,284	639,118	316,058	258,649	97,316	75,480
7	681,319	562,382	278,110	227,595	85,631	66,417
6	588,354	485,645	240,162	196,539	73,947	57,355
5	495,389	408,909	202,215	165,485	62,263	48,292
4	402,424	332,173	164,267	134,429	50,579	39,230
3	309,459	255,437	126,319	103,375	38,894	30,167
2	216,494	178,701	88,371	72,320	27,210	21,105
1	132,724	110,262	54,177	44,623	16,681	13,022

Table A III-5 Obtained IDR due to distributed lateral force from linear static model using SAP2000

floor	2%		10%		40%	
	Δ_x	Δ_y	Δ_x	Δ_y	Δ_x	Δ_y
12	0,0034	0,0049	0,0014	0,0020	0,0004	0,0006
11	0,0035	0,0049	0,0014	0,0020	0,0004	0,0006
10	0,0036	0,0048	0,0015	0,0020	0,0005	0,0006
9	0,0037	0,0047	0,0015	0,0019	0,0005	0,0006
8	0,0038	0,0046	0,0015	0,0019	0,0005	0,0005
7	0,0037	0,0044	0,0015	0,0018	0,0005	0,0005
6	0,0036	0,0040	0,0015	0,0016	0,0005	0,0005
5	0,0034	0,0036	0,0014	0,0015	0,0004	0,0004
4	0,0031	0,0031	0,0013	0,0013	0,0004	0,0004
3	0,0027	0,0025	0,0011	0,0010	0,0003	0,0003
2	0,0021	0,0018	0,0009	0,0007	0,0003	0,0002
1	0,0010	0,0007	0,0004	0,0003	0,0001	0,0001

Table A III-6 Calculated IDR modification factor based on FEMA P-58

floor	2%		10%		40%	
	$H_{\Delta i}(x)$	$H_{\Delta i}(y)$	$H_{\Delta i}(x)$	$H_{\Delta i}(y)$	$H_{\Delta i}(x)$	$H_{\Delta i}(y)$
12	0,595	0,628	0,742	0,754	0,824	0,824
11	0,612	0,645	0,762	0,775	0,847	0,846
10	0,611	0,645	0,762	0,775	0,846	0,846
9	0,601	0,634	0,749	0,762	0,832	0,832
8	0,588	0,620	0,732	0,744	0,813	0,813
7	0,577	0,608	0,719	0,731	0,798	0,798
6	0,574	0,605	0,715	0,727	0,795	0,794
5	0,586	0,618	0,730	0,742	0,811	0,811
4	0,620	0,653	0,772	0,785	0,858	0,857
3	0,686	0,723	0,854	0,869	0,949	0,949
2	0,802	0,846	1,000	1,017	1,111	1,110
1	1,004	1,059	1,251	1,272	1,389	1,389

Table A III-9 Modified PFA based on FEMA P-58 due to seismic input obtained from NBC 2015 spectra

floor	2%		10%		40%	
	PFA _x	PFA _y	PFA _x	PFA _y	PFA _x	PFA _y
12	0,570	0,593	0,265	0,262	0,086	0,083
11	0,390	0,406	0,181	0,179	0,059	0,057
10	0,316	0,329	0,147	0,145	0,048	0,046
9	0,293	0,305	0,136	0,135	0,044	0,043
8	0,301	0,313	0,140	0,138	0,045	0,044
7	0,328	0,342	0,152	0,151	0,049	0,048
6	0,369	0,384	0,171	0,170	0,056	0,054
5	0,412	0,428	0,191	0,189	0,062	0,060
4	0,441	0,458	0,205	0,203	0,066	0,064
3	0,436	0,454	0,203	0,201	0,066	0,064
2	0,386	0,402	0,179	0,178	0,058	0,056
1	0,294	0,306	0,137	0,135	0,044	0,043
0	0,377	0,377	0,131	0,131	0,037	0,037

Table A III-10 Seismic inputs based on NBC 2020 seismic hazard tool

Probability (% in 50 years)	2%	2,50%	3,50%	5%	7%	10%	14%	20%	30%	40%
S _a (0.00) [g]	0,797	0,706	0,585	0,483	0,412	0,341	0,278	0,216	0,152	0,113
S _a (0.05) [g]	0,797	0,706	0,585	0,483	0,412	0,341	0,278	0,216	0,152	0,113
S _a (0.1) [g]	0,797	0,706	0,585	0,483	0,412	0,341	0,278	0,216	0,152	0,113
S _a (0.2) [g]	0,797	0,706	0,585	0,483	0,412	0,341	0,278	0,216	0,152	0,113
S _a (0.3) [g]	0,664	0,599	0,524	0,448	0,382	0,316	0,259	0,202	0,143	0,107
S _a (0.5) [g]	0,579	0,531	0,460	0,391	0,332	0,273	0,221	0,172	0,122	0,091
S _a (1.0) [g]	0,347	0,313	0,265	0,220	0,182	0,146	0,116	0,089	0,062	0,046
S _a (2.0) [g]	0,165	0,147	0,123	0,101	0,082	0,064	0,050	0,037	0,025	0,018
S _a (5.0) [g]	0,046	0,041	0,033	0,026	0,021	0,016	0,012	0,008	0,005	0,004
S _a (10.0) [g]	0,014	0,013	0,010	0,008	0,006	0,005	0,004	0,003	0,002	0,001
PGA [g]	0,481	0,427	0,354	0,298	0,258	0,215	0,177	0,138	0,096	0,070
PGV [m/s]	0,413	0,371	0,313	0,258	0,213	0,169	0,133	0,100	0,069	0,050
S _a (T _{1x} =1.85s)	0,192	0,172	0,144	0,119	0,097	0,076	0,060	0,045	0,031	0,022
S _a (T _{1y} =2.15s)	0,159	0,142	0,118	0,097	0,079	0,062	0,048	0,036	0,024	0,017
S _a =sqrt[S _a (T _{1x} =1.85s) xS _a (T _{1y} =2.15s)]	0,175	0,156	0,131	0,108	0,087	0,069	0,054	0,040	0,027	0,020

Table A III-11 Calculating lateral force distribution coefficient

floor	h_i (m)	W_i (kN)	$W_i h_i^k$ (x)	$W_i h_i^k$ (y)	C_{vx}	C_{vy}
12	45	8264	1.6E+08	633993531	0.17	0.17
11	41.35	7489	1.3E+08	486742204	0.13	0.13
10	37.7	7489	1.2E+08	443777052	0.12	0.12
9	34.05	7489	1.1E+08	400811900	0.11	0.11
8	30.4	7489	9.4E+07	357846748	0.10	0.10
7	26.75	7489	8.3E+07	314881595	0.09	0.09
6	23.1	7489	7.1E+07	271916443	0.08	0.07
5	19.45	7489	6E+07	228951291	0.06	0.06
4	15.8	7489	4.9E+07	185986139	0.05	0.05
3	12.15	7489	3.8E+07	143020986	0.04	0.04
2	8.5	7489	2.6E+07	100055834	0.03	0.03
1	4.85	7817	1.6E+07	61736207	0.02	0.02
0	0		0	0	0.00	0.00
sum	45	90971	9.5E+08	3.63E+09	1	1

Table A III-14 Calculated IDR based on obtained displacement due to distributed lateral force from linear static model using SAP2000

floor	SITE CLASS D															
	2%		2,5%		3,5%		5%		7%		10%		20%		40%	
	Δ_x	Δ_y	Δ_x	Δ_y	Δ_x	Δ_y	Δ_x	Δ_y	Δ_x	Δ_y	Δ_x	Δ_y	Δ_x	Δ_y	Δ_x	Δ_y
12	0,0060	0,0087	0,0054	0,0078	0,0045	0,0065	0,0037	0,0053	0,0030	0,0043	0,0024	0,0034	0,0014	0,0020	0,0007	0,0010
11	0,0063	0,0087	0,0056	0,0078	0,0047	0,0065	0,0039	0,0053	0,0032	0,0043	0,0025	0,0034	0,0015	0,0020	0,0007	0,0010
10	0,0065	0,0086	0,0058	0,0077	0,0049	0,0064	0,0040	0,0053	0,0033	0,0043	0,0026	0,0034	0,0015	0,0019	0,0008	0,0009
9	0,0066	0,0085	0,0059	0,0075	0,0050	0,0063	0,0041	0,0052	0,0033	0,0042	0,0026	0,0033	0,0016	0,0019	0,0008	0,0009
8	0,0067	0,0082	0,0060	0,0073	0,0050	0,0061	0,0041	0,0050	0,0034	0,0041	0,0027	0,0032	0,0016	0,0018	0,0008	0,0009
7	0,0067	0,0078	0,0060	0,0069	0,0050	0,0058	0,0041	0,0048	0,0034	0,0038	0,0026	0,0030	0,0016	0,0018	0,0008	0,0009
6	0,0065	0,0072	0,0058	0,0064	0,0049	0,0054	0,0040	0,0044	0,0033	0,0036	0,0026	0,0028	0,0015	0,0016	0,0007	0,0008
5	0,0061	0,0065	0,0055	0,0058	0,0046	0,0048	0,0038	0,0040	0,0031	0,0032	0,0024	0,0025	0,0014	0,0015	0,0007	0,0007
4	0,0056	0,0056	0,0050	0,0050	0,0042	0,0041	0,0035	0,0034	0,0028	0,0028	0,0022	0,0022	0,0013	0,0013	0,0007	0,0006
3	0,0049	0,0045	0,0044	0,0040	0,0037	0,0033	0,0030	0,0027	0,0025	0,0022	0,0019	0,0017	0,0011	0,0010	0,0006	0,0005
2	0,0038	0,0032	0,0034	0,0028	0,0029	0,0024	0,0024	0,0019	0,0019	0,0016	0,0015	0,0012	0,0009	0,0007	0,0004	0,0003
1	0,0017	0,0013	0,0015	0,0012	0,0013	0,0010	0,0011	0,0008	0,0009	0,0007	0,0007	0,0005	0,0004	0,0003	0,0002	0,0001

Table A III-15 Calculated IDR modification factor based on FEMA P-58

floor	SITE CLASS D															
	2%		2,5%		3,5%		5%		7%		10%		20%		40%	
	$H_{\Delta ix}$	$H_{\Delta iy}$	$H_{\Delta ix}$	$H_{\Delta iy}$	$H_{\Delta ix}$	$H_{\Delta iy}$	$H_{\Delta ix}$	$H_{\Delta iy}$	$H_{\Delta ix}$	$H_{\Delta iy}$	$H_{\Delta ix}$	$H_{\Delta iy}$	$H_{\Delta ix}$	$H_{\Delta iy}$	$H_{\Delta ix}$	$H_{\Delta iy}$
12	0,643	0,669	0,663	0,687	0,692	0,712	0,719	0,736	0,744	0,757	0,768	0,777	0,806	0,809	0,835	0,832
11	0,660	0,687	0,681	0,706	0,711	0,732	0,739	0,756	0,765	0,778	0,789	0,798	0,828	0,831	0,857	0,854
10	0,660	0,687	0,681	0,706	0,711	0,731	0,739	0,756	0,764	0,778	0,789	0,798	0,828	0,830	0,857	0,854
9	0,649	0,676	0,670	0,694	0,699	0,719	0,727	0,743	0,752	0,765	0,776	0,785	0,814	0,817	0,843	0,840
8	0,634	0,660	0,655	0,678	0,683	0,703	0,710	0,726	0,735	0,747	0,758	0,767	0,795	0,798	0,824	0,821
7	0,622	0,648	0,642	0,666	0,670	0,690	0,697	0,713	0,721	0,733	0,744	0,753	0,781	0,783	0,808	0,806
6	0,620	0,645	0,639	0,663	0,667	0,687	0,694	0,709	0,718	0,730	0,740	0,749	0,777	0,780	0,805	0,802
5	0,633	0,659	0,653	0,676	0,681	0,701	0,708	0,724	0,733	0,745	0,756	0,765	0,793	0,796	0,821	0,819
4	0,669	0,696	0,690	0,715	0,720	0,741	0,749	0,766	0,775	0,788	0,799	0,809	0,839	0,841	0,869	0,866
3	0,740	0,771	0,764	0,791	0,797	0,820	0,829	0,847	0,857	0,872	0,884	0,895	0,928	0,931	0,961	0,958
2	0,866	0,902	0,894	0,926	0,933	0,960	0,970	0,992	1,003	1,021	1,035	1,047	1,086	1,090	1,125	1,121
1	1,083	1,128	1,118	1,159	1,166	1,201	1,213	1,240	1,255	1,276	1,295	1,310	1,359	1,363	1,407	1,402

Table A III-16 Modified IDR based on FEMA P-58

floor	SITE CLASS D															
	2%		2,5%		3,5%		5%		7%		10%		20%		40%	
	IDR _x	IDR _y	IDR _x	IDR _y	IDR _x	IDR _y	IDR _x	IDR _y	IDR _x	IDR _y	IDR _x	IDR _y	IDR _x	IDR _y	IDR _x	IDR _y
12	0,0039	0,0058	0,0036	0,0053	0,0031	0,0046	0,0027	0,0039	0,0022	0,0033	0,0018	0,0026	0,0011	0,0016	0,0006	0,0008
11	0,0041	0,0060	0,0038	0,0055	0,0033	0,0047	0,0029	0,0040	0,0024	0,0034	0,0020	0,0027	0,0012	0,0016	0,0006	0,0008
10	0,0043	0,0059	0,0040	0,0054	0,0035	0,0047	0,0030	0,0040	0,0025	0,0033	0,0020	0,0027	0,0013	0,0016	0,0006	0,0008
9	0,0043	0,0057	0,0040	0,0052	0,0035	0,0045	0,0030	0,0039	0,0025	0,0032	0,0021	0,0026	0,0013	0,0016	0,0006	0,0008
8	0,0043	0,0054	0,0039	0,0050	0,0034	0,0043	0,0029	0,0036	0,0025	0,0030	0,0020	0,0024	0,0012	0,0015	0,0006	0,0007
7	0,0041	0,0050	0,0038	0,0046	0,0033	0,0040	0,0029	0,0034	0,0024	0,0028	0,0020	0,0023	0,0012	0,0014	0,0006	0,0007
6	0,0040	0,0047	0,0037	0,0043	0,0032	0,0037	0,0028	0,0031	0,0023	0,0026	0,0019	0,0021	0,0012	0,0013	0,0006	0,0006
5	0,0039	0,0043	0,0036	0,0039	0,0031	0,0034	0,0027	0,0029	0,0023	0,0024	0,0018	0,0019	0,0011	0,0012	0,0006	0,0006
4	0,0038	0,0039	0,0035	0,0035	0,0030	0,0031	0,0026	0,0026	0,0022	0,0022	0,0018	0,0017	0,0011	0,0011	0,0006	0,0005
3	0,0036	0,0034	0,0033	0,0031	0,0029	0,0027	0,0025	0,0023	0,0021	0,0019	0,0017	0,0016	0,0011	0,0009	0,0005	0,0005
2	0,0033	0,0029	0,0030	0,0026	0,0027	0,0023	0,0023	0,0019	0,0019	0,0016	0,0016	0,0013	0,0010	0,0008	0,0005	0,0004
1	0,0019	0,0015	0,0017	0,0014	0,0015	0,0012	0,0013	0,0010	0,0011	0,0008	0,0009	0,0007	0,0005	0,0004	0,0003	0,0002

Table A III-17 Calculated PFA modification height factor based on FEMA P-58

floor	SITE CLASS D															
	2%		2,5%		3,5%		5%		7%		10%		20%		40%	
	H _{aix}	H _{aiy}	H _{aix}	H _{aiy}	H _{aix}	H _{aiy}	H _{aix}	H _{aiy}	H _{aix}	H _{aiy}	H _{aix}	H _{aiy}	H _{aix}	H _{aiy}	H _{aix}	H _{aiy}
12	1,672	1,709	1,742	1,770	1,842	1,855	1,939	1,937	2,028	2,011	2,113	2,081	2,251	2,192	2,357	2,276
11	1,144	1,169	1,192	1,211	1,260	1,269	1,327	1,325	1,388	1,376	1,446	1,424	1,541	1,500	1,613	1,557
10	0,928	0,948	0,967	0,982	1,022	1,030	1,076	1,075	1,125	1,116	1,172	1,155	1,249	1,217	1,308	1,263
9	0,861	0,880	0,897	0,912	0,948	0,955	0,998	0,997	1,044	1,035	1,088	1,071	1,159	1,129	1,214	1,172
8	0,882	0,902	0,919	0,934	0,972	0,979	1,023	1,022	1,070	1,061	1,115	1,098	1,188	1,157	1,244	1,201
7	0,963	0,985	1,004	1,020	1,061	1,069	1,117	1,116	1,168	1,159	1,217	1,199	1,297	1,263	1,358	1,311
6	1,082	1,107	1,128	1,146	1,193	1,201	1,256	1,254	1,313	1,302	1,368	1,347	1,458	1,420	1,527	1,474
5	1,208	1,235	1,259	1,280	1,331	1,341	1,402	1,400	1,466	1,453	1,527	1,504	1,627	1,585	1,704	1,645
4	1,293	1,322	1,347	1,369	1,425	1,435	1,500	1,498	1,568	1,555	1,634	1,609	1,741	1,696	1,823	1,760
3	1,280	1,309	1,334	1,356	1,411	1,421	1,485	1,483	1,553	1,540	1,618	1,594	1,725	1,679	1,806	1,743
2	1,133	1,158	1,180	1,199	1,248	1,257	1,314	1,312	1,374	1,362	1,431	1,410	1,525	1,486	1,597	1,542
1	0,864	0,883	0,900	0,915	0,952	0,959	1,002	1,001	1,048	1,039	1,092	1,075	1,164	1,133	1,218	1,176

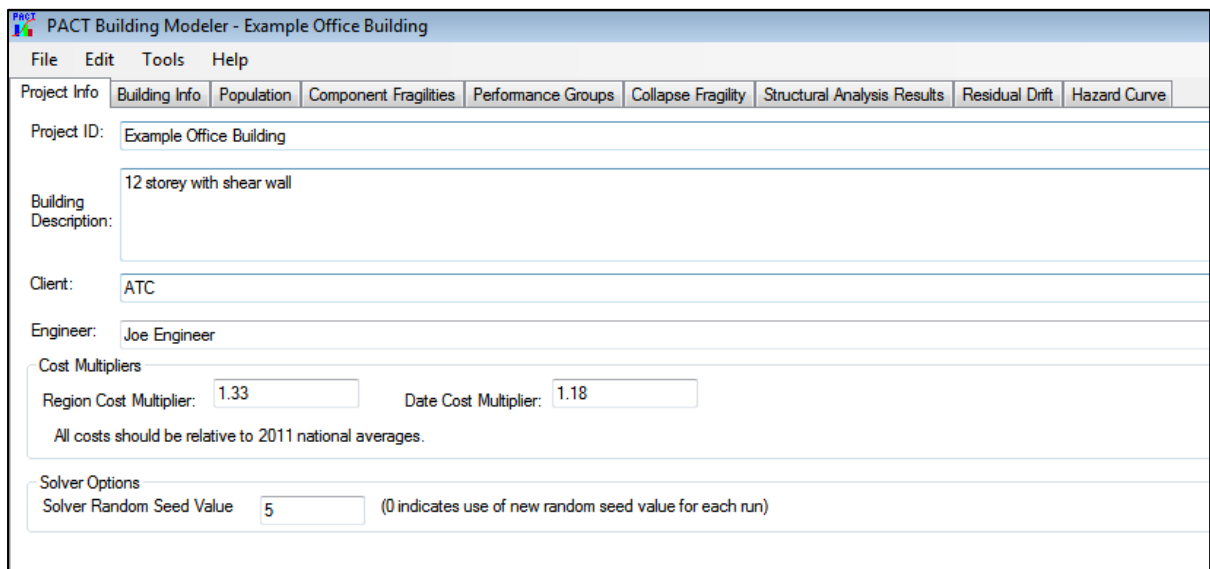
Table A III-18 Modified PFA based on FEMA P-58 due to seismic input obtained from NBC 2020 spectra

floor	SITE CLASS D															
	2%		2,5%		3,5%		5%		7%		10%		20%		40%	
	a _{ix}	a _{iy}	a _{ix}	a _{iy}	a _{ix}	a _{iy}	a _{ix}	a _{iy}	a _{ix}	a _{iy}	a _{ix}	a _{iy}	a _{ix}	a _{iy}	a _{ix}	a _{iy}
12	0,804	0,822	0,744	0,756	0,652	0,657	0,578	0,577	0,523	0,519	0,454	0,447	0,311	0,303	0,165	0,159
11	0,550	0,563	0,509	0,517	0,446	0,449	0,395	0,395	0,358	0,355	0,311	0,306	0,213	0,207	0,113	0,109
10	0,446	0,456	0,413	0,419	0,362	0,364	0,321	0,320	0,290	0,288	0,252	0,248	0,172	0,168	0,091	0,088
9	0,414	0,423	0,383	0,389	0,336	0,338	0,298	0,297	0,269	0,267	0,234	0,230	0,160	0,156	0,085	0,082
8	0,424	0,434	0,392	0,399	0,344	0,346	0,305	0,304	0,276	0,274	0,240	0,236	0,164	0,160	0,087	0,084
7	0,463	0,474	0,429	0,436	0,376	0,378	0,333	0,333	0,301	0,299	0,262	0,258	0,179	0,174	0,095	0,092
6	0,521	0,532	0,482	0,490	0,422	0,425	0,374	0,374	0,339	0,336	0,294	0,290	0,201	0,196	0,107	0,103
5	0,581	0,594	0,538	0,546	0,471	0,475	0,418	0,417	0,378	0,375	0,328	0,323	0,225	0,219	0,119	0,115
4	0,622	0,636	0,575	0,585	0,504	0,508	0,447	0,446	0,405	0,401	0,351	0,346	0,240	0,234	0,127	0,123
3	0,616	0,630	0,570	0,579	0,499	0,503	0,443	0,442	0,401	0,397	0,348	0,343	0,238	0,232	0,126	0,122
2	0,545	0,557	0,504	0,512	0,442	0,445	0,392	0,391	0,354	0,352	0,308	0,303	0,211	0,205	0,112	0,108
1	0,416	0,425	0,384	0,391	0,337	0,339	0,299	0,298	0,270	0,268	0,235	0,231	0,161	0,156	0,085	0,082

APPENDIX IV

PERFORMANCE CALCULATION USING PACT

In this Appendix, the steps of modeling with PACT used in this study to calculate direct economic loss in terms of repair costs for three selected architectural components are shown.



The screenshot displays the PACT Building Modeler software interface for an "Example Office Building". The window title is "PACT Building Modeler - Example Office Building". The menu bar includes "File", "Edit", "Tools", and "Help". The main interface is divided into several sections:

- Project Info:** A tabbed interface with "Project Info" selected. Other tabs include "Building Info", "Population", "Component Fragilities", "Performance Groups", "Collapse Fragility", "Structural Analysis Results", "Residual Drift", and "Hazard Curve".
- Project ID:** A text field containing "Example Office Building".
- Building Description:** A text area containing "12 storey with shear wall".
- Client:** A text field containing "ATC".
- Engineer:** A text field containing "Joe Engineer".
- Cost Multipliers:** A section containing two input fields: "Region Cost Multiplier" with a value of "1.33" and "Date Cost Multiplier" with a value of "1.18". Below these fields is the text: "All costs should be relative to 2011 national averages."
- Solver Options:** A section containing an input field for "Solver Random Seed Value" with a value of "5". A note next to it states: "(0 indicates use of new random seed value for each run)".

Figure A IV-1 Project information including cost multipliers

PACT Building Modeler - Example Office Building *

File Edit Tools Help

Project Info Building Info Population Component Fragilities Performance Groups Collapse Fragility Structural Analysis Results Residual Drift Hazard Curve

Number of Stories:

Total Replacement Cost (\$): Replacement Time (days): Total Loss Threshold (As Ratio of Total Replacement Cost):

Core and Shell Replacement Cost (\$): Max Workers per sq. m.:

Carbon Emissions Replacement (kg): Embodied Energy Replacement (MJ):

Most Typical Defaults

Floor Area (sq. m.): Story Height (m.):

Floor Num	Floor Name	Story Height (m.):	Area (sq. m.):	Height Factor	Hazmat Factor	Occupancy Factor
1	Floor 1	4.85	900.00	1	1	1.2
2	Floor 2	3.65	900.00	1	1	1.2
3	Floor 3	3.65	900.00	1	1	1.2
4	Floor 4	3.65	900.00	1	1	1.2
5	Floor 5	3.65	900.00	1.08	1	1.2
6	Floor 6	3.65	900.00	1.08	1	1.2
7	Floor 7	3.65	900.00	1.08	1	1.2
8	Floor 8	3.65	900.00	1.08	1	1.2
9	Floor 9	3.65	900.00	1.08	1	1.2
10	Floor 10	3.65	900.00	1.08	1	1.2
11	Floor 11	3.65	900.00	1.16	1	1.2
12	Floor 12	3.65	900.00	1.16	1	1.2
13	PH	0.00	36.00	1.16	1	1.2

Figure A IV-2 Building information including geometry, replacement costs, and correction factors

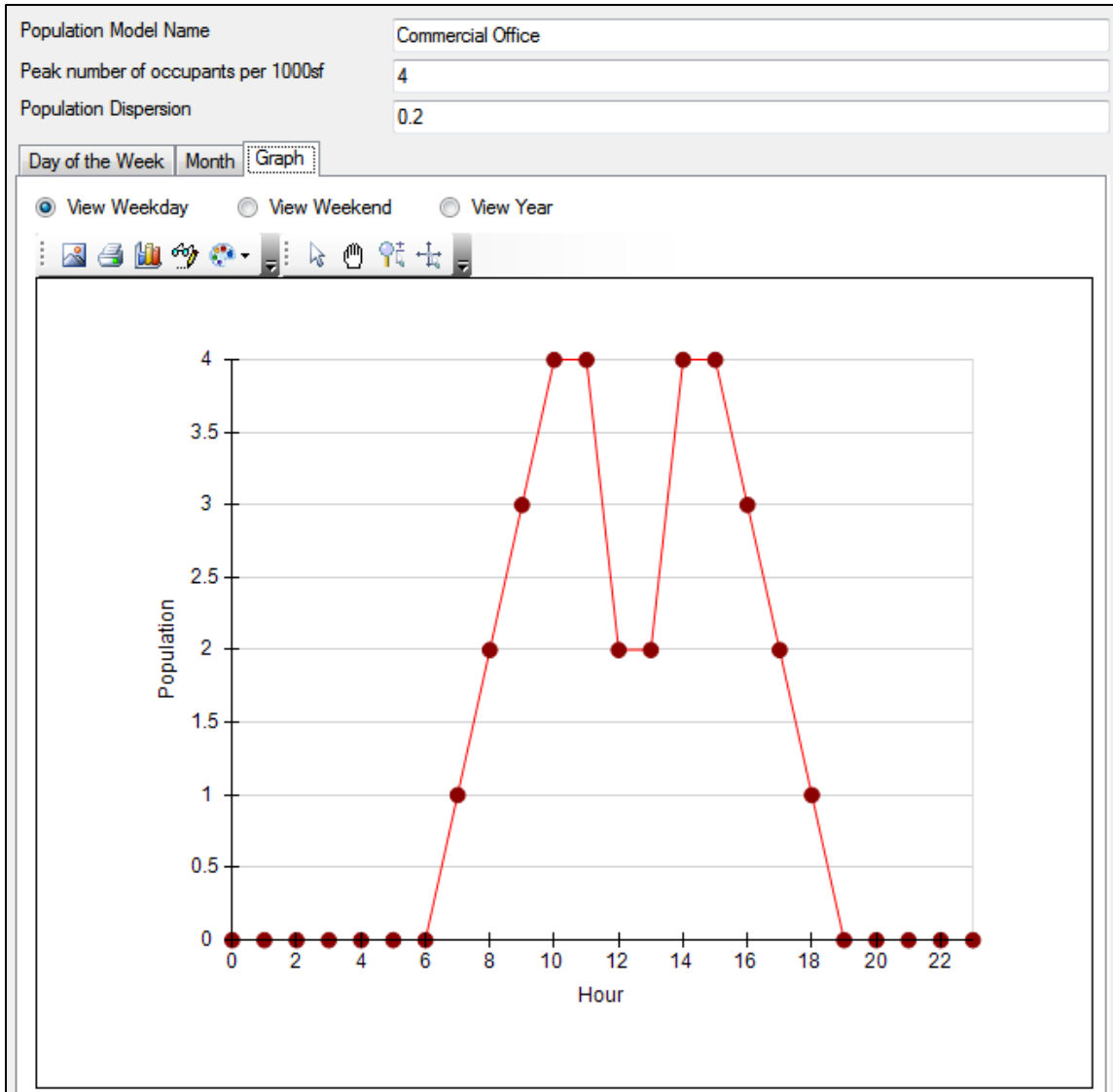


Figure A IV-3 Building population distribution graph

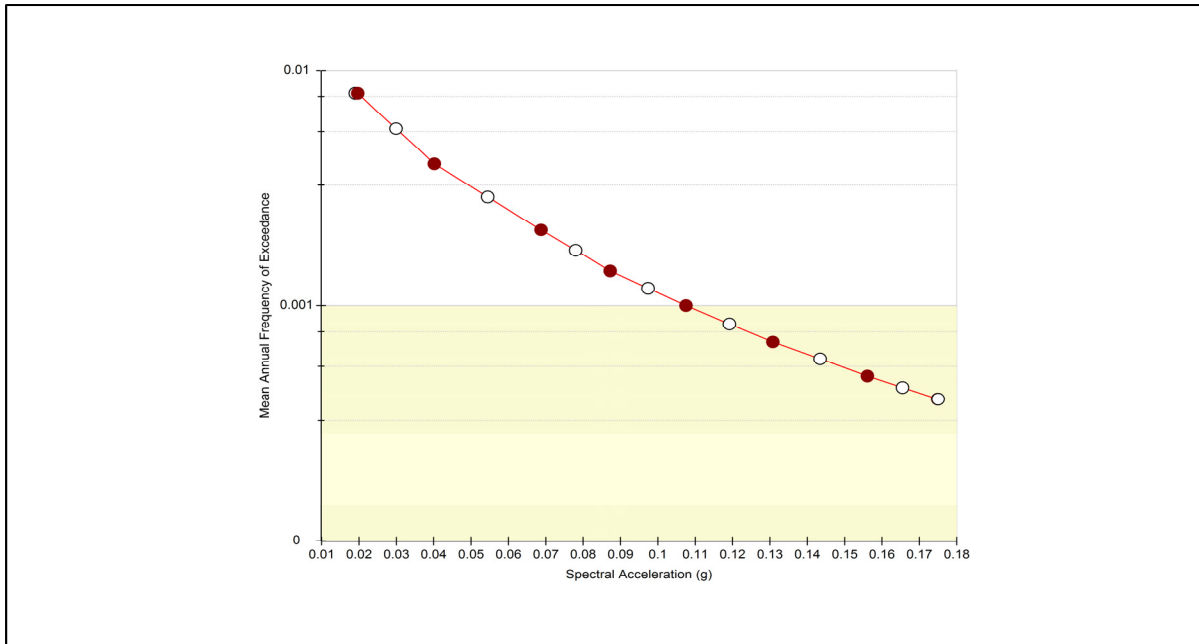


Figure A IV-4 Defined hazard curve based on spectral accelerations and mean annual frequency of exceedance of earthquakes

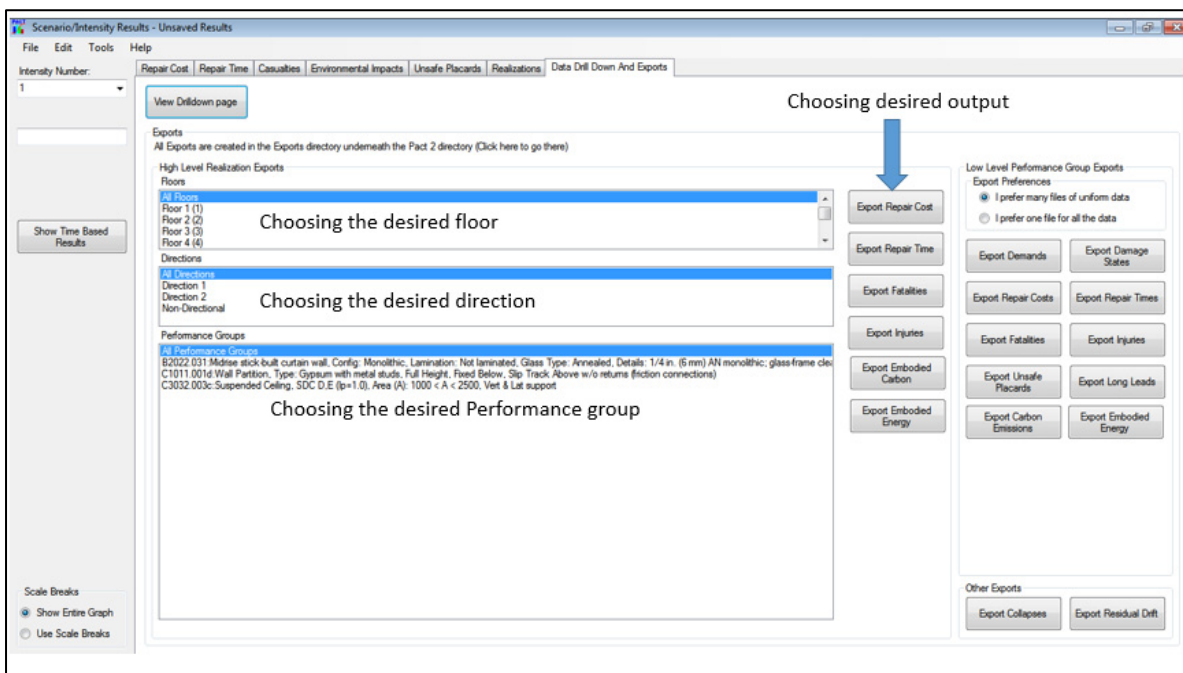


Figure A IV-5 Obtaining numerical outputs by choosing desired floors, directions, and performance groups

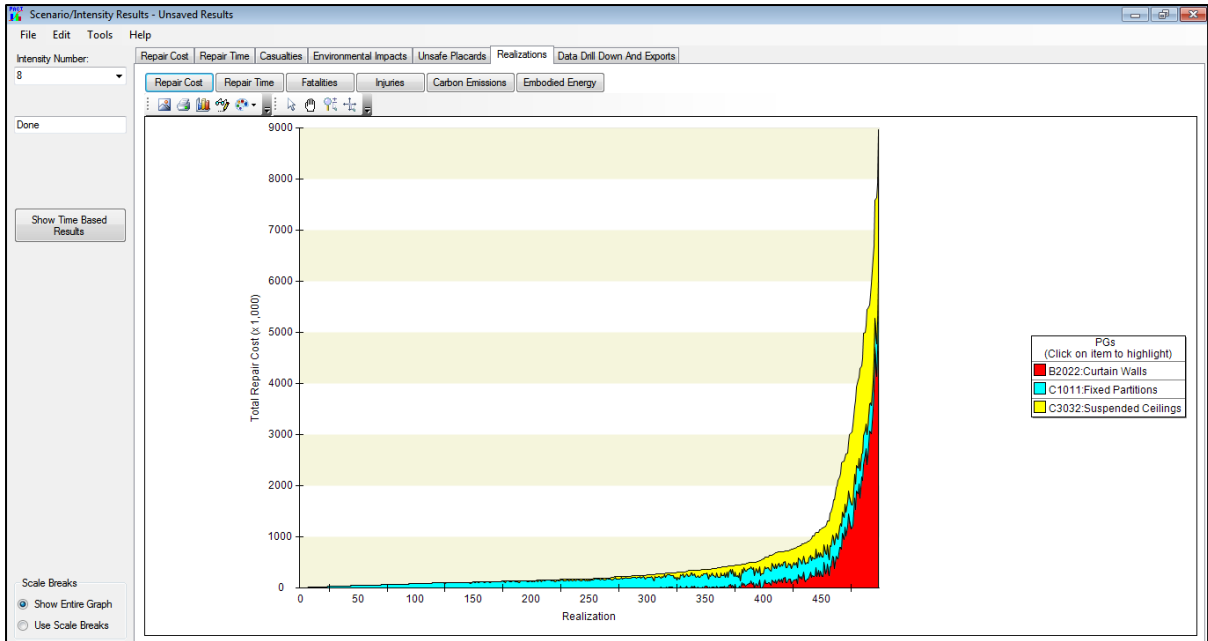


Figure A IV-6 Total repair cost associated with improved condition of all realizations due to the 2% in 50 years earthquake seismic intensity

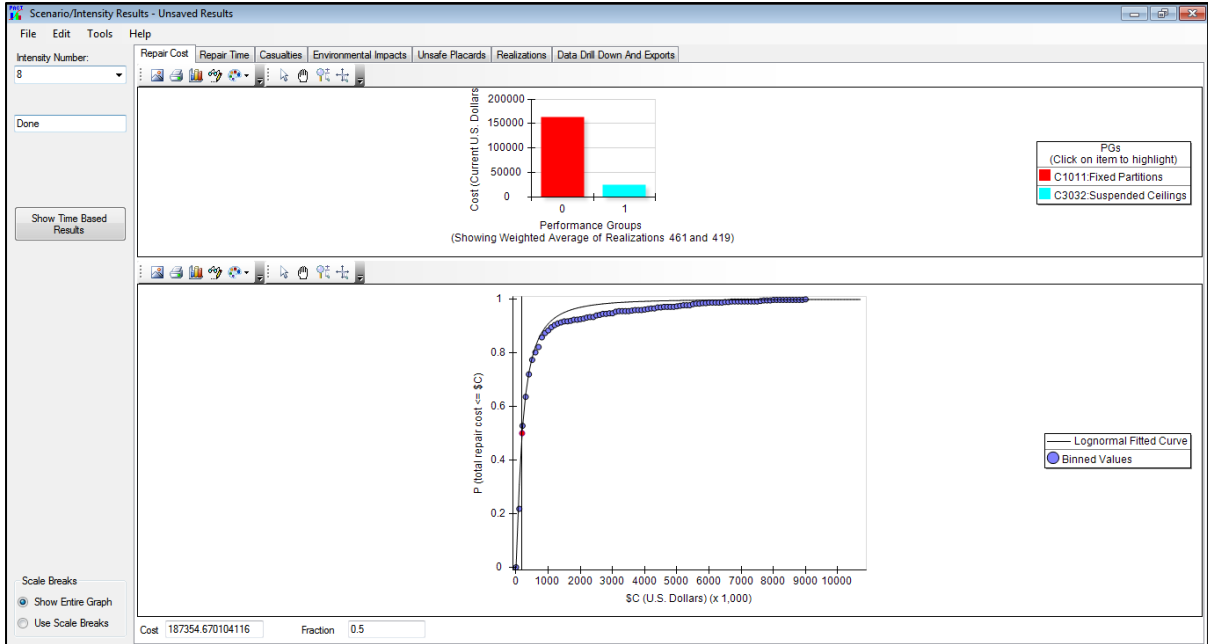


Figure A IV-7 Median of total repair cost associated with improved condition due to the 2% in 50 years earthquake seismic intensity

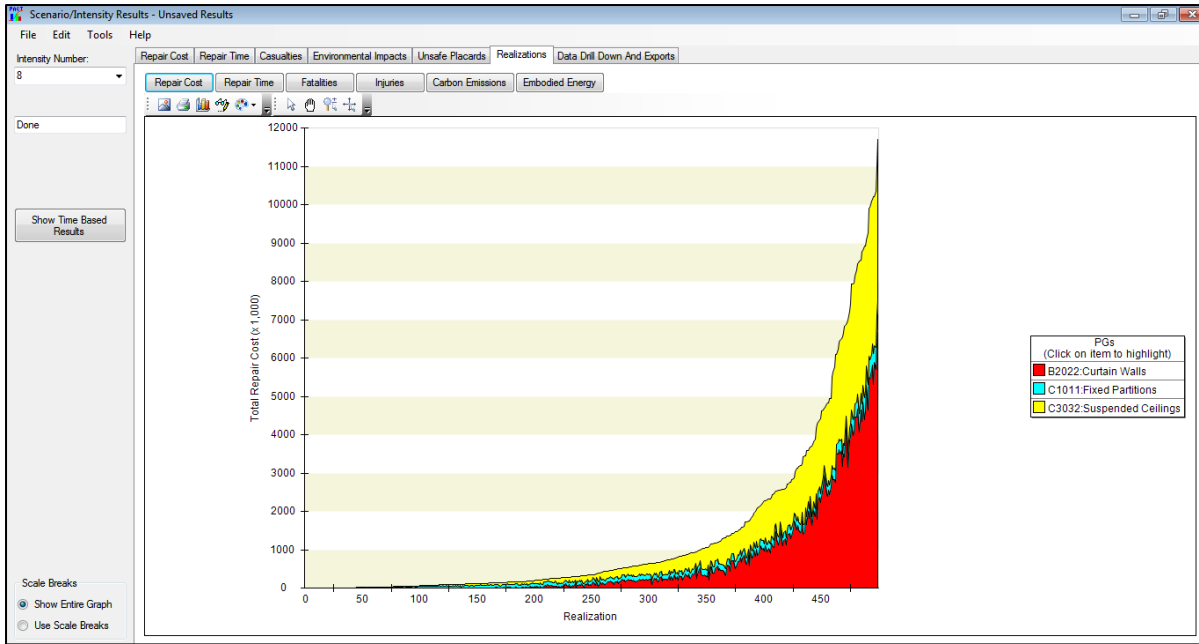


Figure A IV-8 Total repair cost associated with standard condition of all realizations due to the 2% in 50 years earthquake seismic intensity

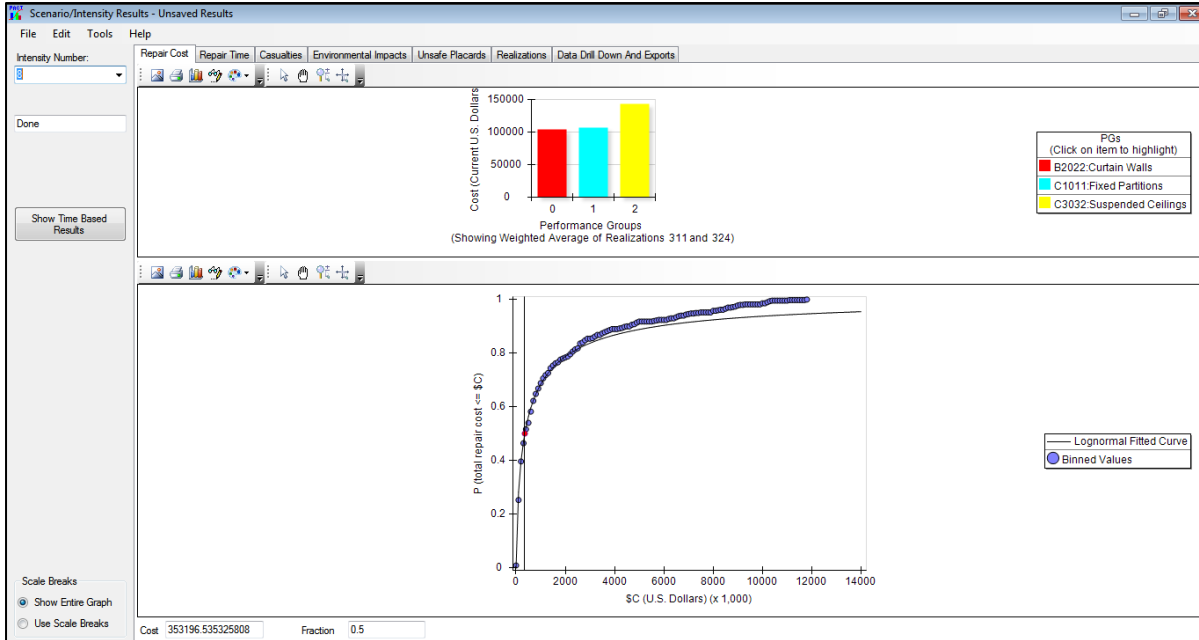


Figure A IV-9 Median of total repair cost associated with standard condition due to the 2% in 50 years earthquake seismic intensity

APPENDIX V

AN EXAMPLE FOR CALCULATION OF REPAIR COST

The following numerical example explains the procedure of loss calculation for a given EDP for a partition wall with the fragility curves shown in the figure (A V-1) and the corresponding consequences functions shown in the figure (A V-2). In order to calculate the repair cost for the surface of 6500 sqft, first the probability of occurrence of each damage state shall be calculated by the fragility curve (Figure A V-1), then, the obtained probability will be multiplied by the estimated cost from the consequence function.

Probability of occurrence of the DS1 for a given IDR=0.01: $P(DS1|IDR = 0.01) = 0.97$

Probability of occurrence of the DS2 for a given IDR=0.01: $P(DS2|IDR = 0.01) = 0.55$

Probability of occurrence of the DS3 for a given IDR=0.01: $P(DS3|IDR = 0.01) = 0.00$

Based on fragility database of FEMA P-58, each 1300 sqft of partition wall is considered as one unite of quantity, therefore, the quantity of NSC is $\frac{6500}{1300} = 5$.

The average repair cost for each damage state can be obtained from the consequence function (Figure A V-2). In this example the interpolation has been utilized in order to obtain more precise results.

Average repair cost for a quantity of 5 while DS1 is occurred:

$$C(1|DS1) = 2677.5 \$ \text{ and } C(10|DS1) = 1428 \$$$

$$\text{Interpolation : } C(5|DS1) = C(1|DS1) + \frac{c(1|DS1)-c(10|DS1)}{1-10} \times (5 - 1) = 2122.17 \$$$

$$\text{So: } C(5|DS1) = 2122.17 \$$$

With the same approach:

$$\text{Average repair cost for quantity of 5 while DS2 is occurred: } C(5|DS2) = 5409.44 \$$$

$$\text{Average repair cost for quantity of 5 while DS2 is occurred: } C(5|DS3) = 9138.89 \$$$

$$\text{Total repair cost} = 0.97 \times 2122.17 + 0.55 \times 5409.44 + 0.00 \times 9138.89 = 5033.7 \$$$

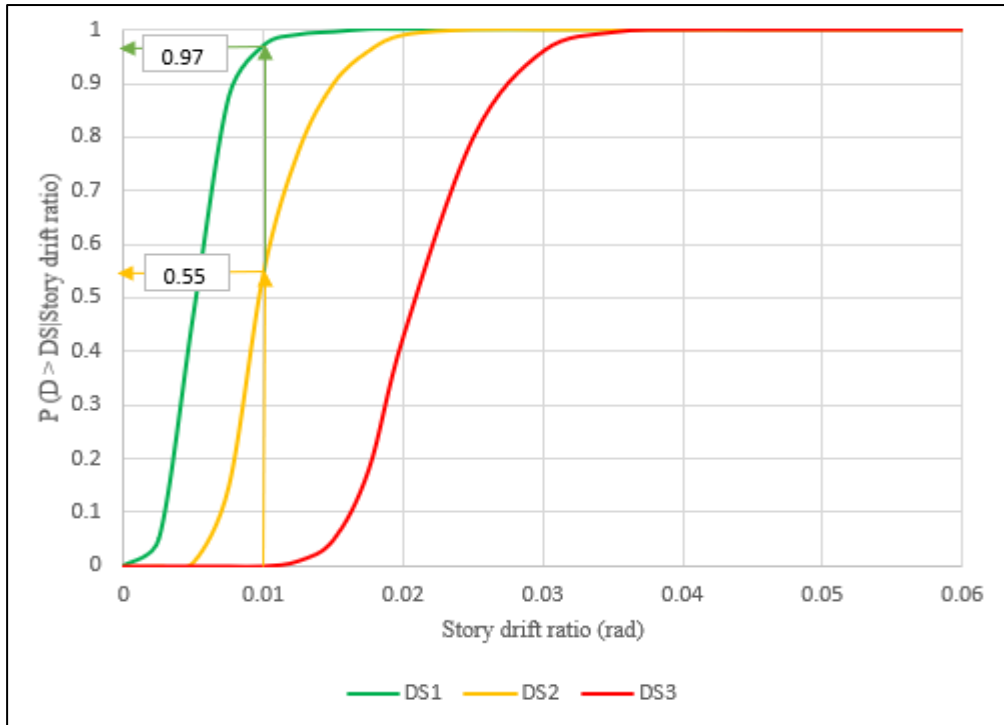


Figure A V-1 fragility curve of the selected NSC

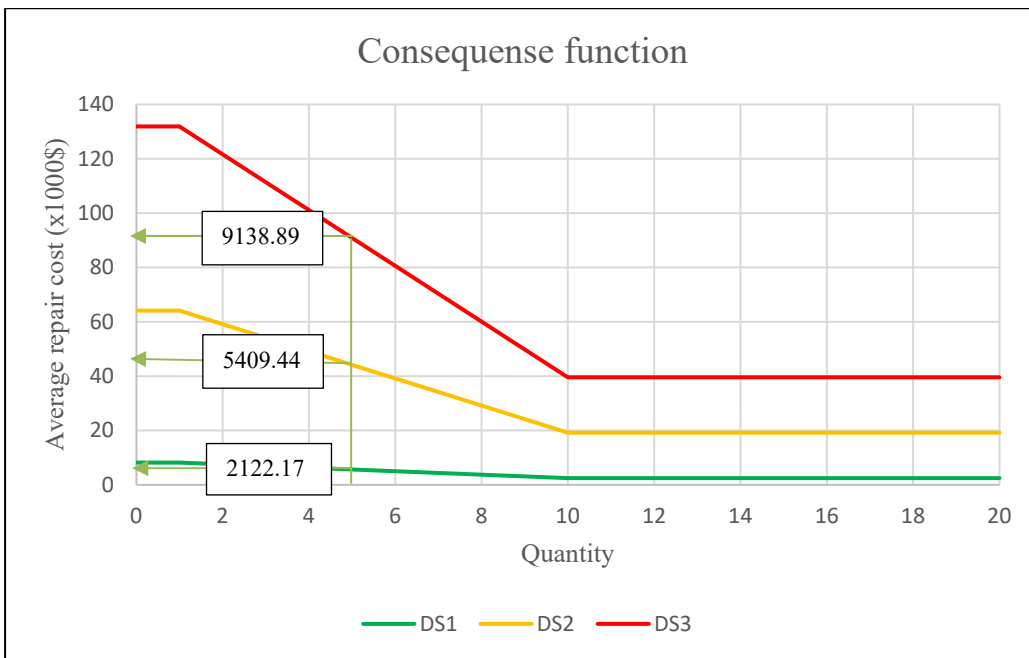


Figure A V-2 Consequence function of selected NSC

APPENDIX VI

CURVE FITTING USING REGRESSION MODEL TO VERIFY ESTIMATED PFA

The curve fitting using regression model in Excel has been conducted to verify the estimated PFA with proposed equations in NBC (NBC, 2015) and ASEC7 (ASCE, 2022) by the equations proposed in the Fathali and Lizundia (2011) as shown in Table VI-1.

In regression analysis, curve fitting involves selecting a model that optimally matches the curves within under study dataset. The correlation coefficient is used to measure the strength of the relationship between two variables.

Table A VI-1 Proposed formula to estimate PFA
Taken from NBC2015, ASCE7-22, and Fathali and Lizundia (2011)

	Code	Fathali ans Lizundia (2011)
NBC 2015	$\frac{PFA}{PGA} = 1 + 2\left(\frac{z}{h}\right)$	$\frac{PFA}{PGA} = 1 + 2\left(\frac{z}{h}\right)$
ASCE 7	$\frac{PFA}{PGA} = 1 + 0.59\left(\frac{z}{H}\right) + 0.94\left(\frac{z}{H}\right)^{10}$	$\frac{PFA}{PGA} = 1 + 1.50\left(\frac{z}{H}\right)^{3.15}$

Table A VI-2 Comparing the height factors
Adapted from ASCE-7, NBC 2015 and Fathali and Lizundia (2011)

Floor	ASCE7-22 elastic PFA profile	Fitted Curve	NBC- PFA height Factor	Fitted Curve
12	2,534	2,500	3,000	3,000
11	1,947	2,149	2,838	2,838
10	1,655	1,859	2,676	2,676
9	1,504	1,623	2,513	2,513
8	1,417	1,436	2,351	2,351
7	1,356	1,291	2,189	2,189
6	1,304	1,184	2,027	2,027
5	1,255	1,107	1,864	1,864
4	1,207	1,055	1,702	1,702
3	1,159	1,024	1,540	1,540
2	1,111	1,008	1,378	1,378
1	1,064	1,001	1,216	1,216
0	1,000	1,000	1,000	1,000
$R^2 = 0,97$			1,00	

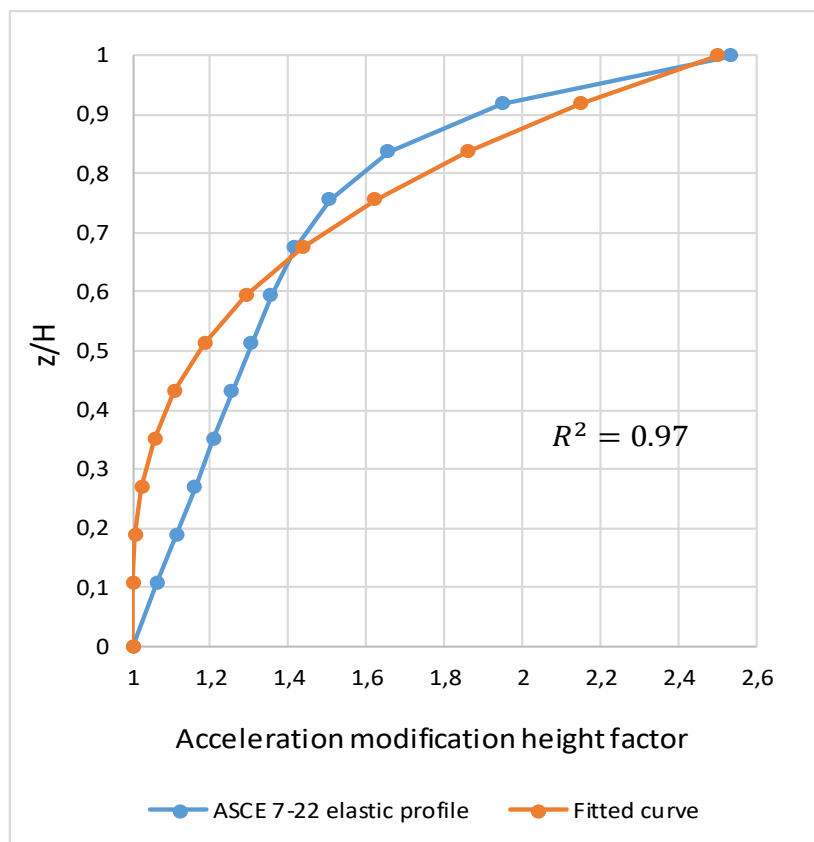


Figure A VI-1 Comparing the height factor obtained from ASCE7 with the fitted curve
Adapted from Fathali and Lizundia (2011)

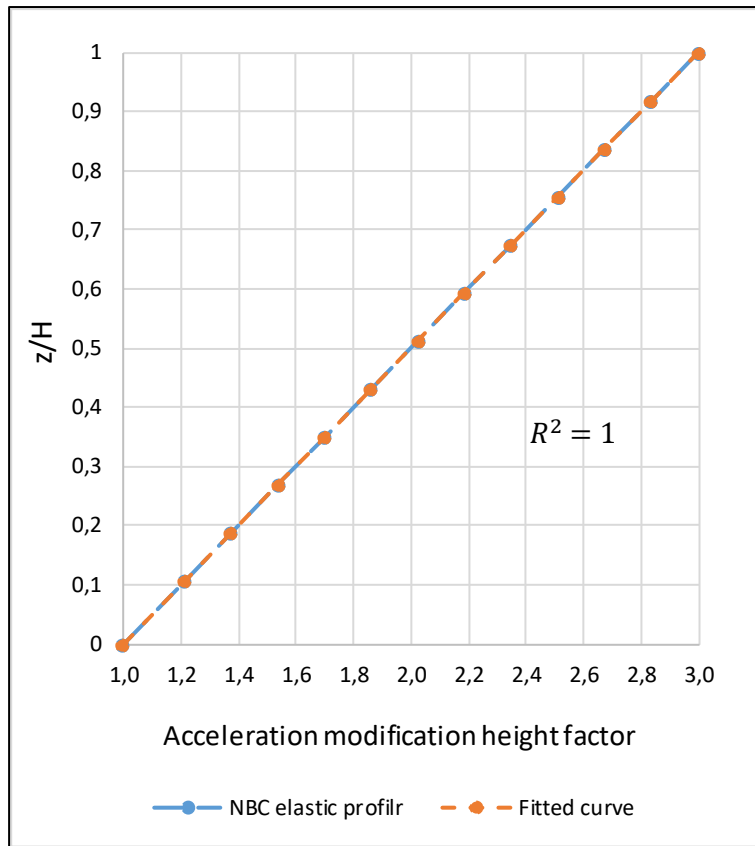


Figure A VI-2 Comparing the height factor obtained from NBC 2015 with the fitted curve
Adapted from Fathali and Lizundia (2011)

LIST OF BIBLIOGRAPHICAL REFERENCES

- Abouda, A. (2022). Caractérisation de l'effet de la non-linéarité sur les accélérations et spectres de plancher horizontaux dans un bâtiment en béton armé avec des murs de refend ductiles. <espace.etsmtl.ca/id/eprint/3005/1/ABOUDA_Amine.pdf>
- Achour, N., Miyajima, M., Kitaura, M., Price, A. (2011). Earthquake-induced structural and nonstructural damage in hospitals. *Earthq Spectra* 27:617–634. <https://doi.org/10.1193/1.3652797>
- Adams, J., Allen, T., Halchuk, S., & Kolaj, M. (2019). Canada's 6th Generation Seismic Hazard Model, as Prepared for the 2020 National Building Code of Canada.
- Arifin, F. A., Sullivan, T. J., Dhakal, R. P. (2020). Experimental investigation into the seismic fragility of a commercial glazing system. *Bull. N. Z. Soc. Earthquake Eng.* 15 (3): 144–149. <https://doi.org/10.5459/bnzsee.53.3.144-149>.
- ASCE 7-22 (2022). Minimum design load and associated criteria for buildings and other structures. Structural Engineering Institute, America society of Civil Engineering
- ASCE 41-13 (2013). Seismic evaluation and retrofit of existing buildings. Structural Engineering Institute, America society of Civil Engineering
- Araya-Letelier, G., Miranda, E., & Deierlein, G. (2019). Development and Testing of a Friction/Sliding Connection to Improve the Seismic Performance of Gypsum Partition Walls. *Earthquake Spectra*, 35(2), 653–677. <https://doi.org/10.1193/123117EQS270M>
- Assi, R., Youance, S., Bonne, A., & Nollet, M.-J. (2016). Effect of non-structural components on the modal properties of buildings using ambient vibration testing. *International Structural Specialty Conference of the Canadian Society for Civil Engineering* pp. 2652-2661.
- Baird, A., Palermo, A., & Pampanin, S. (2011). Facade damage assessment of multi-storey buildings in the 2011 Christchurch earthquake. *Bulletin of the New Zealand Society for Earthquake Engineering*, 44(4), Article 4. <https://doi.org/10.5459/bnzsee.44.4.368-376>
- Baird, A., Palermo, A., Pampanin, S., Riccio, P., & Tasligedik, A. S. (2011). Focusing on reducing the earthquake damage to facade systems. *Bulletin of the New Zealand Society for Earthquake Engineering*, 44(2), Article 2. <https://doi.org/10.5459/bnzsee.44.2.108-120>
- Baker, J. W. (2015). Efficient Analytical Fragility Function Fitting Using Dynamic Structural Analysis. *Earthquake Spectra*, 31(1), 579-599.

<https://doi.org/10.1193/021113EQS025M>

Bersofsky A., 2004. A Seismic Performance Evaluation of Gypsum Wallboard Partitions, MSc Thesis, University of California at San Diego, San Diego, CA.

Bianchi, S., Ciurlanti, J., & Pampanin, S. (2019). Seismic vulnerability of non-structural components: from traditional solutions to innovative low-damage systems.

Bianchi, S., Ciurlanti, J., Perrone, D., Filiatrault, A., Costa, A. C., Candeias, P. X., Correia, A. A., & Pampanin, S. (2021). Shake-table tests of innovative drift sensitive nonstructural elements in a low-damage structural system. *Earthquake Engineering & Structural Dynamics*, 50(9), 2398–2420. <https://doi.org/10.1002/eqe.3452>

Bianchi, S., & Pampanin, S. (2022). Fragility Functions for Architectural Nonstructural Components. *Journal of Structural Engineering*, 148(10), 03122005. [https://doi.org/10.1061/\(ASCE\)ST.1943-541X.0003352](https://doi.org/10.1061/(ASCE)ST.1943-541X.0003352)

Boivin (2006). Assessment of the Seismic Performance of a 12-storey Ductile Concrete Shear Wall System Designed According to the NBCC-2005 and the CSA A23.3-2004 Standards

Bouwkamp, J. G. 1961. Behavior of window panel under in-plane forces. *Bull. Seismol. Soc. Am.* 51 (1): 85–109. <https://doi.org/10.1785/BSSA0510010085>.

Bradley, B. A., Dhakal, R. P., Cubrinovski, M., MacRae, G. A., & Lee, D. S. (2009). Seismic loss estimation for efficient decision making. *Bulletin of the New Zealand Society for Earthquake Engineering*, 42(2), Article 2. <https://doi.org/10.5459/bnzsee.42.2.96-110>

Brandolese, S., Fiorin, L., & Scotta, R. (2019). Seismic demand and capacity assessment of suspended ceiling systems. *Engineering Structures*, 193, 219–237. <https://doi.org/10.1016/j.engstruct.2019.05.034>

Calvi, G. M., Sullivan, T. J., & Welch, D. P. (2014). A Seismic Performance Classification Framework to Provide Increased Seismic Resilience. In A. Ansal (Ed.), *Perspectives on European Earthquake Engineering and Seismology: Volume 1* (pp. 361–400). Springer International Publishing. https://doi.org/10.1007/978-3-319-07118-3_11

Goulet, C. A., Haselton, C. B., Mitrani-Reiser, J., Beck, J. L. (2007). Evaluation of the seismic performance of a code-conforming reinforced-concrete frame building - From seismic hazard to collapse safety and economic losses. *Earthquake Engineering & Structural Dynamics* 36(13):1973-1997, DOI:10.1002/eqe.694

CHD (2016). *Concrete Design Handbook*, Cement Association of Canada, Ottawa (Ontario), Canada, 4th edition.

- Ciurlanti, J., Bianchi, S., Pürgstaller, A., Gallo, P. Q., Bergmeister, K., & Pampanin, S. (2022). Shake table tests of concrete anchors for non-structural components including innovative and alternative anchorage detailing. *Bulletin of Earthquake Engineering*, <https://doi.org/10.1007/s10518-022-01359-2>.
- D'Amore, S., Bianchi, S., Ciurlanti, J., & Pampanin, S. (2023). Seismic assessment and finite element modeling of traditional vs innovative point fixed glass facade systems (PFGFS). *Bulletin of Earthquake Engineering*, 21(5), 2657–2689. <https://doi.org/10.1007/s10518-023-01622-0>
- Davidson, G., Lau, D., Erochko, J., & Kasai, K. (2019). Performance of Suspended Ceilings during Seismic Events. 12th Canadian Conference on Earthquake Engineering (CCEE)
- Davies, D., Retamales, R., Mosqueda, G., Filiatrault, A. (2011). Experimental seismic evaluation, model parameterization, and effects of cold-framed steel-framed gypsum partition walls on the seismic performance of an essential facility. MCEER-11-0005 technical report, NEES non-structural, State university of New York at Buffalo.
- Dhakal, R. P., MacRae, G. A., Pourali, A., & Paganotti, G. (2016). Seismic fragility of suspended ceiling systems used in NZ based on component tests. *Bulletin of the New Zealand Society for Earthquake Engineering*, 49(1), Article 1. <https://doi.org/10.5459/bnzsee.49.1.45-63>
- Djuric-Mijovic, D., Savic, J., Milanovic, D., & Cilic, A. (2018). Seismic damage mitigation of the glazed building façade. *Facta Universitatis - Series: Architecture and Civil Engineering*, 16(3), 343–353. <https://doi.org/10.2298/FUACE171115013D>
- Fathali, S., & Lizundia, B. (2011). Evaluation of asce/sei 7 equations for seismic design of nonstructural components using csmip records. *The Structural Design of Tall and Special Buildings* 20(S1):30 - 46. <https://doi.org/10.1002/tal.736>
- FEMA P-58-1 (2018). *Seismic Performance Assessment of Buildings, Volume 1 – Methodology, Second Edition*. Federal Emergency Management Agency of United States Department of Homeland Security (DHS).
- FEMA P-58-2 (2018). *Seismic Performance Assessment of Buildings, Volume 2 – Implementation Guide, Second Edition*. Federal Emergency Management Agency of United States Department of Homeland Security (DHS).
- FEMA P-58-3 (2018). *Seismic Performance Assessment of Buildings, Volume 3 – Supporting Electronic Material, Third Edition*. Federal Emergency Management Agency of United States Department of Homeland Security (DHS).

- FEMA P-58/BD-3.9.1 (2011). Architectural Glass Seismic Behavior Fragility Curve Development. Federal Emergency Management Agency of United States Department of Homeland Security (DHS).
- FEMA P-58/BD-3.9.2 (2011). Seismic Fragility of Building Interior Cold-Formed Steel Framed Gypsum Partition Walls. Federal Emergency Management Agency of United States Department of Homeland Security (DHS).
- FEMA P-58/BD-3.9.4 (2011). Development of Seismic Fragilities for Acoustical Tile or Lay-in Panel Suspended Ceilings. Federal Emergency Management Agency of United States Department of Homeland Security (DHS).
- FEMA P-58/BD-3.7.16 (2013). PACT Beta Test Example: Building C Reinforced Masonry Shear Wall Building. Federal Emergency Management Agency of United States Department of Homeland Security (DHS).
- Fierro E.A., Miranda E, Perry C.L. (2011). Behavior of nonstructural components in recent earthquakes. AEI 2011. Architectural Engineering Conference (AEI). American Society of Civil Engineers, Oakland, California, United States, pp 369–377
- Filiatrault, A., Uang, C. M., Folz, B., & Christopoulos, C. (2001). Reconnaissance report of the february 28, 2001 nisqually (seattle-olympia) earthquake.
- Filiatrault A, Uang C.M., Folz B, Christopoulos C., and Gatto K. (2001). Reconnaissance Report of the February 28, 2001 Nisqually (Seattle-Olympia) Earthquake. Structural Systems Research Project Report No. SSRP–2000/15, Department of Structural Engineering, University of California, San Diego, La Jolla, CA, 62 pp.
- Filiatrault A., Trembley R., Christopoulos C, Folz B., and Pettinga D. (2013). Elements of Earthquake Engineering and Structural Dynamics, 3rd edition
- Filiatrault A, Perrone D, Merino R.J., Calvi G.M. (2018). Performance-based seismic design of nonstructural building elements. *Journal of Earthquake Engineering* 25:1–33
- Fiorino, L., Pali, T., & Landolfo, R. (2018). Out-of-plane seismic design by testing of non-structural lightweight steel drywall partition walls. *Thin-Walled Structures*, 130, 213–230. <https://doi.org/10.1016/j.tws.2018.03.032>
- Flores, F., Lopez-Garcia, D., & Charney, F. (2015). Acceleration demands on nonstructural components in special steel moment frames. Dans XI Chilean Conference on Seismology and Earthquake Engineering ACHISINA (Vol. 212, pp. 12).
- Fragiadakis, M. (2013). Response Spectrum Analysis of Structures Subjected to Seismic

- Actions. In M. Beer, I. A. Kougiumtzoglou, E. Patelli, & I. S.-K. Au (Eds.), *Encyclopedia of Earthquake Engineering* (pp. 1–18). Springer Berlin Heidelberg. https://doi.org/10.1007/978-3-642-36197-5_133-1
- Haj Najafi, L., Tehranizadeh, M. (2016). *Civil Engineering Infrastructures Journal*, 49(2): 173–196, December 2016 Print ISSN: 2322-2093; Online ISSN: 2423-6691 DOI: 10.7508/cej.2016.02.001
- Hamburger, R. O. (1996). *Implementing Performance Based Seismic Design In Structural Engineering Practice*. Eleventh World Conference on Earthquake Engineering. paper no.2021. ISBN: 0 08 042822 3.
- Hasani, H., & Ryan, K. L. (2022). Experimental Cyclic Test of Reduced Damage Detailed Drywall Partition Walls Integrated with a Timber Rocking Wall. *Journal of Earthquake Engineering*, 26(10), 5109–5129. <https://doi.org/10.1080/13632469.2020.1859005>
- Lee, T.-H., Kato, M., Matsumiya, T., Suita, K., & Nakashima, M. (2007). Seismic performance evaluation of non-structural components: Drywall partitions. *Earthquake Engineering & Structural Dynamics*, 36(3), 367–382. <https://doi.org/10.1002/eqe.638>
- Lim, K. Y. S., King, A. B. (1991). *The behavior of external glazing systems under seismic in-plane racking*. Porirua, New Zealand: Building Research Association of New Zealand.
- Lu, W., B. Huang, S. Chen, and K. M. Mosalam. (2017). Shaking table test method of building curtain walls using floor capacity demand diagrams. *Bulletin of Earthquake Eng.* 15 (8): 31853205. <https://doi.org/10.1007/s10518-016-9866-y>.
- Lu, W., B. Huang, K. M. Mosalam, and S. Chen (2016). Experimental evaluation of a glass curtain wall of a tall building. *Earthquake Eng. Struct. Dyn.* 45 (7): 1185–1205. <https://doi.org/10.1002/eqe.2705>.
- Majdi, A. (2020). Applying ATC FEMA P-58 Approach and Nonlinear History Analysis to Estimate Economic and Social Losses due Earthquake for Reinforced Concrete Building in Iraq. *International Journal of Innovative Science and Research Technology* 5(4), 14.
- McClure, G., Cappai, J., Shapiro, R., Li, M., Dunlop-Brière, G., and Keller, P. (2010). Assessing the postearthquake functionality of critical buildings in Montréal. Proc. 9th US National and 10th Canadian Conference on Earthquake Engineering, 25–29 July, Toronto, Ontario, Canada, Paper No. 993.
- McGavin, G., and H. Patrucco. (1994). *Survey of Non-Structural Damage to Healthcare Facilities in the January 17, 1994, Northridge Earthquake*. Ontario, CA: HMC Group.

- Memari, A. M. (2011). Racking test evaluation of EN-WALL 7250 unitized curtain wall system with 3M™ VHB™ structural glazing tape. State College, CA: Pennsylvania State Univ.
- Memari, A. M., Behr, R. A. and Kremer, P. A. (2004). Dynamic racking crescendo tests on architectural glass fitted with anchored pet film. *Journal of Architectural Engineering* 10 (1): 5–14. [https://doi.org/10.1061/\(ASCE\)1076-0431\(2004\)10:1\(5\)](https://doi.org/10.1061/(ASCE)1076-0431(2004)10:1(5)).
- Miranda, E., Mosqueda, G., Retamales, R., & Pekcan, G. (2012). Performance of Nonstructural Components during the 27 February 2010 Chile Earthquake. *Earthquake Spectra*, 28(1_suppl1), 453–471. <https://doi.org/10.1193/1.4000032>
- NBC 2020 (2020). National Building Code of Canada; Part 4: Structural Design, Canadian Commission on Building and Fire Codes, National Research Council of Canada (NRCC), Ottawa, Canada.
- Ni, N., Anwar, N., Aung, T., & Najam, F. (2018). Seismic loss estimation of Non-structural Components based on actual parameters in high-rise RC shear wall Buildings. Australasian Structural Engineering Conference.
- Pantelides, C. P., and Behr, R. A. (1994). Dynamic in-plane racking tests of curtain wall glass elements. *Earthquake Engineering and Structural Dynamics*, 23 (2):211–228. <https://doi.org/10.1002/eqe.4290230208>.
- Pardalopoulos, S. I., & Pantazopoulou, S. J. (2015). Seismic response of nonstructural components attached on multistorey buildings. *Earthquake Engineering & Structural Dynamics*, 44(1), 139–158. <https://doi.org/10.1002/eqe.2466>
- Petrone, C., Magliulo, G., Manfredi, G. (2017). Shake table tests on standard and innovative temporary partition walls. *Earthquake Engineering & Structural Dynamics* Volume 46, Issue 10 p. 1599-1624, <https://doi.org/10.1002/eqe.2872>
- Perrone, D., Brunesi, E., Dacarro, F., Peloso, S., & Filiatrault, A. (2019). Seismic assessment and qualification of non-structural elements in Europe: A critical review. *International Association for the Seismic Performance Of Non-Structural Elements (SPONSE)*. <https://doi.org/10.7414/4sponse.ID.10>
- Perrone, D., Calvi, P. M., Nascimbene, R., Fischer, E. C., Magliulo, G. (2018). Seismic performance of non-structural elements during the 2016 Central Italy earthquake. *Bulletin of Earthquake Engineering*. 17:5655–5677 <https://doi.org/10.1007/s10518-018-0361-5>
- Porter, K. A. (2003). An Overview of PEER’s Performance-Based Earthquake Engineering Methodology. Ninth International Conference of Applications of Statistics and Probability (ICASP9).

in Civil Engineering.

- Preti, M., & Bolis, V. (2017). Masonry infill construction and retrofit technique for the infill-frame interaction mitigation: Test results. *Engineering Structures*, 132, 597–608. <https://doi.org/10.1016/j.engstruct.2016.11.053>
- Pürgstaller, A., Quintana Gallo, P., Pampanin, S., & Bergmeister, K. (2020). Seismic demands on nonstructural components anchored to concrete accounting for structure-fastener-nonstructural interaction (SFNI). *Earthquake Engineering & Structural Dynamics*, 49(6), 589–606. <https://doi.org/10.1002/eqe.3255>
- Quintana G. P., Moghaddasi M., Pampanin S., Bergmeister K. (2018). Shake table tests of post-installed anchors with supplemental damping. *ACI Struct J* 115(1):595–606
- Retamales, R., Davies, R., Mosqueda, G., & Filiatrault, A. (2013). Experimental Seismic Fragility of Cold-Formed Steel Framed Gypsum Partition Walls. *Journal of Structural Engineering*, 139(8), 1285–1293. [https://doi.org/10.1061/\(ASCE\)ST.1943-541X.0000657](https://doi.org/10.1061/(ASCE)ST.1943-541X.0000657)
- Romano, F., Faggella, M., Gigliotti, R., & Braga, F. (2018). Seismic Loss Analysis of a Non-ductile Infilled RC Building. In M. di Prisco & M. Menegotto (Eds.), *Proceedings of Italian Concrete Days 2016* (Vol. 10, pp. 524–534). Springer International Publishing. https://doi.org/10.1007/978-3-319-78936-1_38
- Rojas, D., Quintana Gallo, P., Pürgstaller, A., Bianchi, S., Ciurlanti, J., Pampanin, S., & Bergmeister, K. (2023). Influence of the anchorage shear hysteresis on the seismic response of nonstructural components in RC buildings. *Bulletin of Earthquake Engineering*, 21(7), 3399–3432. <https://doi.org/10.1007/s10518-023-01642-w>
- Ryu, K. P., Reinhorn, A. M. (2017). Experimental Study of Large Area Suspended Ceilings. *Journal of Earthquake Engineering*, 23(6), 1001–1032. <https://doi.org/10.1080/13632469.2017.1342294>
- SAP2000 (2021). SAP2000 structural analysis program, Computers & Structures Inc., Berekley, CA, USA, student version 21.1.0
- Sousa, L., & Monteiro, R. (2018). Seismic retrofit options for non-structural building partition walls: Impact on loss estimation and cost-benefit analysis. *Engineering Structures*, 161, 8–27. <https://doi.org/10.1016/j.engstruct.2018.01.028>
- Structural Engineers Association of California (SEAOC) (1995). *A Framework for Performance-Based Seismic Engineering*, SEAOC Vision 2000. Sacramento, CA: SEAOC.
- Sucuoǧlu, H., and C. V. G. Vallabhan. (1997). Behaviour of window glass panels during

earthquakes. *Eng. Struct.* 19 (8): 685–694. [https://doi.org/10.1016/S01410296\(96\)001307](https://doi.org/10.1016/S01410296(96)001307).

Trifunac, M., & Todorovska, M. (2008). Origin of the response spectrum method. 14th World Conference of Earthquake Engineering, Beijing, China.

Villaverde R. (2004). Seismic Analysis and Design of Nonstructural Elements, In *Earthquake Engineering: from Engineering Seismology to Performance Based Engineering*, Bozorgnia Y, Bertero V (editors), CRC Press LLC: Boca Raton, FL.

Zeng, X., Lu, X., Yang, T. Y., & Xu, Z. (2016). Application of the FEMA-P58 methodology for regional earthquake loss prediction. *Natural Hazards*, 83(1), 177–192. <https://doi.org/10.1007/s11069-016-2307-z>